DIPARTIMENTO SCIENZE DELLA VITA

DOTTORATO DI RICERCA IN SCIENZE DELLA VITA

LIFE SCIENCES

CICLO XXXVI

COORDINATRICE Prof.ssa Simona Maccherini

Study of lung fibrogenesis induced by several *noxae in vivo* and *in vitro* models

SETTORE SCIENTIFICO-DISCIPLINARE: MED-04

TUTOR: Prof.ssa Monica Lucattelli

Dipartimento di Medicina Molecolare e dello Sviluppo

DOTTORANDA: Chiara Goracci

Chiara Goracci Firmato il 29-04-2024

A.A. 2022-2023

INDEX

ABSTRACT p.4

INTRODUCTION p.7

CHAPTER 1 p.21

- AIM OF THE STUDY p.21
- MATERIALS AND METHODS p.22
- RESULTS p.30
- DISCUSSION p.49
- SUMMARY p.54

CHAPTER 2 p.55

- AIM OF THE STUDY p.55
- MATERIALS AND METHODS p.56
- RESULTS p.64
- DISCUSSION p.80
- SUMMARY p.89

CHAPTER 3 p.90

- AIM OF THE STUDY p.90
- MATERIALS AND METHODS p.91
- RESULTS p.98
- DISCUSSION p.109
- SUMMARY p.117

NOTE p.118

REFERENCES p.119

ABSTRACT

Pulmonary diseases, like chronic obstructive pulmonary disease (COPD) and idiopathic pulmonary fibrosis (IPF), are chronic and progressive disorders that severely affect the airways and other structures of the respiratory system. COPD and IPF, characterized by quite distinct clinical and pathological features, are both related to long-term inhalation of tobacco smoking.

Fibrogenesis is a common pathological feature of many chronic respiratory diseases but the specific mechanisms are still unclear. Repeated insults and/or aberrant repair events are the main processes that lead to fibrosis, and ultimately result in either non-reversible airways obstruction, typical of COPD, and impaired gas exchange and parenchymal consolidation, commonly observed in IPF patients.

A variety of pathogenic mechanisms has been proposed for these diseases, including oxidative stress and accelerated cellular senescence.

In order to achieve new advances in the knowledge of the pathogenetic mechanisms underlying lung fibrogenesis, the study of the fibrogenic process was carried out *in vivo* and *in vitro* models, in which the fibrotic alterations were induced by several etiological agents.

The first study completed our previous works on airways remodelling by using two mice strains, C57 BL/6J and DBA/2. We previously demonstrated that these mice strains present different phenotypical responses after the exposure to cigarette smoke. In particular, the characteristics of the two strains influenced the different changes in parenchymal and airway areas observed at different time points of cigarette smoke exposure. We also demonstrated a correspondence between oxidants-induced DNA damage, cellular senescence and the presence of senescence secreted factors involved in

the onset of fibrous remodelling. Along with these markers in the current study, we investigated whether alterations in the expression of histone deacetylases (SIRT1 and HDAC-2) and factors involved in the inflammatory process and progression of pulmonary lesions (p-p38 and NF-kB) contribute to the pathophysiology of airway remodelling. An earlier upregulation of p-p38 and NF-kB, together with a lower expression of SIRT1 and HDAC-2 is in line with a higher sensitivity to oxidative stress observed in the mice strains that may be one of the key factors in the development of airways fibrotic remodelling.

In another *in vivo* study, the effect of environmental tobacco smoke (ETS) in a model of bleomycin-induced pulmonary fibrosis in C57 BL/6J mice was evaluated, in order to understand the contribution of ETS in fibrogenesis. The combined effect of ETS and BLM was able to seriously compromise the lung regenerative potential, when compared with the effects promoted by the treatment with only bleomycin. In this study, lung fibrosis was accompanied by an increase of extracellular matrix (ECM) proteins (collagens, fibronectin and elastin) and enzymes in charge of ECM reorganization (MMPs and LOXs). Interestingly, overexpression of the Complement system was also observed, together with other senescence-associated markers (cyclin-dependent kinases inhibitors, *SERPINE1*, and Sirtuins) suggesting an earlier induction of cellular senescence.

Finally, *in vitro* studies were performed by using normal human lung fibroblast (NHLF) cells. A first model evaluated the involvement of the Complement system in the fibrotic remodelling. NHLF cells presented a significant increase in gene expression of *COL1A1*, *ACTA2* and *FN1* after the treatment with C3 Complement component. These results highlighted an initial stage of fibroblast differentiation into myofibroblast, a crucial event for the progression of the fibrotic process. A foremost role of the Complement system was further confirmed by exposing fibroblasts to a Complement 3a receptor (C3aR) antagonist,

SB290157, which induced a decline in the gene expression of *COL1A1*, *ACTA2* and *FN1* in a dose-response manner.

In a different model we exposed NHLF cells to cigarette smoke extract (CSE) followed by transforming growth factor-β (TGF-β) treatment. The results obtained from this study suggest the existence of an interference of several stimuli in the fibrogenesis.

Notwithstanding, further studies are still needed to ascertain which pathways promote fibrogenesis and to understand if they can be used as therapeutic targets for both COPD and IPF.

INTRODUCTION

Fibrogenesis is a pathophysiological response of many tissues to chronic injury. Commonly, protective biological mechanisms like wound healing and tissue remodelling are activated in response to stress and damage, to eventually restore the integrity and correct functionality of organs. The process of repair is characterized by removal of damaged or death cells, and represents a mechanism fundamental for survival. In case of persistent insults or deregulation of the repair responses, this process becomes detrimental and results in tissue fibrosis, massive deposition of extracellular matrix (ECM), scarring, and organ failure [1, 2].

Generally, a sequence of events synergistically contributes to the development of fibrosis, starting with epithelial/endothelial barrier damage and TGF-β release, followed by recruitment of inflammatory cells, induction of reactive oxygen species (ROS), and activation of cells capable of collagen production. Therefore, the specific role of each event in the process of fibrogenesis needs to be assessed [1].

Functions and organization of the extracellular matrix components in lung tissue

The main scaffolding of lung tissue consists of the pulmonary extracellular matrix that provides the appropriate stability and elasticity to the lungs [3]. ECM is a highly specialised three dimensional structure organised in two main types: basement membrane and interstitial matrix [4, 5]. Commonly, the composition of the ECM is characterised by an extremely dynamic system of fibrous proteins, glycoproteins, and proteoglycans that changes in response to physiological stimuli, and tissue localization [6, 7].

In particular, basement membranes are thin highly specialised layers of ECM that provide physical support to epithelial and endothelial cells, and surround muscle, fat, and

peripheral nerves [4, 7]. The main collagen constituent of the basement membrane is collagen type IV, which is fundamental for cell migration, proliferation and differentiation [3].

On the other hand, interstitial matrices are responsible for the creation of a three-dimensional fibrillar network that enables structural connection between cells and tissue, thus maintaining the biomechanical features of the lung [3, 4]. The predominant constituents of the interstitial matrix are the fibrillar collagens type I and III and collagen type VI [3].

Nevertheless, these mentioned proteins represent just a fraction of the multiple elements appearing in the pulmonary matrix.

More in detail, among the fibrous proteins, collagens and elastin can be found. The first ones are predominantly triple-helical proteins with intermolecular cross-links that can be further divided into fibrillar and non-fibrillar collagens [6, 8]. Fibrillar collagens like collagen type I, II, III, V and XI present high tensile strength and low elasticity [4], while non fibrillar ones, due to their specific structure, form a dens network that confers tensile strength to the alveolar-capillary barrier. Among these, collagen type IV is the most abundant in the lung [5].

Whereas, collagens are mainly responsible for pulmonary structure maintenance, elastin ensures the elastic properties essential for lung compliance and elastic recoil. Among the elastic fibres, distinguished by high elasticity and low tensile strength, elastin can be considered the essential component [6]. Elastic fibres display further activities, besides mechanical functions; for instance, they can regulate cell-ECM adhesion via interactions with integrin receptors [4].

In the midst of the myriad constituents of the ECM, there is a group of proteins containing oligosaccharide chains known as glycoproteins. These molecules contacts allow ECM assembly, and importantly cell adhesion and signalling [6, 9].

Examples of glycoproteins are laminins, fibronectins, tenascins and vitronectin, which can interact with fibrous proteins [6].

Nowadays, the ability of ECM elements to regulate multiple biological processes, namely cell growth, migration, cytoskeletal re-organization and tissue development, is evident [6, 7]. In brief, the ECM is able to communicate with cells through connections between glycoproteins such as laminins and fibronectins and cell transmembrane proteins like integrins [10]. Besides being the most abundant non-collagen components of basement membranes, laminins present also important cell interactions [11]. In particular, these proteins networks are crucial for cell adhesion, differentiation, proliferation, and many more [10, 12].

Aside from laminins, other proteins deeply associated with specific cellular communications are fibronectins [6]. At first these proteins interface with cells by binding to integrins, then this binding promotes the accumulation of fibronectin on the cell surface, leading to fibronectin-fibronectin interactions [10].

A different class of glycoproteins is represented by proteoglycans. Indeed, these molecules consist of a core of glycoproteins and glycosaminoglycan (GAG) chains [6]. These proteins are mingled within collagen fibrils, and thanks to GAG chains, are able to uptake water and cations. This characteristic gives these molecules the essential ability of space filling and lubrication [9].

Within the ECM, it is likewise possible to identify a cellular component, consisting mainly in mesenchymal and vascular cells. The most essential cell type for ECM remodelling is represent by fibroblasts, mesenchymal cells known as one of the main producer of

collagen fibres. Their ability to secrete ECM proteins is subjective to the presence of cytokines, growth factors, and ECM proteins [8].

Certainly, it is worth to mention that ECM elements undergo constant remodelling and post-transcriptional changes. Notwithstanding, the homeostatic turnover of individual protein differs greatly from one another. In human, the higher turnover is observed for collagens fibres, with a rate of 3 to 10% per day, while the elastic fibres stability is estimated to be of 74 years or more [7, 12].

Extracellular matrix physiological remodelling: a tightly regulated process

The ECM remodelling is an exceedingly multifaceted process where several cell types, enzymes, growth factors and proteins take part. In this perspective, to better represent all the elements that comprise the matrix and play a role in its regulation, the term “matrisome” has been introduce. The “matrisome” is defined as the ensemble of heterogeneous ECM proteins, their associated modifying molecules, and ECM secreted factors regulators [7, 11].

The physiological remodelling of the matrix is a process of degradation and deposition of new ECM components, coordinated by proteases, hydrolases and cross-linking enzymes [8].

Chiefly, some factors in charge of matrix remodelling are matrix metalloproteinases (MMPs) and adamalysins. MMPs are a family of zinc dependent enzymes classified on substrate specificity. More specifically, MMP-1, -8 -13 are collagenases, whose targets are collagen type I, II, fibronectin and fibulin 1; MMP-2 and -9 are gelatinases, responsible of type IV collagen and elastin degradation; MMP-3, -10 and -11 are stromelysins, able to break collagen type II, IV and IX together with proteoglycans, elastin, fibronectin and

laminin [13], and MMP-7 and -12 are elastases, with elastolytic activity, whereas MMP-14, -15, -16, and -17 are separately classified as being anchored to the surface [6, 14].

Instead, the adamalysins family is divided into two categories: ADAMs (a disintegrin and metalloproteinases) and ADAMTS (ADAMs with thrombospondin motif). The former is able to chop transmembrane protein domains, leading to the release of cytokines and growth factors. The latter presents proteinases with proteoglycanolytic activity, and others whose functions are yet to be defined [15].

Since the remodelling of the ECM is a tight controlled process, the cleavage of proteases is controlled by inhibitors of MMPs and adamalysins, also known as tissue inhibitor of metalloproteinases (TIMPs). This family has the vital role of inactivating ECM proteinases, thus avoiding tissue disintegration [6, 15].

Collagen biosynthesis similarly appears to be tightly regulated at the transcriptional level with post-transcriptional modifications. In this perspective, lysyl oxidase enzymes exert a key role [16]. This family of copper-dependent amine oxidases comprises 5 members: LOX (lysyl oxidase) and LOXL1-4 (lysyl oxidase like 1-4). The activation of these enzymes relies on copper concentrations and availability of proteinases responsible for the proteolytically activation of the pro-form enzymes [17]. LOXs are known to create cross-links between collagens and elastin fibres, consequently increasing ECM stiffness. Therefore, it is not surprising that the expression of these enzymes is accurately coordinated [18].

Apart from the general ability of connecting collagens and elastin, these enzymes display additional properties. For instance, LOX affects myofibroblasts dedifferentiation into fibroblasts, inactivating transforming growth factor beta (TGF-β) and fibroblast growth factor 2 (FGF-2) [19]. Furthermore, other pathways emerged to be impaired by altered LOX expression, these include ERK, NF-kB, PI3K/AKT, SMAD, MAPK, and so forth. As a

result, several pulmonary, vascular, cardiac, and kidney disorders were linked to LOX dysregulation [17, 20].

Similarly, the other isoforms present peculiar features: LOXL1 has the elastin as its preferred substrate, while LOXL4 favours collagens. Interestingly, both these enzymes are associated with vascular remodelling. LOXL2 instead interacts majorly with collagen type IV, enhancing its deposition and stability, therefore increasing the solidity of basement membranes [19, 21]. On the other hand, LOXL3 exhibits an enhanced affinity for collagen type XI (alpha 1 and 2) and II (alpha 1), major component of cartilage, which explains LOXL3 involvement in cartilage development [19].

The process of matrix remodelling is finely regulated, therefore whenever there is an insult this delicate mechanism is altered with potentially harmful consequences. Dysregulation of ECM composition causes modifications on lung structure, with failure of mechanical functions, and morphological changes in fibroblasts, which are necessary for tissue repair [8, 22].

Though, one single insult is not sufficient for inducing a significant alteration of pulmonary structure; usually, in case like that, repair pathways are activated without major consequences. On the contrary, when lungs are chronically exposed to different insults, like cigarette smoke, the reparative mechanisms are significantly impaired [8].

As a matter of fact, it is known that within the lungs reparative mechanisms can resolve the fibrosis through ECM degradation and removal of myofibroblasts and inflammatory cells [23]. Currently, which mechanisms lead to an almost complete resolution are not yet clarified; however, it seems to be correlated to the duration or intensity of the fibrotic stimulation [23].

Cellular senescence as a common pathogenic mechanism of COPD and IPF

The most common lung chronic conditions are represented by chronic obstructive pulmonary disease (COPD), and idiopathic pulmonary fibrosis (IPF). Even if, these pathologies present some dissimilarity, they share several common features. First, the incidence of COPD and IPF is higher in male and elderly people. Secondly, both these disorders are characterized by progressive loss of parenchyma, which ultimately leads to respiratory failure. Of note, there is a relative new syndrome known as combined pulmonary fibrosis and emphysema (CPFE), which presents both areas of pulmonary fibrosis and emphysema [24].

There are several pathogenic mechanisms proposed to be responsible for COPD development, yet there is a limited understanding of its pathogenesis. Among them, a chronic inflammation affecting airways, parenchyma and pulmonary vasculature; an increased influx of macrophages, neutrophils and T lymphocytes capable of releasing a huge plethora of mediators; the proteinases/anti-proteinases imbalance and the oxidative stress can be found [25]. As for the COPD, the pathogenesis of IPF remains elusive. It is believed that in response to a damage, epithelial cells evoke inflammatory cells and stimulate fibroblasts proliferation and activation by releasing growth factors and pro-inflammatory cytokines. Thus, there is the instauration of a fibrotic microenvironment that favours the onset of pulmonary fibrosis, which may also represent a failure of fibrogenesis suppression [26, 27].

Besides these differences recently, lung cellular senescence was pointed out as a common pathogenic feature to COPD and IPF [24]. Senescent cells are in a state of cell cycle arrest that might be induced by DNA damage, telomere shortening, genomic instability, epigenetic alterations, mitochondrial dysfunction and loss of proteostasis.

Nevertheless, these cells are metabolically active and secrete cytokines, chemokines, and growth factors also known as senescence-associated secretory phenotype (SASP) [28].

Generally speaking, aged lungs are characterized by lower levels of antioxidants and a reduced innate and adaptive immunity response that make the lung more susceptible to damage by environmental stressors as smoking [29]. Senescent cells are found both in COPD and IPF patients. Probably, the accumulation of senescent epithelial and endothelial cells prompts the small airways fibrosis and the emphysema typical of COPD. On the other hand, the accumulation of senescent fibroblasts and alveolar epithelial cells favours the progression of lung fibrosis in IPF [29].

Pathophysiology of COPD

Overall, COPD is defined as a progressive, not completely reversible, airflow limitation associated with an aberrant inflammatory response to harmful agents [25, 30]. Of the risk factors for developing this pathology, cigarette smoke is the most common; nonetheless, non-smokers are also likely to develop this specific condition, hence other detrimental agents might be involved [30, 31]. Indeed, many evidences pointed to a contribution of genetic predisposition, sex, ethnicity, and, recently, ageing in the development of COPD [32]. Despite the prime role of inflammation in the initiation and progression of this illness, a proteinases and anti-proteinases imbalance and oxidative stress are seen as other major contributors to the pathogenesis of COPD [25, 33].

Due to the complexity of this disease, several pathological manifestations, together with particular structural modifications, can be identified. The principal one, known as emphysema, consists in the enlargement of alveolar spaces, with the disruption of lung parenchyma. In particular, this phenomenon is related to the loss of elastin causing the reduction in lung elastic recoil [34]. This aspect is exceptionally crucial for ECM

remodelling if we consider the turnover rate of elastin. More in-depth, there is a very little synthesis of elastin, which account for the high longevity of mature elastin [12, 35]. One of the primary mechanisms to make up for the lack of elastin, is the deposition of more collagen fibres, however this compromises the elastic recoil of lungs and increases the stiffness of the matrix [20].

Frequently, COPD patients present mucus hypersecretion and mucus accumulation subsequent to ciliary dysfunction, leading to chronic cough and ultimately to chronic bronchitis [25, 36].

Two other anatomic lesions often observed are small airways and vascular remodelling. The former usually referred to as SAR (small airways remodelling) determines airways shrinkage through an accumulation of fibrous tissue, smooth-muscle cells, fibroblasts, and inflammatory cells right at the base of the bronchial epithelial cells [37, 38]. The triggers of airways wall thickening might be due to repeated insults that prompt as many inflammatory responses; alternatively, excessive production of growth factors may be at the origin of this abnormal tissue rearrangement [37]. Although, none of these theories is mutually exclusive.

Instead, the vascular remodelling comprehends numerous pulmonary vascular changes, such as intima hyperplasia, media hypertrophy, elastin and collagen deposition, and muscularization of the arteries [39]. In COPD, the vascular remodelling is distinguished by a narrowing of muscular and bronchiolar arteries due to the thickening of the intima. As a result, there is a general alteration of blood circulation in the lungs, leading ultimately to pulmonary hypertension [40].

It is worth pointing out that these four anatomical lesions are not often observed simultaneously in patients diagnosed with COPD, and the distribution of these injuries differs widely.

Pathophysiology of IPF

Another chronic and progressive lung condition is the idiopathic pulmonary fibrosis (IPF). This illness is classified among the heterogeneous group of interstitial lung disorders (ILD), and is characterised by lung parenchyma damage with a wide degree of inflammation and fibrotic scars formation [41, 42]. As stated in the name, the aetiology of this interstitial lung condition is unknown, yet a histopathological pattern of usual interstitial pneumonia (UIP) may be recognized [43, 44]. IPF has an exceptionally high mortality rate due to an unstoppable destruction of lung architecture, that culminates in respiratory failure within 2-5 years from the diagnosis [45, 46]. Other than that, it is important to point out that this pathology is more often diagnosed in old patients [45]. Within the lungs, it is possible to pinpoint normal and altered areas; the latter are usually associated to honeycombing fibrosis and fibrotic foci, where fibroblasts and inflammatory cells perpetuate the fibrosis [47, 48].

Even if the aetiology of IPF is not clear, some potential risk factors have been identified. As already mentioned, the incidence is significantly higher with age, sign of a strong contribution of ageing in this disorder [49]. Moreover, men are more susceptible of developing this condition, when compared to women [50, 51]. Withal, should not be overlook the evidences suggesting a not minor contribution of genetic predisposition. Indeed, many studies reported that polymorphisms of genes relate to inflammatory and immune response, like transforming growth factor β (TGF-β), interleukin 1 receptor α (IL1RN), interleukin 8 (IL-8), along with genes associated with cell cycle regulation such as cyclin-dependent kinase inhibitor 1A (CDKN1A) and tumour protein P53 (TP53) have been associated with IPF risk or progression [52]. Additionally, epigenetic modifications, mostly induced by cigarette smoke exposure and ageing, are proved to play a central role in IPF [53, 54]. Still, the constant exposure of lungs to noxious environmental particles (i.e.

microbes, fumes, cigarette smoke, and pollutants) might create a never-ending cycle of damage and repair. Lastly, virus infections like herpesvirus, Epstein-Bar-virus, hepatitis C virus and adenovirus are believed to act as initiators or exacerbating agents of IPF [54, 55].

Notwithstanding, the understanding of IPF pathogenesis remains elusive. More in general, fibrosis can be defined as an excessive pathologic deposition of ECM during wound healing [56], however due to its complexity, even the pathobiology is yet to be completely comprehend. As a matter of fact, initially the IPF was describe as an inflammatory disease, still patients were not responsive to anti-inflammatory therapies [54, 57].

Currently, IPF is seen as an epithelium-driven disease, where epithelial injury and dysregulated repairs end up with the activation of multiple signalling, the proliferation of cell types able to secrete ECM components, and the release of cytokines and chemokines. Though, the involvement of inflammation is not in doubt [41, 54, 56, 58].

Role of fibroblasts proliferation and activation in the repair process

Under physiological conditions, following an injury, lung tissue activates a repair process with the aim of restoring the homeostasis. Normally, wound healing is characterised by two phases: first, there is a regenerative phase, where there is a replacement of damaged cells; second, a fibrosis phase can be found, where parenchymal tissue is replaced with connective tissue [54, 57, 59]. A non-regulated reparative process is the key element in the establishment of fibrogenesis.

Usually, epithelial injury activates the inflammatory response, with inflammatory mediators' release, and the coagulation cascade [57]. The loss of alveolar epithelial cell type I (AT1) is physiologically overcome with proliferation and subsequent differentiation of alveolar epithelial cells type II (AT2). Conversely, in IPF the ability of AT2 cells of regenerating

damaged cells is compromised [56]. Thus, repeated insults to the epithelium not only prompt a chronic inflammation, but also trigger a series of linked dysfunctional events like epithelial-mesenchymal transition (EMT), related to a rupture of basement membranes, abnormal secretion of pro-fibrotic chemokines [41], such as TGF-β, PDGF (platelet derived growth factor), VEGF (vascular endothelial growth factor) and FGF (fibroblasts growth factor), fibroblasts activation and differentiation, collagen deposition and new vessels formation [54, 57].

Among the fibrotic chemokines, TGF-β is the most relevant pleiotropic factor. This molecule is not only secreted from epithelial cells, but also macrophages, neutrophils, T cells, platelets, fibroblasts, mast cells and many more [60, 61]. Several researches pointed out the chemotactic and proliferative properties of TGF-β, but it is now evident that a wider range of pathways is actually affected by it.

Nonetheless, the reason why these specific abilities have a major impact in IPF is because they induce the recruitment and facilitate the proliferation of fibroblasts [61]. Fibroblasts are peculiarly affected by TGF-β. Indeed, following TGF-β stimulation, a morphological modification is observed in fibroblasts. In detail, these cells, called myofibroblasts, assume a contractile phenotype, characterised by mesenchymal features, but also an enriched network of actin fibres [60]. Myofibroblasts are a distinctive population of cells founded in great number in fibroblast' foci [62]; they share several similarities with fibroblasts, yet activated myofibroblasts express higher levels of collagens [60]. Multiple theories are trying to shed light on the origin of these cells, but further investigations are still needed. The most accepted one is that resident lung fibroblasts populations differentiate into myofibroblasts. Other potential progenitors seem to be fibrocytes, a population of circulating mesenchymal cells, that co-express mesenchymal markers like collagen type I,

fibronectin and α-SMA (α smooth muscle actin); and leukocyte and hematopoietic antigens (CD45 and CD34 respectively) [61, 63].

Several studies reported as source of myofibroblasts AT1 and AT2 cells, through the epithelial-mesenchymal transition (EMT) [56, 64, 65]. This transition, facilitated by TGF-β exposure, arises from the loss of epithelial markers (i.e. cytokeratins, zonula occludens protein 1 (ZO-1) and acquaporins) and the acquisition of mesenchymal proteins (i.e. vimentin, collagen type I, and α-SMA) [64].

Recent researches suggest that an additional source of myofibroblasts might be deriving from endothelial-mesenchymal transition (EndMT). Under the influence of TGF-β, endothelial cells may decrease the expression of endothelial factors like CD31, as they begin *de-novo* expression of canonical mesenchymal markers [61, 66].

In addition, another mesenchymal cell type, the pericytes, may be involved. These mesenchymal mural cells can be found around vessels, where they regulate angiogenesis and vascular permeability. Many studies reported that even these cells might be myofibroblasts precursors. As a consequence of this shift, loss of pericyte functions results in vascular leak and dysregulated angiogenesis also suggesting a foremost role of these cells in fibrogenesis [67].

Regardless of myofibroblasts' origin, the expansion of these cell populations, as well as fibroblasts' one, represents the spark for fibrosis. In the past few years, these specific cell populations gained more attention, because of their potential involvement in several lung chronic conditions, like IPF and COPD. In addition, this aspect highlights the presence of some overlapping features between different lung chronic disorders that require more in-depth investigations.

In this thesis, the lung fibrotic remodelling was evaluated in different *in vitro* and *in vivo* models. Due to a great number of harmful elements able to start the process of

fibrogenesis, several agents were employed. Nevertheless, the main focus of every work was to identify or better characterized a pathway majorly involved in the fibrotic remodelling.

CHAPTER 1

AIM OF THE STUDY

In this chapter we investigated whether alterations in the expression of histone deacetylases (SIRT1 and HDAC-2) and factors involved in the inflammatory process and progression of pulmonary lesions (p-p38 and NF-kB) contribute to the pathophysiology of airway remodelling. For this specific purpose, we used two distinct animal models characterized by a pre-existing sensitivity to oxidative stress to evaluate if this characteristic affects the airway changes induced by the exposure to cigarette smoke.

MATERIALS AND METHODS

ANIMAL EXPERIMENTS

Male C57 BL/6J and DBA/2 mice (8 weeks old) used in this study were purchased from Charles River (Calco, Italy). The mice were housed in a controlled environment (22°C ± 2°C, humidity 55% ± 15%, light/dark cycle 12:12); food (Mucedola Global Diet 2018; Harlan, Correzzana, Italy) and water were supplied *ad libitum.* All animal experiments were conducted in conformity with the "Guiding Principles for research Involving Animals and Human Being" [68] and were approved by the Ethics Committee of the University of Siena and the Italian Health Ministry.

CHRONIC EXPOSURE TO CIGARETTE SMOKE

C57 BL/6J and DBA/2 mice were exposed to either room air or to the smoke of three cigarettes (CS) per day, 5 days/week for 1, 4, and 7 months (Marlboro Red, 10 mg of tar and 0.8 mg of nicotine), in specifically designed Makrolon cages (Tecniplast, Buguggiate, Italy). The methodology for smoke exposure was previously established in our laboratory [69, 70]. More in detail, mice were placed in Makrolon cages (42.5 x 26.6 x 19 cm) equipped with a disposable filter with 15 holes (10mm of diameter) that allows continuously renewal of the airflow. The smoke of a burning cigarette is introduced into the chamber thanks to a mechanical ventilator (7025 Rodent Ventilator, Biological Research instrument, Comerio, Italy) at a rate of 33ml/min. In addition, the cages are provided with a second ventilator that allows a dilution of the smoke stream (1:8) with room air. By using this methodology, the mice were exposed to the smoke originated by three cigarettes once a day for the duration of 90 min. In a pilot study, the efficiency of the smoke delivery system was tested by measuring blood carboxyhemoglobin (COHb) in 12 mice by CO oximetry.

Control animals were exposed to room air under the same conditions. At the different time points, animals were anesthetized and sacrificed by severing the abdominal aorta.

RNA ISOLATION AND REAL TIME RT-PCR

Six mice for each group were used for RNA isolation. Total RNA was extracted from lungs of mice using Tri Reagent (Ambion; Austin, TX; Cod AM9738) according to the manufacturer's instructions. RNA was re-suspended in RT-PCR Grade Water (Ambion. Cod 03315843001), and the amount and purity of RNA were quantified by measuring the optical density at 260 and 280 nm with a spectrophotometer. Integrity was checked by agarose gel electrophoresis. 2µg of total RNA were treated with TURBO DNase (TURBO DNA-free kit; Ambion; Cod AM1907) for 30 minutes and reverse transcribed using the RETRO script kit (Roche; Cod 04896866001) according to the manufacturer's instructions. 200 µL of the final volume of RT were used for real-time RT-PCR.

Real-time RT-PCR was performed in triplicate for each sample on the MJ Opticon Monitor 2 (MJ Research Co.; Waltham, MA) with specific locked nucleic acid probes from the Mouse Universal Probe Library Set (Roche; Indianapolis, IN; Cod 04683641001). Primers were designed using the free online Probe-Finder software version 2.53 (Roche Molecular Systems Inc.; Branchburg, NJ), which shows a pair of specific primers for each probe from the Universal Probe Library set (Roche) (Table 1). The primers were designed to span an exon–exon junction, with one of the amplification primers potentially spanning the actual exon–intron boundary. The combination of primers and probes provides the specific amplification and detection of the target sequence in the sample. Polymerase chain reaction reactions were performed in a volume of 25 µL and contained 12.5 µL of FastStart TaqMan Probe Master (Roche; Cod 04673417001), 300 nmol/L forward and reverse primers (TIB Molbiol; Genova, Italy), 200 nmol/L Universal Probe Library Set probes, and 5

µL of cDNA. Reactions were incubated at 95°C for 10 minutes and then amplified for 40 cycles, each cycle comprising an incubation step at 94°C for 15 seconds followed by 60°C for 1 minute. A minus reverse transcription control (-RT control) was included in all RT-qPCR experiments to test for contaminating DNA. The real-time RT-PCR assay included a no-template control and a standard curve of four serial dilution points (in 10-fold steps) for each of the test cDNAs, and this was performed according to the method reported in detail in previous studies [71 - 73]. The analysis of the results was based on the Ct comparative method (ΔΔ Ct), in which Ct represents the cycle number at which the fluorescent signal, associated with an exponential increase in polymerase chain reaction (PCR) products, crosses a given threshold. The specific gene's cycle threshold (Ct) values were normalized to the housekeeping gene 18S rRNA and compared with the control group, which was assigned a value of 1 to calculate the relative fold change in expression, as previously described [74]. Ctgf and Rps18 gene expression was assessed by SYBR-Green-based real-time PCR using SsoAdvanced Universal SYBR-Green Supermix (Bio-Rad) protocol and amplification thermocycler machine (PCR Detection System CFX Opus 96, Bio-Rad). Rps18 expression was used as the endogenous control to normalize the sample data. The gene-specific primers for Ctgf and Rps18 were purchased from the Bio-Rad company, which supplied the PrimePCR Assay Validation Report for them (Table 2). The specificity of the primers was determined by melting curve analysis and agarose gel electrophoresis. Polymerase chain reaction reactions for Ctgf and Rps18 genes were performed in a volume of 20 µL and contained 10 µL of SsoAdvanced Universal SYBRGreen Supermix (Bio-Rad), 1 µL of forward and reverse primers (PrimePCR SYBR Green Rps18, mouse and/or PrimePCR SYBR Green Ctgf mouse; Bio-Rad, Italy), 2,5 µL of cDNA, and 6.5 µL of PCRgrade H2O.

Table 1: Primers Sequence and Probe Catalog Number

Gene	Primer Sequence	Probe	Amplicon Length (nt)
rRNA 18S MGI:97943 NR 003278.2	FW: 5'-AATCAGTTATGGTTCCTTTGGTC-3' Rev: 5'-GCTCTAGAATTACCACAGTTATCCAA-3'	#55	67nt
PDGFb MGI:97528 NM011057.3	FW: 5'-CGGCCTGTGACTAGAAGTCC-3' Rev: 5'-GAGCTTGAGGCGTCTTGG-3'	#32	61nt
TGFb MGI:98725 NM011577.1	FW: 5'-TGGAGCAACATGTGGAACTC-3' Rev: 5'-GTCAGCAGCCGGTTACCA-3'	#72	73nt

Table 2: Amplicon sequences for Ctgf and Rps18 expression

Gene	Amplicon Length (nt)
Rps 18 MGI: 98146 NM.324762	TCATAGGTATATAAACTATTTATTAACAGCAAAGGCCCAGAGACTCATT TCTTCTTGGATACACCCACAGTTCGGCCCCTGCGGCCAGTG **(60nt**)
Ctgf MGI: 95537 NM.390287	TCGATAGCCTCAAACTCCAAACACCATAGGTAGGACACGAAGCTTATC TGTGATTCAAAACAAAGGAGATACTGCAGTGGGAATTGTGACCTGAGT GACTCTCT **(74nt**)

MASSON*'S TRICHROME STAINING*

Mice lungs were fixed intra-tracheally with buffered formalin (5%) at a constant pressure of 20 cm H_2O. Then, lungs were processed and embedded in paraffin for histologic examination. The entity of collagen deposition around the airways was evaluated on lung slices after Masson's trichrome staining [71]. In details, sagittal sections (7 μm) of lungs were cut and deparaffinised by passing through a series of xylene and graded alcohol. Next, slides were soaked for 3 minutes in tap water. Haematoxylin stain was applied for 10 minutes, after the lung sections were thoroughly washed for 10 minutes. Subsequent a

solution of 6% Picric acid was applied for 2 minutes, this was followed by a Ponceau-Fuchsin solution, where slides were immerged for 15 minutes. After a brief rinse in tap water, sections were soaked in a 1% phosphomolybdic acid solution for other 15 minutes. After that, each slide was drenched in “sea green colour” solution for 5 minutes and then in a 1% acetic acid solution for 30 seconds. Finally, sections were quickly dehydrated, cleared in xylene and mounted.

Areas of peribronchial trichrome staining were outlined and quantified using a light microscopy (BX 40 Olympus) equipped with the software NIS-Elements 5.01.00 (Nikon). Results are expressed as the area of staining per μm length of basement membrane of bronchioles with 150/200 μm internal diameter. At least eight bronchioles for each mouse were counted for statistics. Six animals for each group were used.

IMMUNOHISTOCHEMICAL ANALYSIS

Mice lungs were fixed intra-tracheally with buffered formalin (5%) at a constant pressure of 20 cm H_2O. Then, lungs were processed for histological and immunohistochemical examination.

Tissue sections (4 μm) were stained for Sirtuin 1 (SIRT1), phosphorylated mitogen-activated protein kinase (p-p38), histone deacetylase 2 (HDAC-2), and nuclear factor kappa B (NF-kB). SIRT1 and p-p38 were revealed using the streptavidin-alkaline phosphatase method, while HDAC-2 and NF-kB were revealed with the immuno-peroxidase method.

The primary antibodies used were: mouse monoclonal Ab to SIRT1 (1:1000; Invitrogen Life Technologies, Irvine, CA, USA), rabbit polyclonal Ab to p-p38 (1:50; Santa Cruz Biotechnology, Inc., Dallas, TX, USA), rabbit polyclonal Ab to HDAC2 (1:20; Invitrogen,

Carlsbad, CA, USA), and rabbit monoclonal Ab to NF-kB p65 (1:400; Biolegend, San Diego, CA, USA).

First, lung sections (4 μm) were deparaffinised by xylene, rehydrated with decreasing concentration of ethanol (100% and 95%), and quickly washed with water. Next, antigen retrieval was performed by heating the section in a microwave (750W) in 0.01M pH 6.0 citrate buffer. All sections were cooled at room temperature; then, SIRT1 and p-p38 slides where incubated with 1% acetic acid for 10 minutes to inhibit the endogenous alkaline phosphatases, while HDAC-2 and NF-kB p65 slides were incubated with 3% H_2O_2 for 10 minutes to inhibit the endogenous peroxidases. Next, all the sections were rinsed in tris buffer saline (TBS) and then blocked for 1 hour at room temperature with 3% bovine serum albumin (BSA). In addition, in order to detect SIRT1 on mouse tissues, we used the Vector M.O.M. Immunodetection Kit (Vector Laboratories, Burlinghame, CA, USA) containing a novel blocking agent designed specifically to reduce the undesired background staining. All the antibodies were then incubated overnight at 4°C.

The following day, after rinsing in TBS the appropriate secondary antibodies were applied.

SIRT1 slides were incubated with the secondary antibody (anti-mouse IgG biotin-conjugated) of the Vector M.O.M. Immunodetection Kit (Vector Laboratories, Burlinghame, CA, USA).

p-p38 and NF-kB p65 sections were incubated with a polyclonal goat anti-rabbit IgG biotin-conjugated (1:200; Vector Laboratories, Burlingame, CA, USA), at room temperature, for 30 minutes.

HDAC-2 sections were incubated with a polyclonal goat anti-rabbit IgG HRP-conjugated (1:200; Invitrogen, Carlsbad, CA, USA) for 40 minutes at room temperature.

SIRT1 and p-p38 antibodies were incubated with streptavidin–alkaline phosphatase (BD Pharmingen, Buccinasco, Italy) for 30 minutes. After a quick rinse in TBS, colour

development was performed using NBT/BCIP stock solution (Roche Diagnostics, Milan, Italy) as a chromogen, diluted in 0.1 M TBS, pH 9.5, 0.05 M MgCl2, 0.1 M NaCl, and 2 mM levamisole.

NF-kB slides were incubated with streptavidin-HRP conjugated (BD Pharmingen, Buccinasco, Italy) for 30 minutes at room temperature and then rinsed in TBS. In conclusion, HDAC-2 and NF-kB p65 were revealed with 3,3'-diaminobenzidine tetrahydrochloride (DAB) substrate.

As negative controls for each immunostaining, the primary Ab was replaced by non-immunized serum.

IMMUNOFLUORESCENCE STAINING

The expression of few antigens evaluated with the immunohistochemistry method, was also assessed through immunofluorescence.

Initially lungs sections were rinsed in phosphate buffered saline (PBS) and then incubated with 3% BSA for 30 minutes at room temperature. Next, to avoid not specific background fluorescence, slides were incubated with M.O.M. blocking agent (Vector Laboratories, Burlinghame, CA, USA). Then, lung sections were incubated with primary antibodies: goat polyclonal Ab to α-SMA (1:100; Sigma, St Louis, MO, USA) and mouse monoclonal Ab to $p16^{ink4A}$ (1:200; Abcam, Cambridge, UK).

Lastly, all sections were rinsed with phosphate buffered saline (PBS) and probed with: Alexa Fluor-488-labelled donkey anti-goat antibody (1:200; Molecular Probes, Eugene, OR) and Alexa Fluor-546-labelled donkey anti-mouse antibody (dilution 1:200; Molecular Probes, Eugene, OR) for 45 minutes in the dark and at room temperature.

As negative controls for each immunostaining, the primary Ab was replaced by non-immunized serum.

Double-immunofluorescence analysis was visually examined under immunofluorescence microscopy using a Zeiss LSM510 META confocal microscope (Carl Zeiss, Oberkochen, Germany). Images were processed with Zeiss LSM510 software version 4.2 SP1.

STATISTICAL ANALYSIS

Data are presented as mean ± SD. The significance of the differences was calculated using one-way analysis of variance followed by Bonferroni's post hoc test. $P<0.05$ was considered significant. All data were plotted and analysed using GraphPad Prism software version 5.0 (GraphPad, San Diego, CA, USA).

RESULTS

The results reported in this section complete previous analyses described and discussed in the doctoral thesis "Immunohistochemical studies of pulmonary remodeling in mice exposed to chronic cigarette smoke" of Dr. Emilia Balzano and comprehend some results already published in the paper "Immunohistochemical study of airways fibrous remodeling in smoking mice" [73].

LUNG CHANGES AND FIBROUS AIRWAY REMODELLING IN DBA/2 AND C57 BL/6J MICE FOLLOWING EXPOSURE TO CIGARETTE SMOKE

Morphological evaluation of damaged induce by CS exposure was evaluated through histological staining. Air-exposed controls from both strains showed a normal appearance at every time points examined (Figure 1). Following the chronical exposure to CS, the two strains developed enlargement of air spaces (Figure 1, asterisks). Withal, DBA/2 and C57 BL/6J mice were affected to a different extent by fibrotic airway remodelling from 4 months of exposure onward.

Masson's trichrome staining depicted the morphological changes in lung from both strains (Table 3; Figure 1). A progressive collagen accumulation was observed around peripheral airways in the lungs of DBA/2 and C57 BL/6J mice. At 7 months of CS exposure, a significant increase around peribronchial areas from both strains (Figure 1) was observed as compared with the respective non-smoking control DBA/2 (2.12 ± 0.10 vs 0.49 ± 0.02 $\mu m^2/\mu m$), and C57 BL/6J mice (1.90 ± 0.13 vs 0.43 ± 0.05 $\mu m^2/\mu m$) (Table 3).

In DBA/2 mice, collagen accumulation was seen earlier compared to the other mice strain, and was already evident after 4 months of smoking exposure (Figure 1C), when the values

of the trichrome stained areas (sea green stain) for air control and smoking DBA/2 mice were 0.46 ± 0.02 $\mu m^2/\mu m$ and 0.85 ± 0.03 $\mu m^2/\mu m$, respectively (Table 3).

At 4 months of CS exposure, the values of stained areas of smoking C57 BL/6J mice were not significantly different when compared to air control mice (0.50 ± 0.13 vs 0.42 ± 0.07 $\mu m^2/\mu m$, respectively) (Table 3; Figure 1D). Interestingly, at 7 months following the exposure to CS, both strains displayed a similar degree of remodelling around peribronchial areas (Table 3; Figure 1E-F).

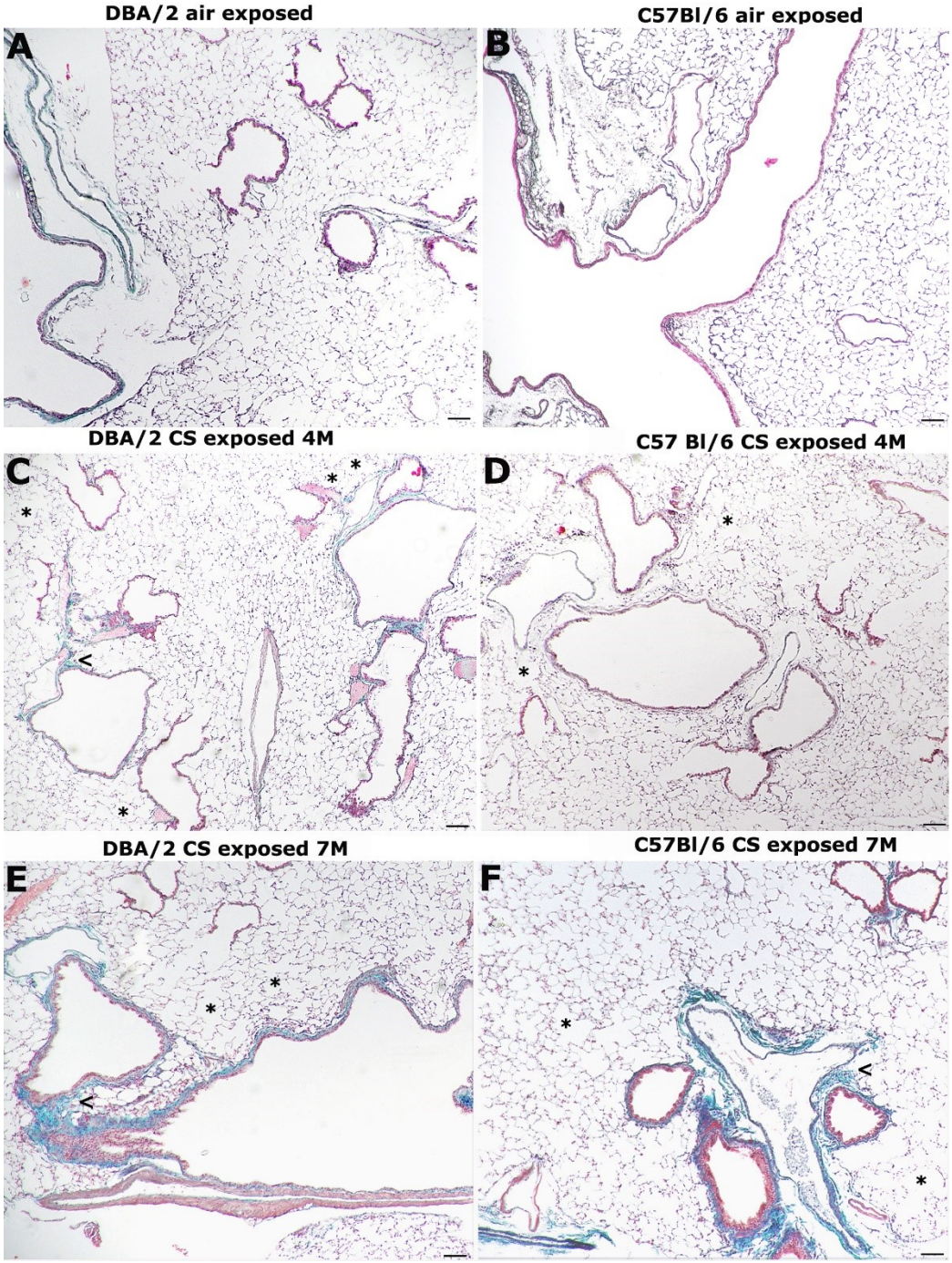

Figure 1: *Masson's trichrome staining was performed on lung sections from DBA/2 and C57 BL/6J mice exposed to air or cigarette smoke (CS). (A-B) Lung from control DBA/2 and C57 BL/6J mice showing a normal architecture. (C) Areas of fibrotic remodelling are seen around bronchioles (arrowhead). Emphysematous changes (*). (D) Minor emphysematous changes (*) but no areas of airway fibrotic remodelling are seen. (E) Airway fibrotic remodelling changes (arrowhead) are more severe (sea green areas) around bronchioles. (F) Patchy areas of lung emphysema (*) and areas of fibrotic remodelling around bronchioles (arrowhead). (A-F) 10x, scale bars = 100 µm (n=6/group).*

Table 3: Peribronchial trichrome stained area (peribronchial fibrosis, PF) after CS (cigarette smoke) exposure.

Strain	Exposure	PF ($\mu m^2/\mu m$)
DBA/2	Air (1 month)	0.40 ± 0.02
DBA/2	CS (1month)	0.39 ± 0.02
C57 BL/6J	Air (1 month)	0.39 ± 0.02
C57 BL/6J	CS (1 month)	0.40 ± 0.03
DBA/2	Air (4 months)	0.46 ± 0.02
DBA/2	CS (4 months)	0.85 ± 0.03*
C57 BL/6J	Air (4 months)	0.42 ± 0.07
C57 BL/6J	CS (4 months)	0.50 ± 0.13
DBA/2	Air (7 months)	0.49 ± 0.02
DBA/2	CS (7 months)	2.12 ± 0.10*
C57 BL/6J	Air (7 months)	0.43 ± 0.05
C57 BL/6J	CS (7 months)	1.90 ± 0.13*

*Trichrome stained areas are expressed as the area of staining per μm length of basement membrane of bronchioles with 150-200 μm internal diameter. At least 10 bronchioles per mouse were counted (n=6/group). Data are presented as mean ± SD. *P<0.05 vs control mice of the same strain.*

AIRWAYS REMODELLING IS CHARACTERIZED BY AN INCREASED EXPRESSION OF α-SMA AND p16^{ink4A}

In a previous study [73], we performed the immunohistochemical staining of α-SMA and p16^{ink4A}. Briefly, at 7 months of cigarette smoke exposure, the expression of α-SMA increased beneath the intraparenchymal bronchi and bronchioles in both strains, when compared with respective control groups. Withal, DBA/2 mice showed significant difference between smoking and air-control mice already after 4 months of exposure. A quantification of α-SMA positive staining areas is reported in Table 4.

Table 4: Peribronchial α-smooth muscle actin (α-SMA) stained area after CS exposure.

Strain	Exposure	α-SMA (μm^2/μm)
DBA/2	Air (1 month)	0.32 ± 0.02
DBA/2	CS (1month)	0.31 ± 0.02
C57 BL/6J	Air (1 month)	0.35 ± 0.02
C57 BL/6J	CS (1 month)	0.35 ± 0.03
DBA/2	Air (4 months)	0.34 ± 0.02
DBA/2	CS (4 months)	0.71 ± 0.06*
C57 BL/6J	Air (4 months)	0.34 ± 0.03
C57 BL/6J	CS (4 months)	0.38 ± 0.04
DBA/2	Air (7 months)	0.35 ± 0.03
DBA/2	CS (7 months)	0.98 ± 0.10*
C57 BL/6J	Air (7 months)	0.35 ± 0.03
C57 BL/6J	CS (7 months)	0.79 ± 0.04*

*α-SMA stained areas are expressed as the area of staining per μm length of basement membrane of bronchioles with 150-200 μm internal diameter. At least 10 bronchioles per mouse were counted (n=6/group). Data are presented as mean ± SD. *P<0.05 vs control mice of the same strain.*

Thickening of the peribronchial smooth muscle layer induced in DBA/2 and C57BL/6J mice after chronic exposure to cigarette smoke (Table 4) was accompanied by increased expression of the senescence marker $p16^{ink4A}$ especially under the intraparenchymal bronchi and bronchioles in both strains of mice.

At 7 months of smoke exposure, DBA/2 and C57 BL/6J mice displayed a remarkable increment of $p16^{ink4A}$ expression when compared to air-exposed mice [73].

In this study, the analysis of the co-expression α-SMA and $p16^{ink4A}$ was performed with specific fluorescent probes on confocal microscopy.

Air control DBA/2 (Figure 2) and C57 BL/6J (Figure 3) mice presented very few positive cells for α-SMA and $p16^{ink4A}$. Instead, the co-localization and an increased expression of these markers was evident after 7 months of smoking (Figures 2-3). A marked positivity was seen beneath the intraparenchymal bronchi and bronchioles in both DBA/2 (Figure 2) and C57 BL/6J mice (Figures 3). These results corroborated what we previously observed with the immunohistochemical analysis [73].

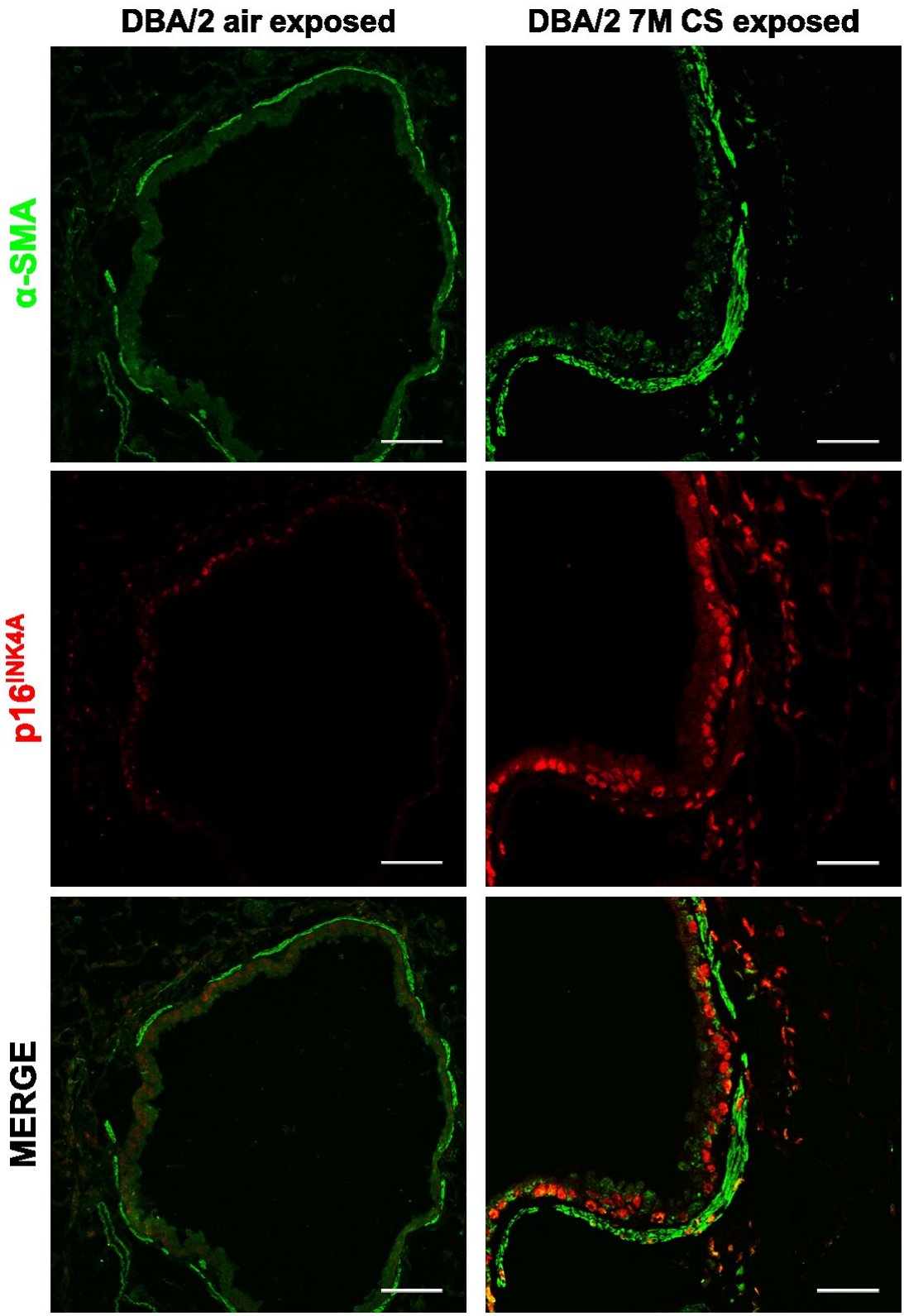

Figure 2: *Double immunofluorescence for α-SMA (green) and p16^{ink4A} (red) in DBA/2 mouse lungs from the different experimental groups. α-SMA positive cells are increased following the exposure to CS. A faint positivity for p16^{ink4A} is present on lung slides of air control mice, while a significant increment in the expression of this marker is seen at 7 months of CS exposure. 20x, scale bar = 50 µm, (n=6/group).*

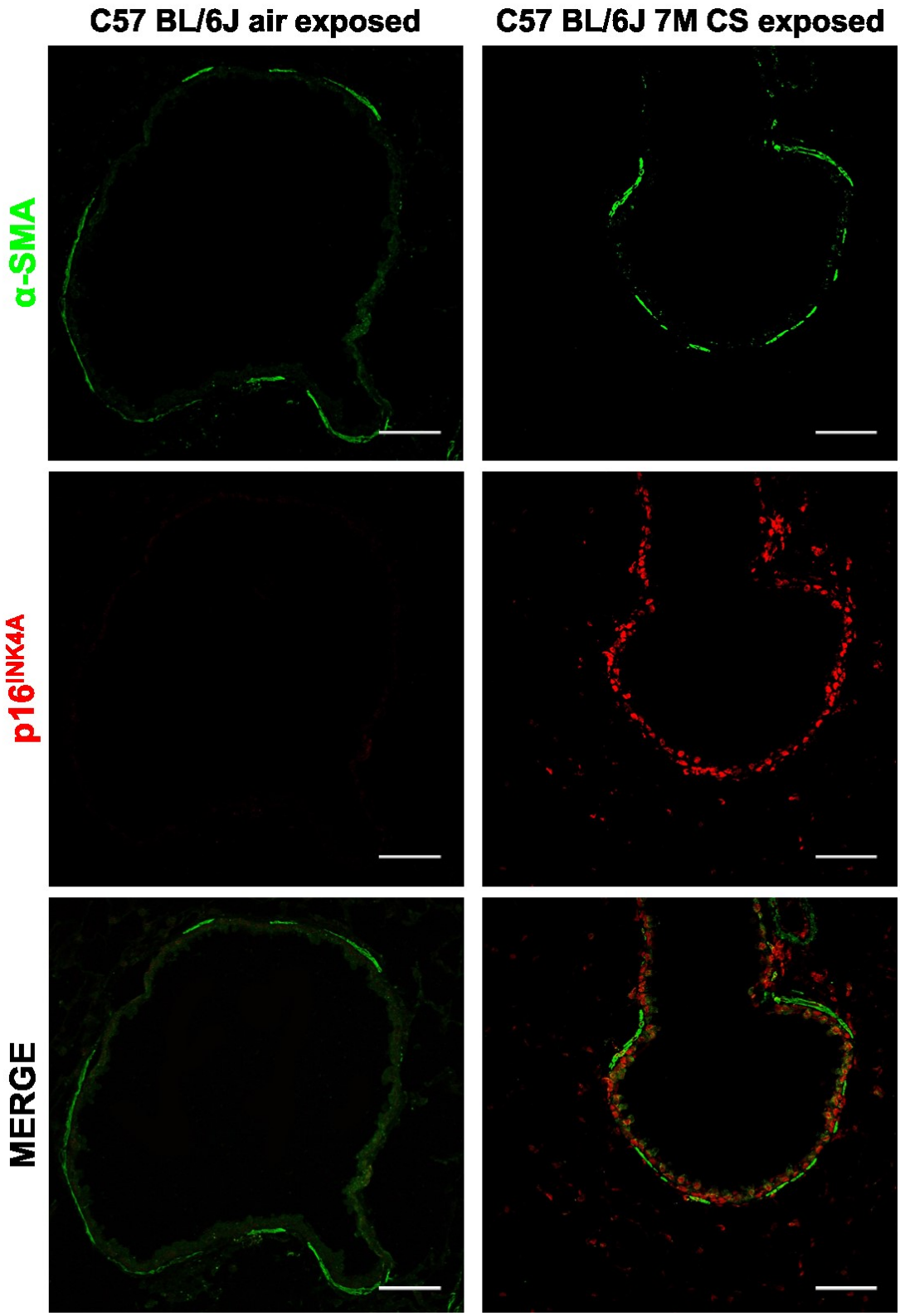

Figure 3: *Double immunofluorescence for α-SMA (green) and p16^{ink4A} (red) in C57 BL/6J mouse lungs from the different experimental groups. α-SMA positive cells are increased following the exposure to CS. No signals for p16^{ink4A} are present on lung slides of air control mice, while a significant increment in the expression of this marker is seen at 7 months of CS exposure. 20x, scale bar = 50 µm, (n=6/group).*

In the previous work of Balzano et al. [73], it was also demonstrated that the airways remodelling was accompanied by the expression of the transcription factor MyoD. Of note, DBA/2 mice exhibited MyoD-positive cells already at 4 months of smoke exposure, while C57 BL/6J mice did not presented MyoD-positive cells until 7 months of CS. The expression of $p16^{ink4A}$ and MyoD is essential for terminal differentiation of fibroblasts, but also plays a crucial role in cellular senescence, by promoting cell cycle arrest in G1 phase.

OXIDATIVE DAMAGE OF PERIBRONCHIAL AREAS IS ASSOCIATED WITH THE UPREGULATION OF FIBROTIC CYTOKINES

As illustrated in our work [73], the amplified expression of α-SMA majorly observed in DBA/2 mice after 4 months of smoking was accompanied with significant oxidative DNA damage. The latter was characterized by a marked positivity for 8-hydroxy-2'-deoxyguanosine (8-OHdG), associated with increased levels of senescence-associated secretory phenotype (SASP) factors (TGF-β, PDGF-B, and CTGF), known also as fibrotic cytokines involved in myofibroblasts differentiation. As already mentioned, an increased number of α-SMA-positive cells was observed at the peribronchial level. Of interest, in the same area, a great number of cells were also positive for 8-OHdG, TGF-β, PDGF-B, and CTGF markers, thus confirming a chief role of oxidative DNA damage and pro-fibrotic cytokines in the airways remodelling.

Real-time PCR analysis of mRNA for TGF-β, PDGF-B and CTGF carried out on lungs from six mice for each experimental group confirmed a marked and significant increase of these cytokines between air and smoking groups within the same strain (Figure 4). At 4 months after smoke exposure, the increase in the expression of these cytokines with respect to control mice appears more evident in DBA/2 mice (Figure 4A), while a mild but significant increase is observed in C57 BL/6J mice (Figure 4B). At 7 months, the expression levels of

TGF-β, PDGF-B, and CTGF do not appear substantially different between the two strains of mice.

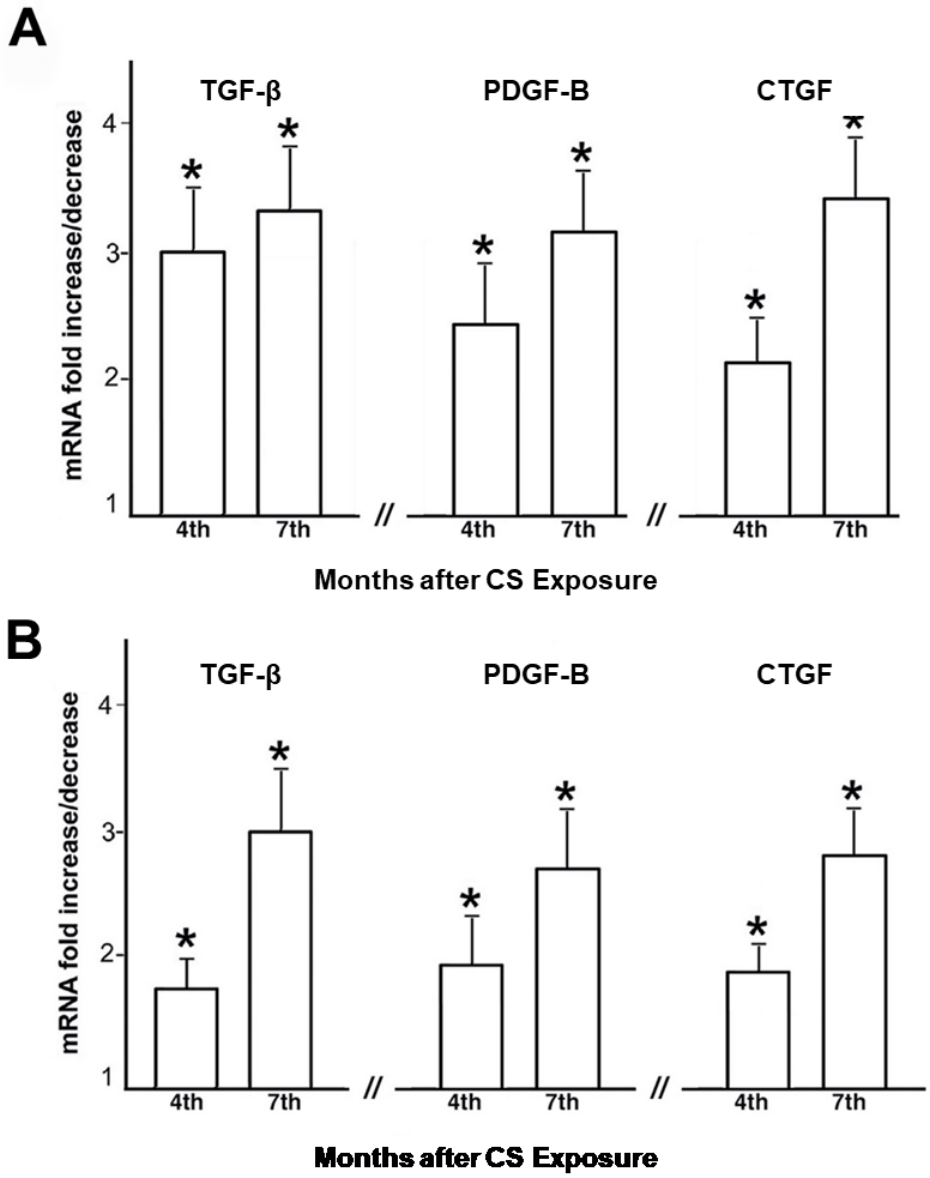

Figure 4: *Real-time PCR analysis of mRNA for TGF-β, PDGF-B and CTGF carried out in lungs from six DBA/2 mice (A) and C57 BL/6J (B) at 4 and 7 months after CS exposure reveals a marked and significant increase of these cytokines. Values of transcripts for TGF-β, PDGF-B and CTGF are corrected for 18S rRNA and normalized to a median control value of 1.0. Error bars indicate mean ± SD. *P<0.05 versus controls. (n=6/group).*

EARLY CHANGES OF EPIGENETIC FACTORS EXPRESSION AFTER CIGARETTE SMOKE EXPOSURE

Of interest, the oxidative DNA damage can favour the onset of cellular senescence, characterized by a marked increment of senescence-associated factors (i.e. SASPs) involved in transcription processes (epigenetics alterations), metabolism (i.e. fibrotic cytokines) and apoptosis.

Recently, it has been described that NAD-dependent deacetylase sirtuin 1 (SIRT1) avoids lung cellular responses and airway remodelling in mice and COPD patients by regulating the gene expression of pro-inflammatory cytokines through the deacetylation of NF-kB subunits, which in turn reduce premature cellular senescence [75]. As already demonstrated in a previous work [72], chronic exposure to cigarette smoke in C57 BL/6J mice reduces the expression of two important deacetylases, SIRT1 and HDAC-2. In this study, we proceeded to investigate the chronic effect of cigarette smoke on SIRT1 and HDAC-2 expression in DBA/2 mice, sensitive to oxidative stress.

In this work, a positive staining for SIRT1 was observed in the lungs of air-exposed animals from both strains, especially in airways epithelial cells (Figure 5A-B). SIRT1 expression in airways epithelial cells was attenuated with the exposure to CS; in DBA/2 mice, a significant drop in SIRT1 positivity was appreciable since 1 month from the beginning of the experiment (Figure 5C). In contrast, in C57 BL/6J mice a weak SIRT1 positivity was maintained after 1 month of cigarette smoke exposure (Figure 5D). Eventually, a complete disappearance of this marker was beheld at 4 months from the beginning of the experiment in DBA/2 and C57 BL/6J mice (Figure 5E-F).

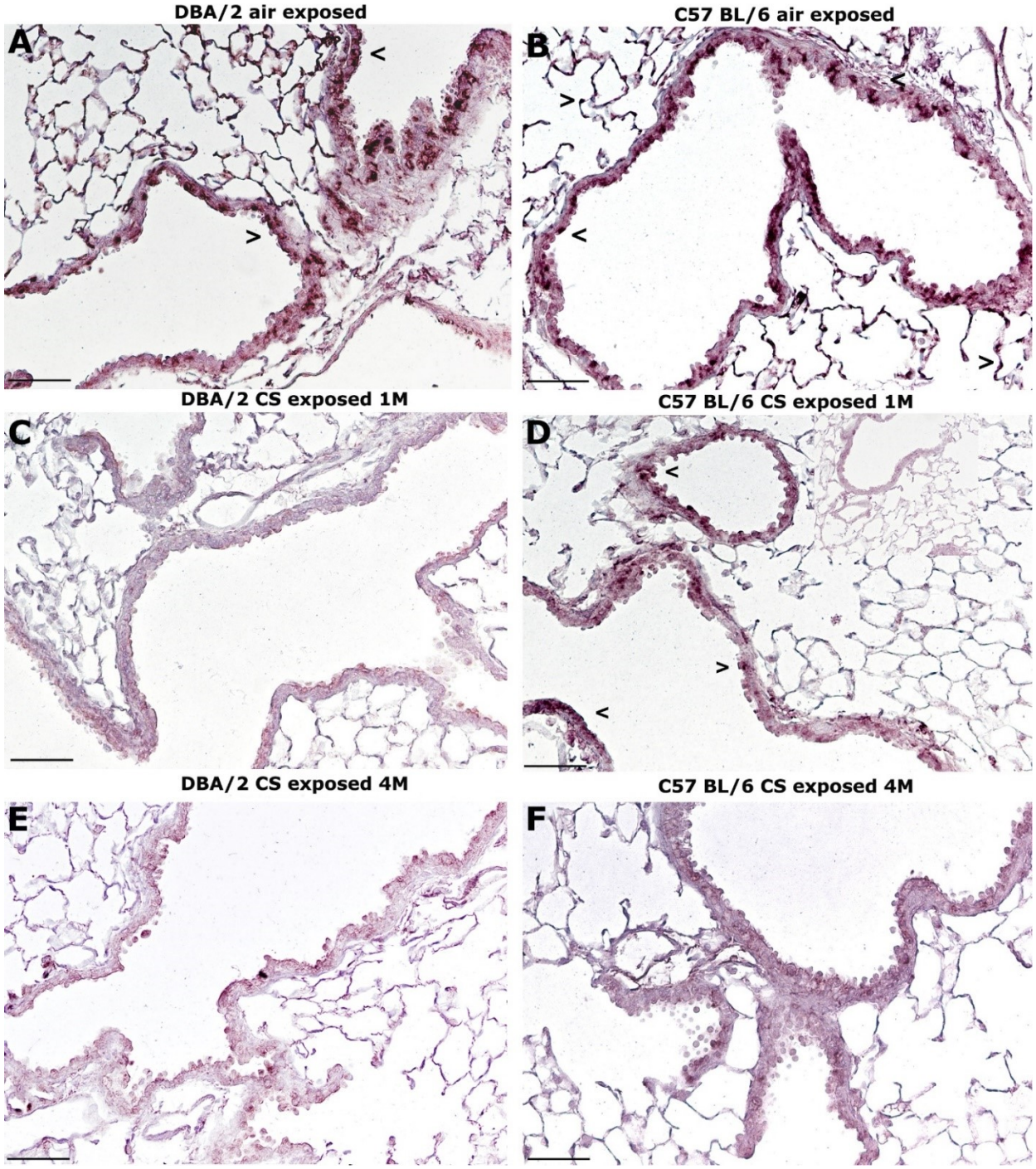

Figure 5: *Immunohistochemical reaction for NAD-dependent deacetylase 1, SIRT1. Positive staining for SIRT1 in the lungs of air-exposed DBA/2 (A) and C57 BL/6J (B) mice is seen in alveolar and airway epithelial cells (>). At 1 month of CS exposure, decreased expression of SIRT1 is observed in DBA/2 mice (C), while a faint positivity is still seen in C57 BL/6J mice (D). At 4 months of CS exposure, very little or no reaction is observed in DBA/2 (E) and C57 BL/6J (F) mice. (A–F) 10x, scale bar = 100 µm, (n=6/group).*

The number of SIRT1 positive cells in small airways of both mouse strains at various times is plotted in a graph (Figure 6). In DBA/2 mice, a significant reduction in the number of SIRT1-positive cells was observed after 1 month of CS exposure. While, at the same time point, C57 BL/6J mice presented a similar value of air-exposed mice. After 4 months of smoking, SIRT1 expression was drastically reduced in both strains. A longer exposure to CS (7 months) further reduced the number of SIRT1-positive cells in both strains (Figure 6).

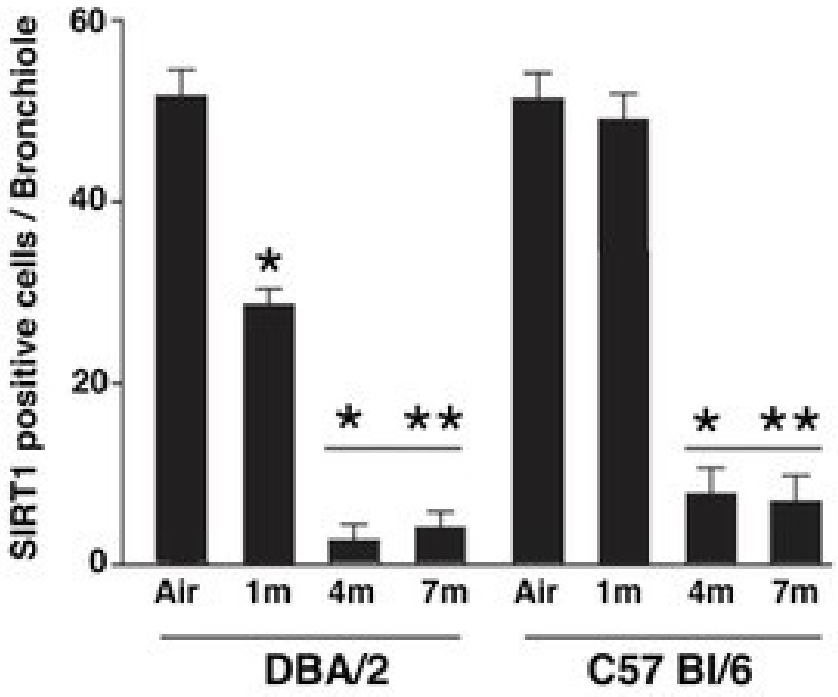

Figure 6: *The bar graph reports the SIRT1 positive cells in small airways at different time points. The number of individual SIRT1 positive cells in small airways structures was counted using a light microscopy and expressed as the number of cells per bronchiole with 150–200 μm internal diameter. A minimum of ten bronchioles was counted per each animal, (n=6/group). Error bars indicate mean ± SD. *P<0.05 versus air controls; **P<0.05 versus smoking mice at 1 month of exposure.*

The expression of histone deacetylase-2 (HDAC-2), resulted downregulated in both mice strains after the exposure to cigarette smoke in comparison to the respective control groups (Figure 7). In addition, DBA/2 mice showed an evident reduction in HDAC-2 expression after 1 month of CS exposure (Figure 7C), when compared to C57 BL/6J mice at the same time point of exposure (Figure 7D). Longer exposure to cigarette smoke keeps HDAC-2 expression level low; in particular, no positive cells can be seen in lung parenchyma and at the peribronchial level from 4 months of CS exposure onwards in both strains (Figure 7E-F).

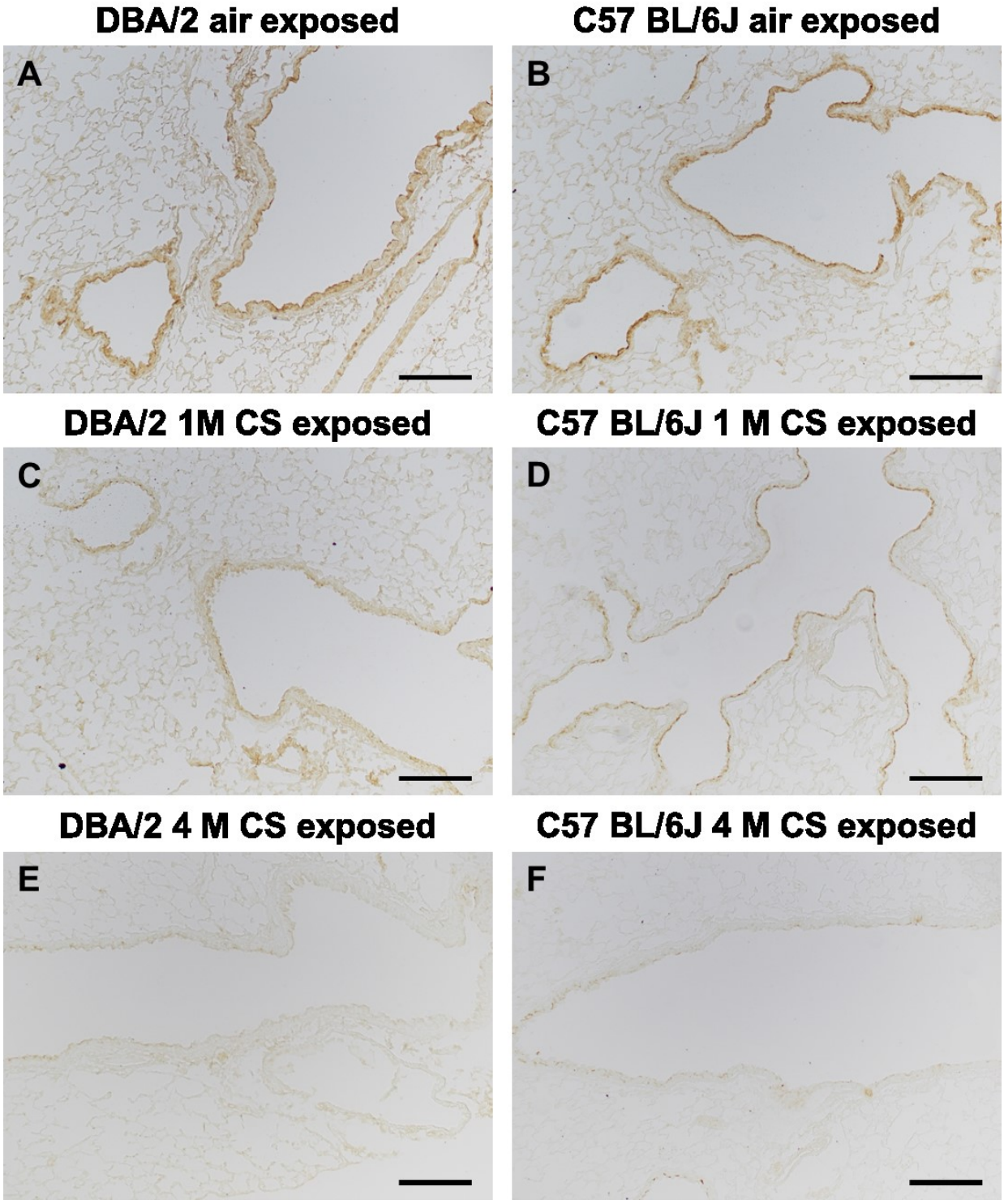

Figure 7: *Immunohistochemical reaction for histone deacetylase 2 HDAC-2. Control mice from DBA/2 (A) and C57 BL/6J (B) presented a low positivity to this marker both in alveolar and airway epithelial cells. At 1 month of CS exposure, DBA/2 mice (C) displayed an apparent decline in HDAC-2 expression, while only minor alterations can be appreciated in C57 BL/6J strain (D). After 4 months of CS exposure, a more evident reduction in the expression of this deacetylase was observed in lung parenchyma of both DBA/2 (E), and C57 BL/6J mice (F). (A-F) 10x, scale bar = 100 µm, (n=6/group).*

In recent times, promising data showed that the nuclear factor kappa B (NF-kB) signalling system plays a crucial role in the induction of SASP [76]. NF-kB is a pleiotropic transcription factor involved in many biological processes as inflammation, immunity, differentiation, cell growth, tumorigenesis and apoptosis. Several pathways can activate NF-kB signalling; for instance, p38 mitogen-activated protein kinase (p38 MAPK) is known to stimulate NF-kB. Of interest, p38 MAPK can also induce cellular senescence when triggered by DNA damage. These evidences propose a main role of NF-kB and p38 MAPK in cellular senescence induction [76].

Therefore, we evaluated the expression of NF-kB and p-p38 MAPK in our *in vivo* model.

As reported in Figure 8, DBA/2 mice displayed a significant increase of NF-kB after 1 month of smoke exposure (Figure 8C), while in C57 BL/6J mice we observed a milder upregulation of this factor at the same time point (Figure 8D). After 4 months of cigarette smoke exposure, a greater number of NF-kB positive cells were found in the airways, lung parenchyma, lung vessels and peribronchial smooth muscle layer in both strains (Figure 8E-F).

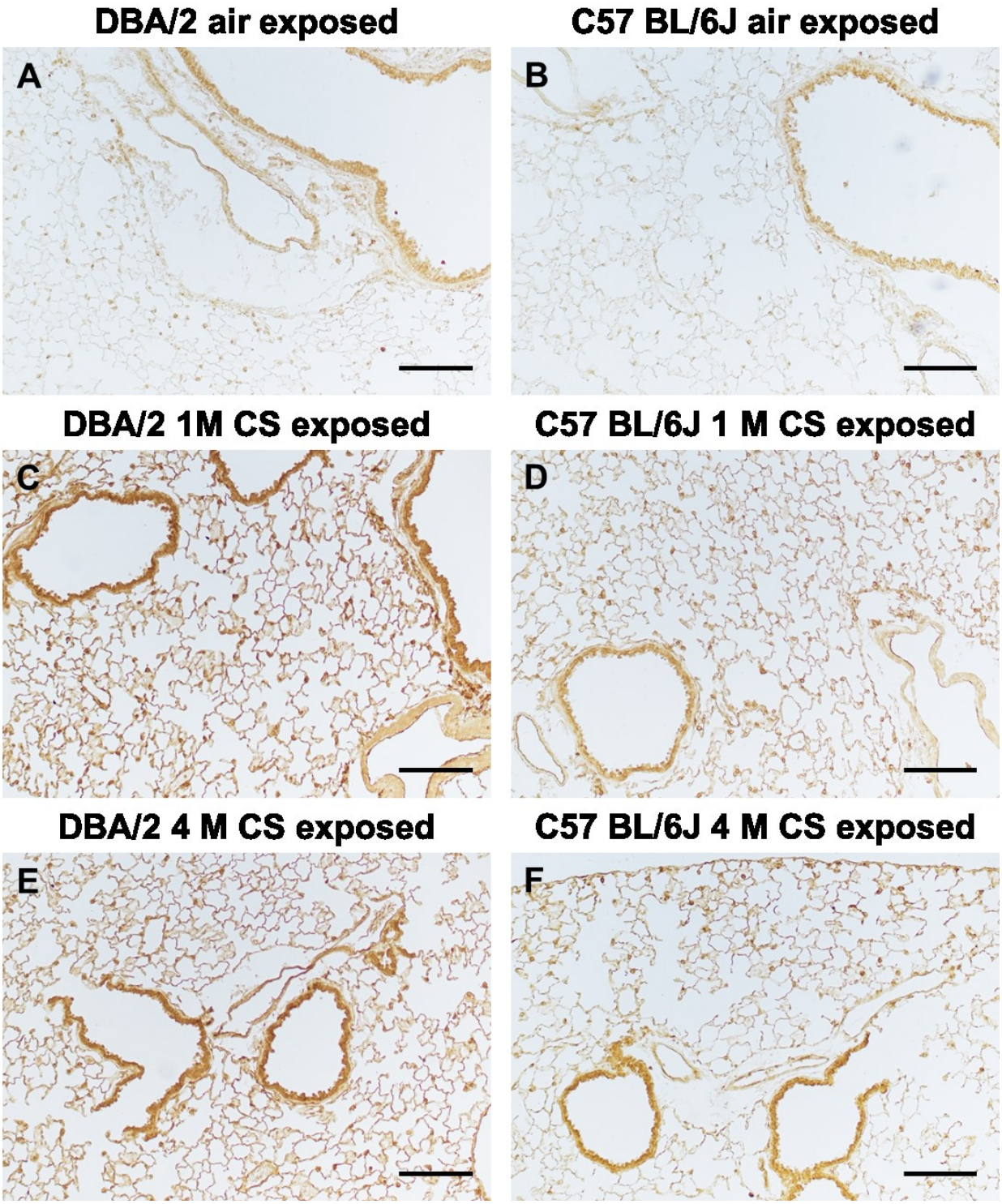

Figure 8: *Immunohistochemical reaction for phosphorylate nuclear factor kappa B. A light positive staining for NF-kB is seen in the lungs of air-exposed DBA/2 (A) and C57 BL/6J (B) mice. At 1 month of CS exposure, an increment in the expression of NF-kB is evident in DBA/2 mice (C), while in C57 BL/6J mice (D) a modest positivity can be observed. At 4 months of CS exposure, a stronger reaction is visible in DBA/2 (E) and C57 BL/6J (F) mice, both in alveolar and airway epithelial cells. (A-F) 10x, scale bar = 100 μm, (n=6/group).*

As expected, the expression of phosphorylated p38 mitogen-activated protein kinase (p-p38 MAPK) increased in both strains after the exposure to CS. DBA/2 mice exposed to smoke for 1 month already displayed a remarkable positivity to p-p38 MAPK in bronchial epithelial cells, peribronchial smooth muscle layer, and lung parenchyma (Figure 9C). The continuous exposure to CS for 4 months maintained p-p38 expression levels higher than air-exposed mice (Figure 9E). C57 BL/6J mice presented an increment in the p-p38 expression from 1 month of CS exposure, but a more evident increase can be appreciated from 4 months of CS exposure (Figure 9F). The areas of major positivity corresponded to DBA/2 mice ones.

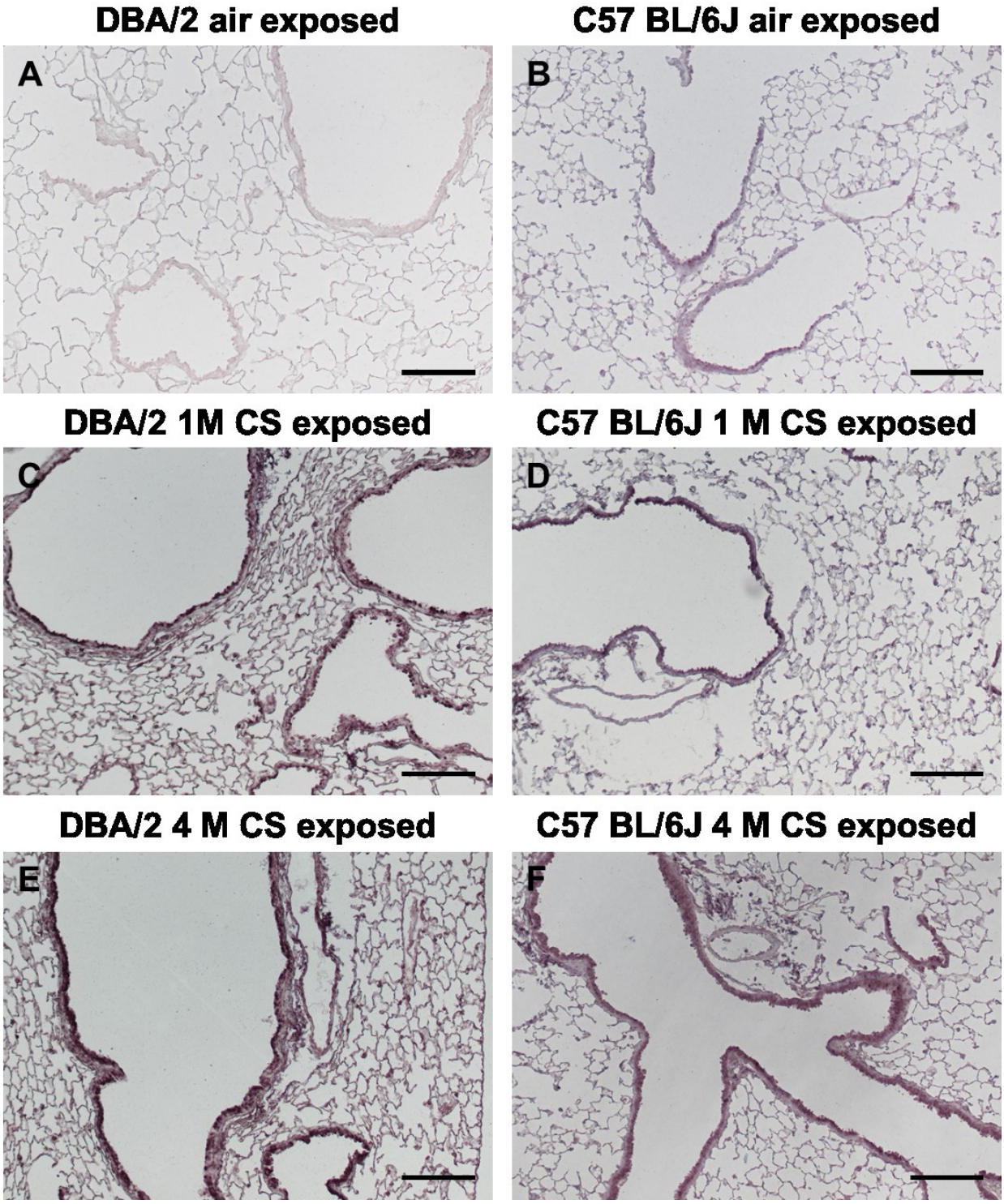

Figure 9: *Immunohistochemical reaction for phosphorylate p38 mitogen-activated protein kinase. No positive staining for p-p38 in the lungs of air-exposed DBA/2 (A) and C57 BL/6J (B) mice is appreciated in alveolar and airway epithelial cells. At 1 month of CS exposure, increased expression of p-p38 is observed in DBA/2 mice (C), while a modest positivity is seen in C57 BL/6J mice (D). At 4 months of CS exposure, a stronger reaction is visible in DBA/2 (E) and C57 BL/6J (F) mice. (A-F) 10x, scale bar = 100 μm, (n=6/group).*

DISCUSSION

Airway remodelling consists in a modification of structural cells and tissues leading to the development of a new airway-wall structure, which can be present in lung chronic disease such as asthma or COPD. Clinical studies carried out in patients within each GOLD stage shown that as the disease progresses there is an increase in airway wall thickness, which can also be largely attributed to airways fibrous remodelling [77]. Currently, this condition is untreatable, and a limited understanding of the pathogenic mechanisms that lead to collagen accumulation is detrimental to therapeutic success.

Several stimuli and putative mediators in the induction of fibrous remodelling in COPD have been considered. These include DNA damage induced by oxidants, cellular senescence with the expression of SASPs involved in processes affecting transcription (i.e., epigenetic alteration) and metabolism (i.e., fibrotic cytokines), and the lack of apoptosis mechanisms.

This study was meant to complete previous researches on airways remodelling on the same mouse strains (C57 BL/6J and DBA/2) here analysed. Indeed, it was formerly demonstrated in our laboratories that the emphysematous lesion develops more rapidly and uniformly in DBA/2 mice compared to C57 BL/6J mice [78]. In addition, following chronic exposure to cigarette smoke, was interesting to notice that other lesions, as goblet cells metaplasia, were observed. Although, the appearance and severity of those were different in the two mice strains [78].

Here, we highlighted how a diverse susceptibility to oxidative stress would lead to different responses after exposing the two mice strains to cigarette smoke for several months. In particular, we paid attention to the potential mechanisms of airway epithelial cells senescence in COPD, which is reported to be involved in the development and severity of the disease [75].

In a recent study, we demonstrated that fibroblasts transition to myofibroblasts was associated with an increased expression of $p16^{ink4A}$ and MyoD and other senescence-secreted factors, including some fibrotic cytokines such as TGF-β, PDGF-B, and CTGF [73]. Cigarette smoke causes an upregulation of fibrotic cytokines, like TGF-β and CTGF, leading to airways remodelling [79]. In this study, the mRNA expression of TGF-β, PDGF-B and CTGF was tested and demonstrated a statistically significant upregulation in both strains after 4 months of CS exposure. Nonetheless, DBA/2 mice displayed higher levels of these growth factors when compared to C57 BL/6J mice.

It is well known that in COPD smokers, the oxidants and free radicals released by cigarette smoke are involved in both the onset and maintenance of inflammation and in the modifications of proteins and enzymes causing the loss of their functions [72, 80]. It has recently been described that NAD-dependent deacetylase sirtuin 1 (SIRT1) prevents lung cellular responses and airway remodelling in mice and COPD patients by regulating the gene expression of pro-inflammatory cytokines through the deacetylation of NF-kB subunits, which in turn reduce premature cellular senescence [75].

Of interest, where airways fibrous remodelling develops, the phenotypic change in fibroblasts is preceded by the decreased expression of SIRT1. Changes in SIRT1 expression appear very early in DBA/2 mice, also preceding the development of lung air space enlargements and airways changes. In C57 BL/6J mice, changes in SIRT1 expression appear later but still precede airways remodelling as well as alveolar changes. The decreased expression of SIRT1 in both strains of mice enhances cellular senescence through the expression of a cyclin-dependent inhibitor, $p16^{ink4A}$, which leads to cell cycle arrest at G1 phase, determining resistance to apoptosis [73, 81].

It is well known that damage related to oxidative stress can induce cell senescence and may favour aging and the development of several associated diseases [82, 83]. In this

regard, DBA/2 strain's peculiar sensitivity to oxidative stress appears to be a significant factor in the different extent and time of development of these phenotypic changes that we observed after exposure to CS when compared to the other strain.

Furthermore, the NAD^+ dependent deacetylase not only plays a key role in premature cellular senescence and aging, but also modulates oxidative stress responses, and inflammation [84, 85]. Indeed, Yeung and colleagues demonstrated that a pharmacological modulation of SIRT1 in cells would result in a reduced transcription of the nuclear factor kappa B (NF-kB) following the TNF-α stimulation [86], suggesting an interesting interaction between these factors.

The activation of nuclear factor kappa B (NF-kB) pathways are involved in pulmonary fibrosis, asthma, COPD, pulmonary tuberculosis, lung carcinoma and many other lung conditions associated to an inflammatory response [87].

Thus, in our study, we assessed the expression of NF-kB and we compared its expression levels with SIRT1 expression. Our results confirmed a deep correlation between the nuclear factor and the deacetylase. As a matter of fact, following the exposure to CS, a steady upregulation of NF-kB was observed in association with a strong downregulation of SIRT1 in both strains. More in detail, DBA/2 mice at 1 month of smoke exposure, showed a statistically significant reduction in SIRT1 expression, and a concomitant upregulation of NF-kB. On the other hand, C57 BL/6J mice first showed a marked reduction of SIRT1 and an evident increment of NF-kB after 4 months of cigarette smoke exposure. These evidences yet confirmed what was reported by other authors [84-87], but also highlighted, once again, a role of oxidative stress.

Activation of NF-kB leads to a translocation of this pleiotropic transcription factor into the nucleus, where it regulates the expression of several genes, including inflammatory cytokines and chemokines responsible for histone deacetylases modification [72]. As

reported in this work, C57 BL/6J mice exposed to smoke presented a reduced expression of SIRT1 but also HDAC-2; but more importantly, the expression of these enzymes was not restored with smoke cessation. Moreover, in their experimental conditions, they also observed a marked upregulation of phosphorylated p 38 mitogen-activated protein kinase (p-p38 MAPK) [72].

Since the expression of the histone deacetylase 2 (HDAC-2) is influenced by oxidants levels, we also tested its expression in our study. As for SIRT1, DBA/2 mice showed an earlier downregulation of this enzyme at 1 month of CS exposure, while C57 BL/6J mice has a major reduction later at 4 months of CS exposure. In line with the previous work [72], HDAC-2 expression remained low at later time points in both strains.

Another signalling pathway responsible for an increased senescence burden in the lung is p38 MAPK, which is also induced by SASP and oxidative stress (e.g. tobacco smoke) [28, 88]. Interestingly, bronchial epithelial cells, macrophages and lymphocytes from COPD and asthma patients showed increased phosphorylation levels of p38 MAPK [28, 88]. p38 MAPK is also reported to upregulate the expression of microRNA-570 (miR-570), a small RNA molecule responsible for SIRT1 inhibition and increased NF-kB activity and consequently in the expression of SAPS [28, 29]. Several researches also reported that p38 activity is crucial for immune and inflammatory responses, and multiple inflammatory mediators as chemokines, cytokines, and chemoattractant can activate its pathway [89].

Hence, we also assessed the expression of p-p38 MAPK in our model. Here, cigarette smoke exposure prompts an upregulation of p-p38 MAPK in both mice strains. As for NF-kB expression levels, DBA/2 mice already displayed an important increment in p-p38 MAPK expression after 1 month of smoke exposure. At later time point, the immunohistochemistry highlighted a persistent upregulation of this kinase. On the other hand, a less pronounced upregulation of the phosphorylated form of p38 MAPK was

observed in C57 BL/6J mice at the earliest time point. Withal, at 4 months of cigarette smoke exposure, even this strain presented a great increase in p-p38 MAPK expression, confirming the analysis performed previously in our laboratory [72].

In conclusion, we can state that an earlier upregulation of p-p38 and NF-kB, together with a lower expression of SIRT1 and HDAC-2 especially detected in DBA/2 mice is in line with a higher sensitivity to oxidative stress, and may be one of the key factors in the development of airways fibrotic remodelling. Moreover, our data suggest that the same signalling pathways may contribution to the airways remodelling through induction of cellular senescence.

Future researches to better understand the mechanisms involved in senescence, and their contribution to COPD pathogenesis are needed and will definitely aid in the development of novel therapies that could prevent the progression and may reverse this condition. In particular, the identification of novel senolytic, able to selectively induce senescent cells death, or senomorphic agents, which suppress the effects of senescence mediators (SASPs), could enhance the development of new therapies [90, 91].

SUMMARY

The chronic obstructive pulmonary disease (COPD) no longer represents a rare condition, nonetheless the pathogenic mechanisms that lead to this illness are still under investigation, therefore an effective treatment is still missing. Despite this, it is obvious that multiple insults are needed to actually induce the onset of this condition.

In this chapter was reported the latest finding regarding a previous work that aim to evaluate whether a pre-existing sensitivity to oxidative stress could contribute to the damage induced by a chronic cigarette smoke exposure.

In summary, we demonstrate that DBA/2 mice, which are sensitive to oxidative stress, developed structural damages at earlier time points when compared with another strain, C57 BL/6J mice. In both strains, the airways remodelling and the emphysematous lesions were preceded by epigenetic alterations of SIRT1, HDAC-2, NF-kB and p-p38 MAPK. The upregulation of NF-kB and p-p38 MAPK together with a downregulation of SIRT1 and HDAC-2 not only highlighted the instauration of an inflammatory response, but also the early onset of cellular senescence. These findings, associated with the previous evaluation of fibrotic cytokines (TGF-β, PDGF-B, and CTGF), myofibroblasts marker (α-SMA), cellular senescence makers ($p16^{ink4A}$ and MyoD), and oxidative stress marker (8-OHdG), confirmed the pivotal role of oxidative stress predisposition in the development of lung injuries after chronic exposure to cigarette smoke.

Future analysis are required to develop new therapies that may slow down the progression and even reverse this condition.

CHAPTER 2:

AIM OF THE STUDY

Here, we hypothesized that sub-chronic exposure to environmental tobacco smoke (ETS) favours the fibrogenesis induced by bleomycin (BLM) administration causing an inflammatory response. Thus, we investigated whether previous exposure to ETS could support the dysregulation of collagen dynamics (synthesis and degradation) induced by BLM. Besides probing the expression of several ECM components, we also analysed markers of cellular senescence to determine whether the exposure to ETS would favour the early onset of senescence.

An additional study was performed to further evaluate the effects of the Complement system activation in normal human lung fibroblasts (NHLF). Indeed, this system resulted significantly upregulated in the animal model, suggesting a relevant role of the Complement in the early induction of cellular senescence and therefore a potential role in pulmonary fibrosis progression.

MATERIALS AND METHODS

ANIMALS AND TREATMENTS

4-5 months *C57 BL/6* male mice were housed in a 12-hour-light/12-hour-dark cycle in the inhalation core facility at the University of Rochester. First, animals were exposed to ETS for a total of 30 days, 5 days/week, via the Teague machine with 100 total particular matter (TPM, mg/m^3). After 6 weeks of exposure, bleomycin (BLM) (1.5U/kg) or PBS (50μL) were oropharyngeal administered. After 14 days from this treatment, mice were sacrificed with intraperitoneal (i.p.) injection of sodium pentobarbital (100mg/kg). Air-exposed control groups of mice were housed separately.

For each animal, right lung lobes were snap-frozen for RNA and protein analysis, while left one was inflated with 1% low-melting agarose for histological analysis.

The animal experiments performed in this study followed the standards from the United States Animal Welfare Act, NIH, and protocol approved by the Animal Research Committee of the University of Rochester.

RNA ISOLATION AND NANOSTRING MEASUREMENT

Lungs lobes were mechanically homogenized with QIAzol reagent, then each sample was mixed with chloroform and vortexed vigorously for 10 sec. Next, the samples were centrifuged at 20,000*g* for 15 min at 4°C; after that, the aqueous phase was moved to new RNase-free tubes and mixed with isopropanol for 2 hr at -20°C. The mixtures were spun down at 20,000*g* for 15 min at 4°C, and the supernatant was removed. RNA pellets were washed with 75% EtOH and then centrifuged at 20,000*g* for 15 min at 4°C. Discarded the EtOH and re-suspended RNA with RNase-free water. All of the RNA samples were cleaned up by RNeasy Plus Mini Kit following the manufacturer's protocol (Qiagen,

Germantown, MD, USA). RNA samples were quantified using a NanoDrop spectrophotometer ND-1000 (NanoDrop Technologies, Wilmington, DE, USA).

A total of 100ng of RNA samples were used for NanoString analysis. In this study, we used the nCounter Fibrosis Panel (Cat# XT-CSO-MFIB2-12, NanoString Technologies, Inc., Seattle, WA, USA). Briefly, the hybridization reaction mix was prepared by RNA samples, reporter codeset, and capture codeset. The mixtures were incubated at 65°C for 16 hrs and stored at 4°C until further profiling. NanoString running cartridge was used to load all the sample mixtures and performed gene expression profiling via nCounter SPRINT Profiler (NanoString Technologies, Inc., Seattle, WA, USA). After profiling, gene expression results were analysed by nSolver 4.0 software, and reported as normalized count for data presentation and statistical analysis.

WESTERN BLOT

First, snap-frozen lungs were mechanically homogenized in RIPA buffer (Cat# 78442 Thermo Fisher Scientific, Waltham, MA, USA) with protease inhibitor (Cat# 78442 Thermo Fisher Scientific, Waltham, MA, USA). Then, protein concentration of each sample was quantified by Pierce BCA Protein Assay (Cat# 23225 Thermo Fisher Scientific, Waltham, MA, USA). Precast gels (Cat# 5671085, Cat# 4568126 BioRad, Hercules, CA, USA) were loaded with 30 µg of protein for each lane for electrophoresis. After that, proteins were transferred onto a nitrocellulose membrane (Cat# 1704159, BioRad, Hercules, CA, USA) through a semi-dry system. The membranes were washed with tris buffer saline containing 0.1% Tween 20 (TBS-T) for 15 min, then blocked with 5% bovine serum albumin (BSA) for 1 hour at room temperature. Next, the membranes were probed overnight at 4°C with primary antibodies: rabbit anti-COLLAGEN 1α1 (1:1000, Novus Biologicals, Centennial, CO, USA); rabbit anti-COLLAGEN 4α1 (1:1000, Abcam, Cambridge, UK); rabbit anti-LOX

(1:1000, Abcam, Cambridge, UK); rabbit anti-FIBRONECTIN (1:1000, Abcam, Cambridge, UK); rabbit anti-MMP2 (1:1000, Abcam, Cambridge, UK); rabbit anti-C3 (1:1000, Abcam, Cambridge, UK). The next day each membrane was incubated with the secondary antibody goat anti-rabbit IgG (H+L) HRP-conjugated (1:5000, BioRad, Hercules, CA, USA) for 90 minutes at room temperature. After each antibody incubation, the membrane was washed 3 times in TBS-T (15 minutes/wash). Ultimately, the luminescence signals were developed using a chemiluminescence substrate (Thermo Fisher Scientific, Waltham, MA, USA).

The membranes exposure and band intensities were detected via the Bio-Rad ChemiDoc MP imaging system (BioRad, Hercules, CA, USA). Protein quantification was done by densitometry, and β-ACTIN (1:2500, Abcam, Cambridge, UK) was used as housekeeping control. Densitometry analysis was performed by Image Lab software (v4.1, BioRad, Hercules, CA, USA) and data was presented as fold change compared to the PBS group.

H&E STAINING

The H&E staining has been performed as previously described [92]. Briefly, lung sections (5 μm) were deparaffinised by xylene 3 times, and rehydrated with decreasing concentration of ethanol (100%, 95%, and 70%). Next, slides were quickly washed with water, and stained with haematoxylin for 1 minute. Then, sections were cleansed with water and blued with 0.1% ammonia water for 10 seconds. After a brief rinse in water, the sections were submerged in Eosin for 1 minute. Sections were washed with 95% ethanol for 1 minute, then dehydrated with 95% and 100% ethanol, 2 times, and xylene, 3 times. Finally, slides were mounted in Permount mounting for microscopy.

GOMORI'S TRICHROME STAINING

Gomori's trichrome staining has been used to visualize the amount of collagen deposition in the lungs from different experimental groups. Lung sections (5 μm) were deparaffinised, rehydrated, and finally rinsed with tap water. Sections were then subjected to Gomori's trichrome staining using the Thermo Fisher Scientific kit (Cat# 87020, Thermo Fisher Scientific, Waltham, MA, USA). In brief, sections were placed in Bouin's solution at 56°C for 1 hour, and then washed with water until the complete removal of the yellow color. Next, sections were immersed in Working Weigert's Iron Hematoxylin Stain for 10 minutes and washed with water for other 10 minutes. Sections were soaked in Trichrome Stain for 15 minutes and immediately immerged in acetic acid 1% for 1 minute. After, sections were rinsed with water for 30 seconds and dehydrated. Lastly, the slides were mounted by Permount for microscopy observation. For each sample, 10 pictures (20x magnification) have been taken by Nikon microscopy (Eclipse Ni-U) and the amount of collagen has been quantified by Colour Deconvolution via FIJI ImageJ.

IMMUNOHISTOCHEMISTRY STAINING

The staining protocol has been performed as previously described [93]. Serial lung sections (5 μm) were deparaffinised and rehydrated, and then the antigens were unmasked with antigen retrieval solution (10x) (Dako, Carpinteria, CA, USA). Sections were blocked with 10% normal goat serum at room temperature before being incubated overnight at 4°C with primary antibodies: anti-Collagen 1α1 (1:100, Novus Biologicals, Centennial, CO, USA); anti-Collagen 4α1 (1:100, Abcam, Cambridge, UK) and anti-LOX (1:50, Abcam, Cambridge, UK). The next day, slides were rinsed with tris buffer saline (TBS) and soaked in 0.3% hydrogen peroxide for 15 minutes. After few washes with TBS, secondary antibody goat anti-rabbit IgG (H+L) HRP-conjugated (1:1000, Abcam,

Cambridge, UK) was applied to the sections at room temperature for 1 hour. The immunohistochemistry was developed with DAB Quanto Chromogen and Substrate (Thermo Fisher Scientific, Waltham, MA, USA) and then counter-stained with haematoxylin. Finally, the slides were dehydrated and mounted for further analysis. These markers have been evaluated in sequential sections and for each sample, 10 pictures (20x magnification) have been taken and compared between groups. The positive staining has been quantified using Colour Deconvolution via FIJI ImageJ.

CELL CULTURE AND TREATMENTS

Primary human lung fibroblasts (NHLF) (Cat# CC-2512) were purchased from Lonza (Lonza, Morristown, NJ, USA). Lung fibroblasts were cultured in FGM-2 Fibroblast Growth Medium (Cat# CC-3132, Lonza, Morristown, NJ, USA) and maintained under 5% CO_2 and 95% humidity.

First, NHLF cells were seeded into 12 well plates ($2.5x10^5$ cells/well), after 24 hours, the cells were serum deprived for at least 6 hours before starting the treatments which were conducted in a serum-free media. Fibroblast cells were treated for 48 hours with 0.2 μM human C3 Complement component (Abcam, Cambridge, UK) or different concentrations (50nM, 100nM) of SB290157 C3aR antagonist (Cat# 559410, Sigma-Aldrich, St. Louis, MO, USA). A detailed scheme of treatments is reported in Figure 10. At the end of the experiments, the cells were lysed for RNA quantification. In addition, NHLF cells exposed to C3 Complement component were fixed with 4% paraformaldehyde for immunofluorescence staining.

Figure 10: Schematic representation of cell treatments.

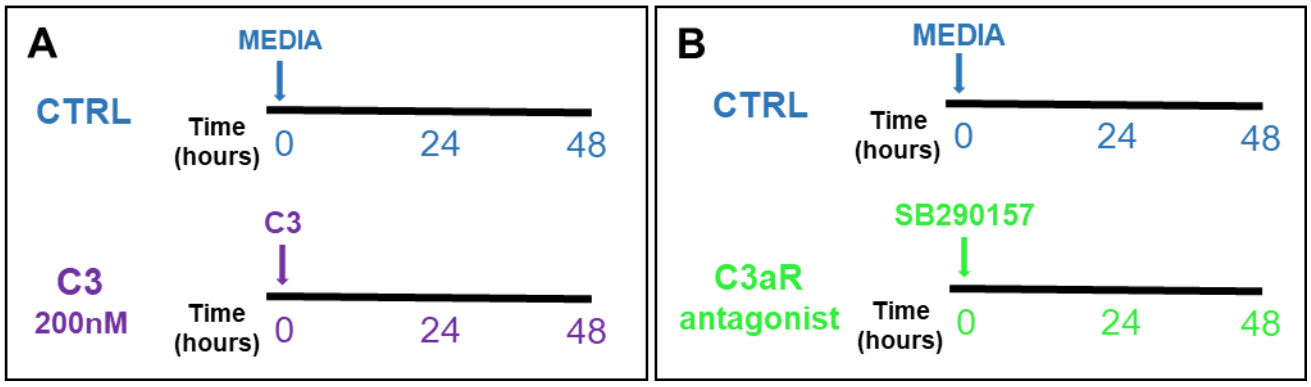

LACTATE DEHYDROGENASE CYTOTOXICITY ASSAY

Lactate dehydrogenase (LDH) was quantified to assess the cytotoxicity of treatments (i.e. C3 and C3aR antagonist). After 48 hours, media was collected and immediately place on ice. The LDH release was determined by using the Cytotoxicity Detection Kit ^{PLUS} (LDH) (Roche Diagnostic Corporation, Indianapolis, IN, USA). In brief, a 96-well plate was loaded with 50 µL of each sample in duplicate and 100 µL of reaction mixture, which was incubated at room temperature. After 15 minutes, 50 µL of stop solution was used to stop the reaction. Absorbance was recorded at 490 nm using a microplate spectrophotometer system.

RNA ISOLATION AND qRT-PCR

At end of the exposure, cells were washed with phosphate buffer saline (PBS) and incubated for 15 minutes at room temperature with QIAzol lysis reagent (Cat#79306, Qiagen, Germantown, MD, USA). The RNA isolation was obtained using the miRNeasy Mini Kit following the manufacturer's instructions (Cat#217004, Qiagen, Germantown, MD, USA). At the end of RNA extraction, concentrations and qualities of RNA were measured

with Nano-drop spectrophotometer ND-1000 (NanoDrop Technologies, Wilmington, DE, USA).

RT^2 First Strand Kit (Qiagen, Germantown, MD, USA) was used to synthetized the cDNA. Equal amounts of cDNA for each sample were used for real-time PCR quantification based on RT^2 SYBR Green Fluor qPCR Mastermix (Cat# 330513, Qiagen, Germantown, MD, USA). The primers used were: COL1A1 (Human, qHsaCED0043248), ACTA2 (Human, qHsaCID0013300), and FN1 (Human, qHsaCID0012349). All primers were purchased from BioRad. The qPCR thermal cycle applied consists in 10 minutes at 95 °C, and 40 cycles of 95 °C (15 seconds) and 60 °C (1 minute). At the end, a melting curve was performed to check cDNA amplification quality.

The BioRad CFX96 was used as qPCR detection system, and data were presented as fold change, calculated based on $2^{-\Delta\Delta Ct}$ methods with GAPDH as housekeeping control.

IMMUNOFLUORESCENCE

Fibroblasts were seeded on coverslips, and treated as indicated in Figure 10A. After 48-hours treatment with C3 Complement component, NHLF cells were fixed with 4% paraformaldehyde for 15 minutes at room temperature. After two washes with TBS, they were blocked with 10% normal goat serum. Then, cells were incubated overnight at 4°C with primary antibodies: rabbit anti-fibronectin (1:50, Abcam, Cambridge, UK) and mouse anti-α-SMA Alexa Fluor 594 conjugated (5 µL/10^6 cells, R&D System, Minneapolis, MN, USA). The coverslips were washed with TBS three times and incubated with donkey anti-rabbit IgG (H+L) secondary antibody Alexa Fluor 488 (1:1000, Thermo Fisher Scientific, Waltham, MA, USA) for 1 hour at room temperature on a rocker. Following three washes, the slides were mounted with Prolong Diamond Antifade Mountant with DAPI (Life

Technologies, Carlsbad, CA, USA). Images were acquired through a fluorescence microscopy.

ImageJ was used to quantify the fluorescence intensity with the following equation: integrated Density (IntDen) − (Area of cells * Mean fluorescence of background).

STATISTICAL ANALYSIS

All data were analysed through one-way ANOVA with Šidák correction using GraphPad Prism software version 9.0 (GraphPad, San Diego, CA, USA). Results were presented as mean ± SEM and $P<0.05$ was considered significant.

RESULTS

EFFECTS OF ENVIRONMENTAL TOBACCO SMOKE EXPOSURE IN BLEOMYCIN-INDUCED LUNG INJURY

Male mice were exposed to ETS for 30 days and then BLM was administered to evaluate to what extent ETS exposure contributes to BLM-induced lung injury. BLM treatment induced body weight decline, the reduction was evident after 7 days post-BLM injury. ETS exposure only (ETS+PBS) did not alter body weight compared with control group (Air+PBS), likewise ETS exposure did not affect the body weight reduction induced by BLM administration (ETS+BLM) (Figure 11A).

H&E-stained lung sections depicted similar lung injury between Air+BLM and ETS+BLM groups, characterised by several areas of scaring, inflammatory cells infiltration and cell proliferation. Limited airspace enlargement was seen in the ETS+PBS group compared to the Air+PBS group (Figure 11B).

In order to evaluate the collagen dysregulation with every treatment, we performed the Trichrome staining. BLM significantly augments the amount of collagen in the lungs either with exposure to Air (Air+BLM) or ETS (ETS+BLM), in comparison to Air+PBS or ETS+PBS groups. ETS exposure only (ETS+PBS) did not affect the amount of collagen within the tissue compared with the control group (Air+PBS). Mice exposed both to ETS and BLM presented a similar increment in collagen deposition to the one observed in mice exposed to BLM (Air+BLM) (Figure 12).

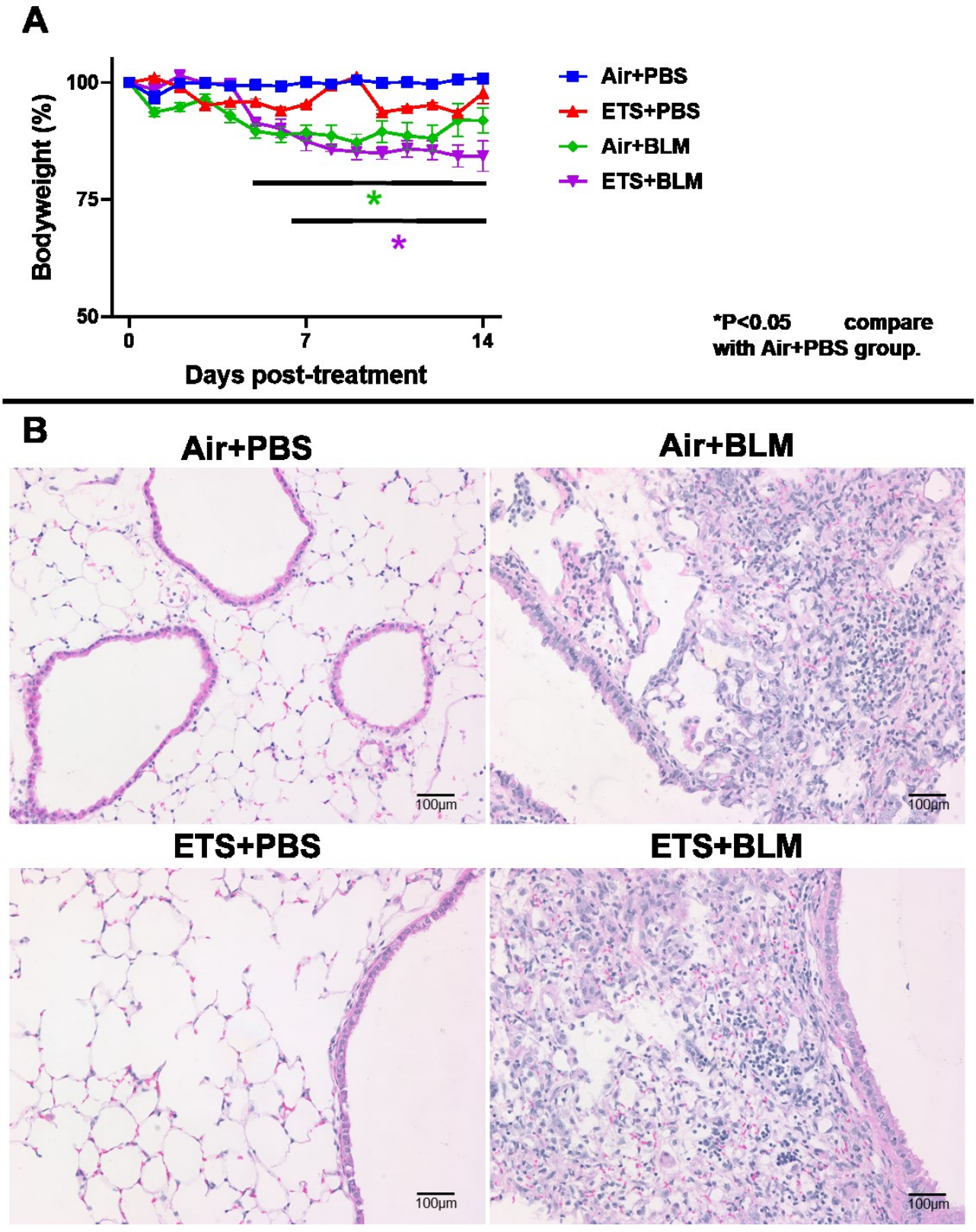

Figure 11: *ETS exposure and BLM administration induced a lung injury characterized by collagen deposition, and impaired lung function. (A) Changes in body weight 14 days post-BLM. (B) H&E staining (20x, scale bar = 100 μm) shows the lung injury induced by both agents (n=3-4/group).*

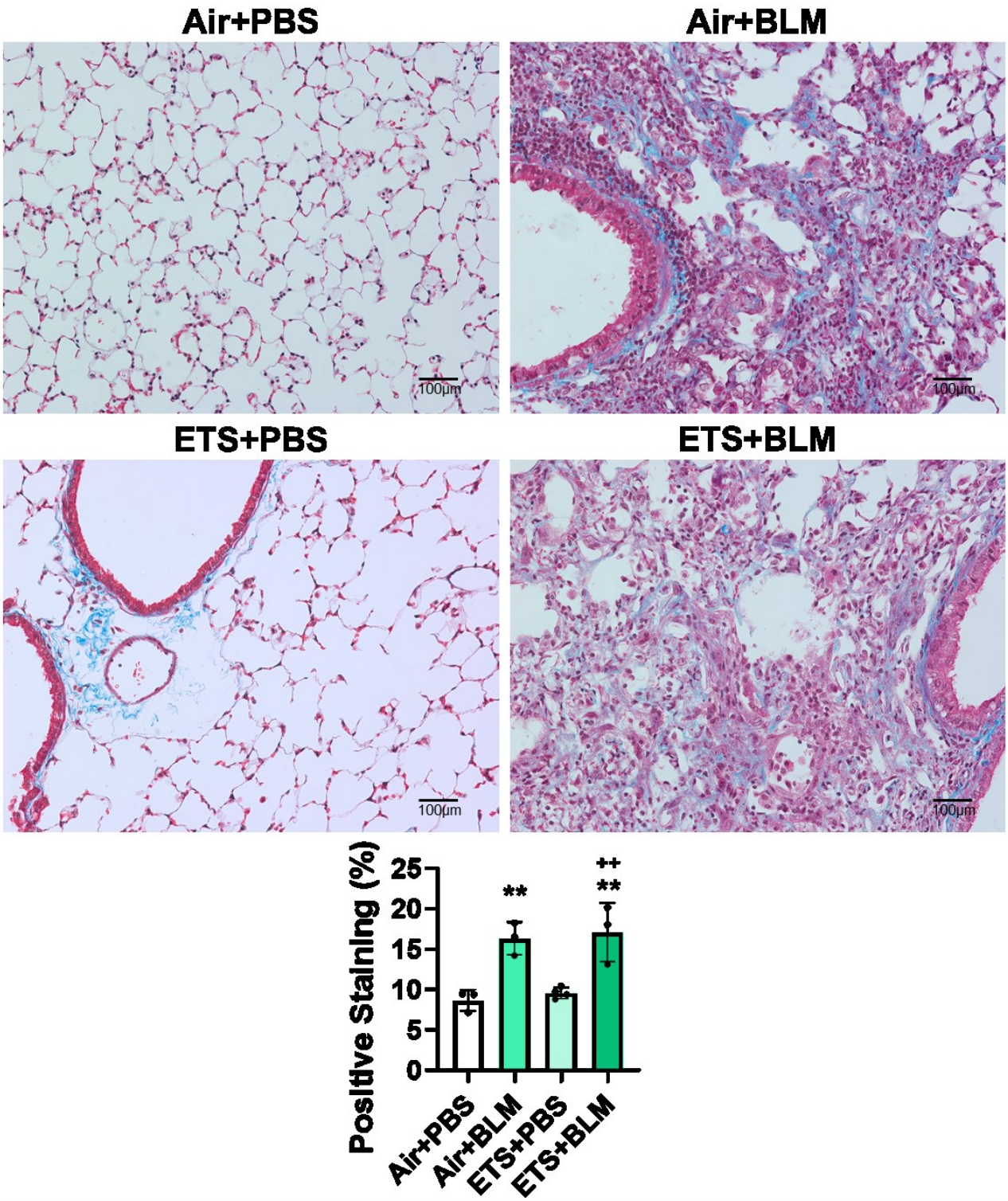

***P<0.05, **P<0.01, compare with Air+PBS group; +P<0.05, ++P<0.01, compare with ETS+PBS group.**

Figure 12: *Trichrome staining (20x, scale bar = 100 µm) was performed to highlight the collagen deposition. The positive staining was quantified using Colour Deconvolution via FIJI ImageJ. The collagen deposition percentage is reported in the bar graph. Data are presented as mean ± SEM (n=3-4/group).*

ETS EXPOSURE FURTHER DISREGULATED BLEOMYCIN-INDUCED ABNORMAL ECM COMPONENTS BIOSYNTHESIS AND MODIFICATION

To define the effect of a sub-chronic exposure to tobacco smoke in BLM-induced lung injury in mice, RNA was isolated from lung homogenates, and fibrotic genes were measured via NanoString profiling.

BLM administration, either with the exposure to ETS (ETS+BLM) or with air (Air+BLM), displayed increased collagens gene expression. In details, ETS+BLM treatment augmented the upregulated transcription levels of *COL1A1, COL1A2, COL3A1, COL4A1, COL4A2,* and *COL5A3.* Of interest, among all the sub-types of collagen, *COL4A1* and *COL5A3* gene expression levels were significantly increased in ETS+BLM compared to Air+BLM (Figure 13).

Other ECM genes, like elastin (*ELN)* and fibronectin (*FN1)* were overall upregulated after bleomycin treatment. A further increment was noticed with ETS exposure, even if it was not significant when compared to Air+BLM mice (Figure 13). No evident variations of these ECM components genes (collagens, elastin and fibronectin) were observed in mice exposed exclusively to ETS (Figure 13).

The transcription levels of lysyl oxidase enzymes (LOXs) and matrix metalloproteinases (MMPs) were also assessed (Figure 13). Increased expression levels of *LOXL1* and *LOXL2* genes were found in Air+BLM animals as opposed to the control group (Air+PBS), although the difference was not significant. *LOX* expression level in this experimental group (Air+BLM) was not dissimilar from the one observed for the control group (Figure 13). ETS exposure showed no significant variation in the expression of lysyl oxidase enzymes compared to the Air+PBS group (Figure 13). The combined exposure to ETS and BLM induced a major increment in the expression of *LOX, LOXL1* and *LOXL2*, with

respect to control mice. No significant differences between Air+BLM and ETS+BLM groups were appreciated (Figure 13).

Following bleomycin administration (Air+BLM) gene expression of *MMP2* and *MMP14*, were significantly upregulated in comparison to control animals (Air+PBS), while *MMP12* and *MMP13* were not significant upregulated (Figure 13). The expression levels of *MMP2, MMP12, MMP13,* and *MMP14* were significantly higher in mice treated with bleomycin after the tobacco exposure, than the control mice (Figure 13). Of interest, MMP2 gene was downregulated in ETS+BLM mice as opposed to Air+BLM. Overall, gene expression levels of MMPs were not upregulated in ETS+PBS mice (Figure 13).

The MMPs inhibitor, *TIMP1*, showed increased gene expression levels in Air+BLM group with respect to the Air+PBS group. Of note, the expression levels of *TIMP1*, in ETS+BLM group, presented a noteworthy rise compared to either Air+PBS or ETS+PBS groups; nonetheless, ETS+PBS group did not present significant changes when compared to Air+PBS group (Figure 13).

As the most well-known fibrogenesis regulators, TGFβ signalling was also tested. *TGFB1*, *TGFBR1*, and *TGFBR2* gene expression levels were augmented post-bleomycin either with air or ETS exposure, with no significant differences from the control group or between the two groups (Air+BLM vs ETS+BLM) (Figure 13). ETS+BLM group presented a significant increment in the expression of *TGFB1* and *TGFBR1* genes as opposed to ETS+PBS mice (Figure 13). Also in this case, mice exposed only to ETS showed no variations compared to air exposed mice (Figure 13).

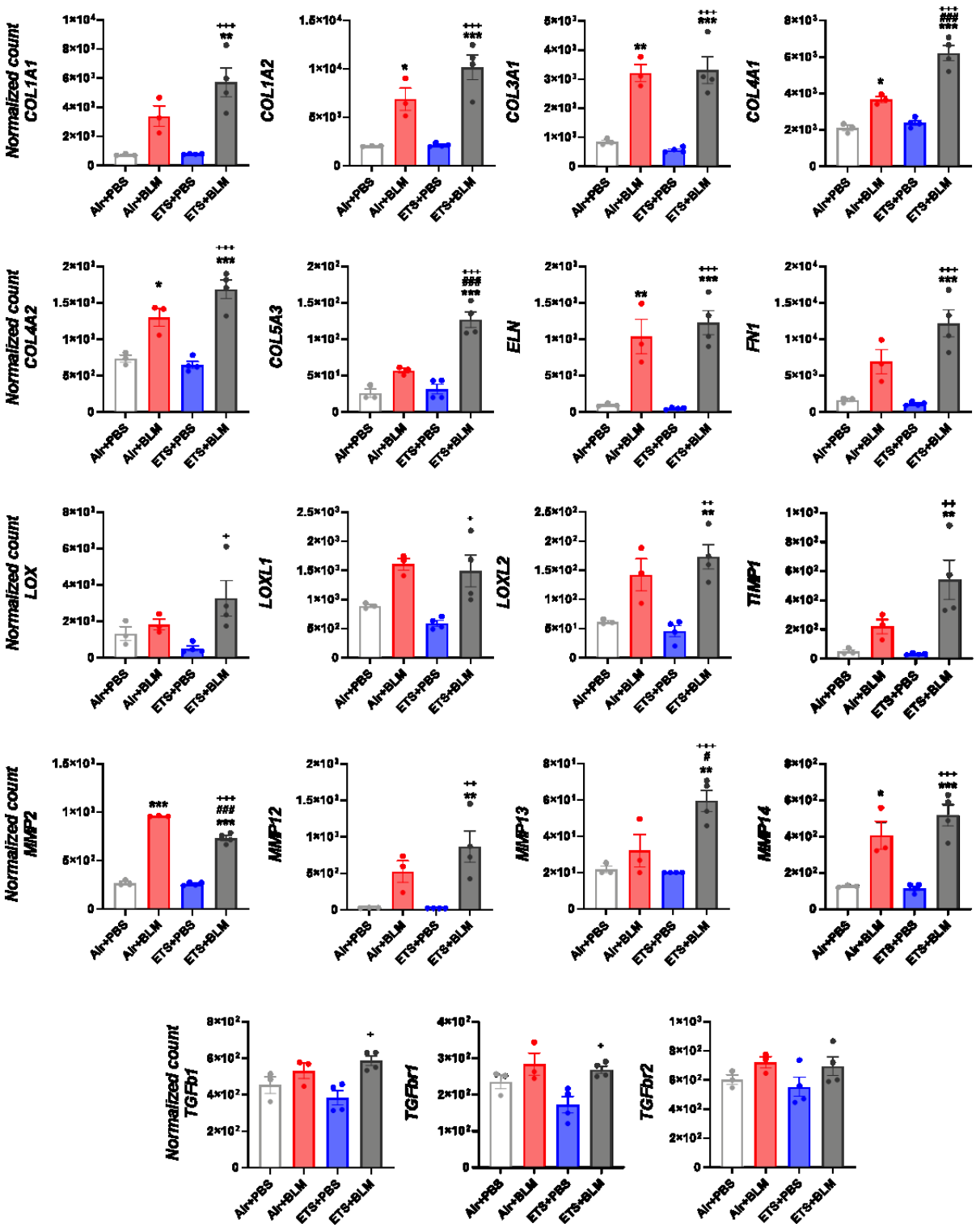

***P<0.05, **P<0.01, ***P<0.001, compare with Air+PBS group; #P<0.05, ##P<0.01, ###P<0.001 compare with Air+BLM group; +P<0.05, ++P<0.01, +++P<0.001 compare with ETS+PBS group.**

Figure 13: *NanoString nCounter Fibrosis panel was used to identify fibrotic gene transcript levels. RNA expression levels were normalized by nSolver software, and the normalized count was used for statistical analysis. Selected genes are shown as bar graphs. Data are shown as mean ± SEM (n=3-4/group).*

The protein expression of dysregulated ECM elements, like COL1A1, LOX, and MMP2, was measured with immunoblot. COL1A1, LOX, and the activated forms of LOX and MMP2 were upregulated after BLM administration. Notably, the protein expression of COL1A1 and activated LOX showed a significant increase in ETS+BLM with respect to the Air+BLM group. LOX and activated MMP2 expression was increased after ETS+BLM administration but not significantly compared to Air+BLM group. In ETS+PBS group, the protein levels of these factors (COL1A1, LOX and MMP2) were not dissimilar from those observed in Air+PBS group (Figure 14A). Blot images are shown in Figure 14B; the active form of MMP2 is represented by the lower bands in the blot images of MMP2.

To better visualise the localization of these proteins in the lesion areas, IHC staining was performed. The protein expression of COL1A1, COL4A1, and LOX was increased in Air+BLM and ETS+BLM groups with respect with the control groups (Air+PBS or ETS+PBS). Of interest, the protein expression levels of COL4A1 and LOX in the lesion areas were significantly increased in the ETS+BLM group compared to Air+BLM, while COL1A1 showed non-significant increased protein expression whit respect to the Air+BLM group (Figure 15).

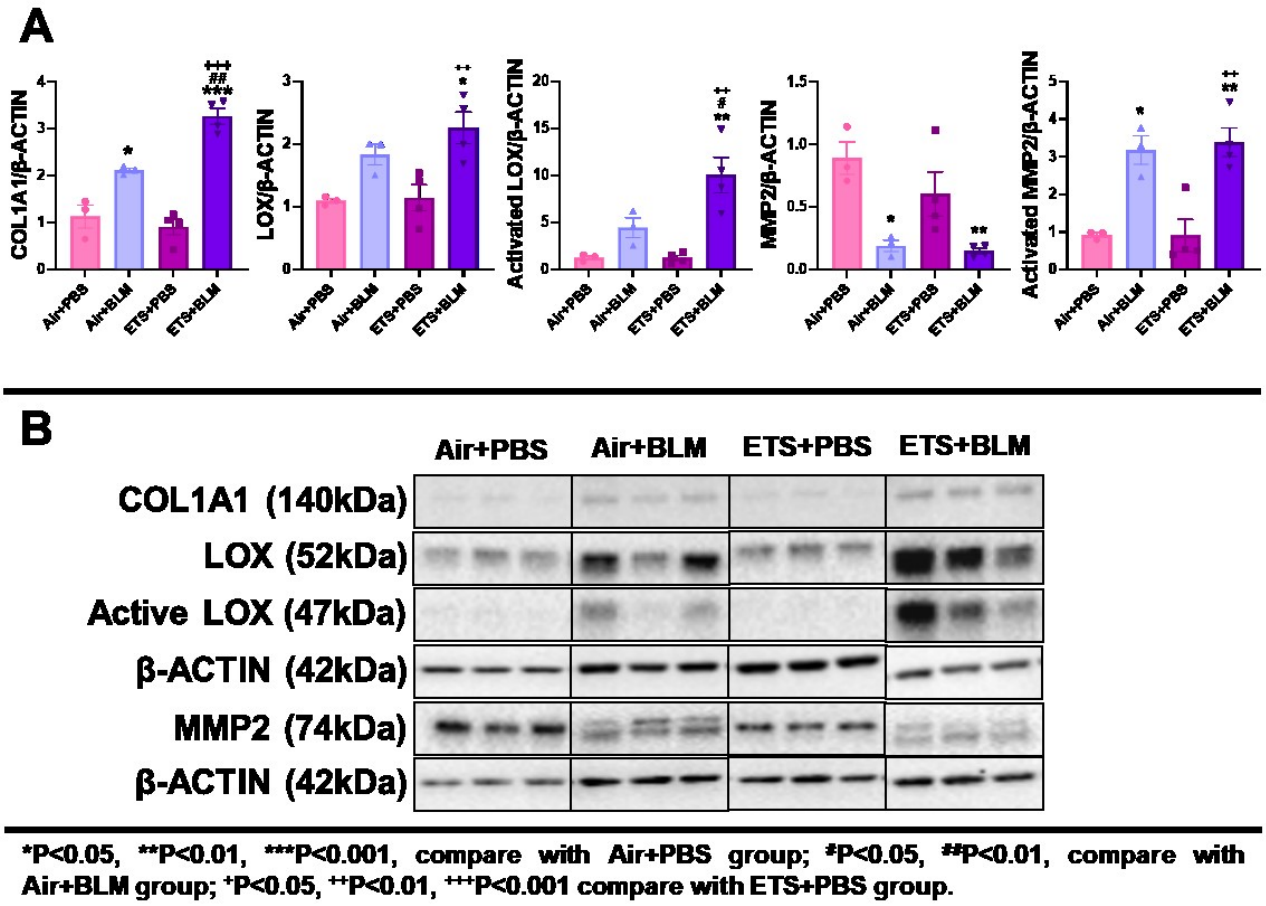

Figure 14: *Protein expressions were analysed by Western blotting from lung homogenates. (A) The bar graphs show the proteins expressions (fold change) of COL1A1, LOX, active-LOX, MMP2 and active-MMP2. (B) Blot images of each experimental group. The active form of MMP2 is represented by the lower bands in the MMP2 blot. These bands are exclusively visible in Air+BLM and ETS+BLM groups. Densitometry analyses are done individually, and β-ACTIN was used as an endogenous control. Data are shown as mean ± SEM (n=3-4/group).*

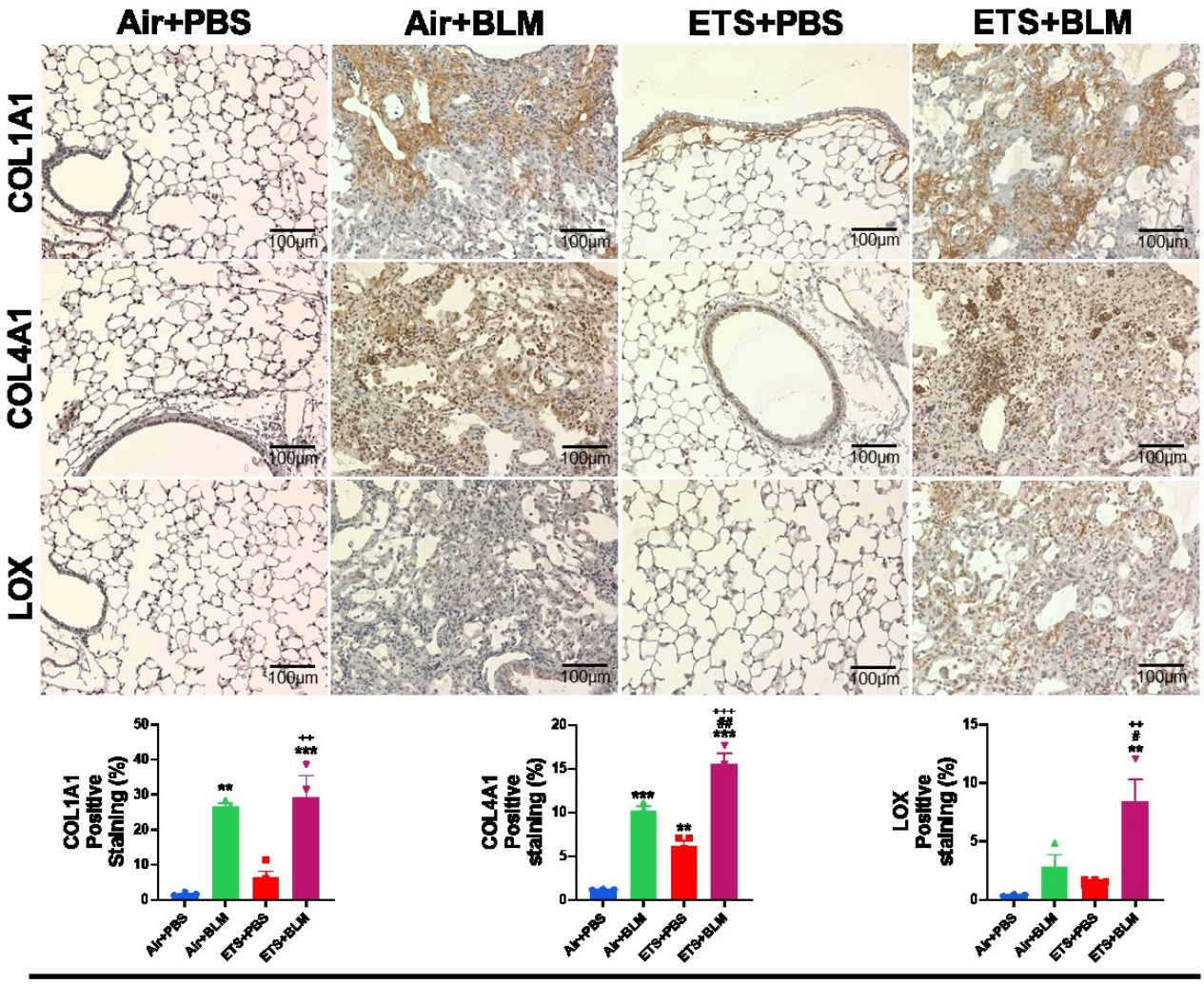

***P<0.05, **P<0.01, ***P<0.001, compare with Air+PBS group; #P<0.05, ##P<0.01, ###P<0.001 compare with Air+BLM group; +P<0.05, ++P<0.01, +++P<0.001 compare with ETS+PBS group.**

Figure 15: *COL1A1, COL4A1, and LOX proteins abundance and localization were evaluated via IHC staining (20x, scale bar = 100 µm) and quantified as a positive staining percentage. The positive staining has been quantified using Colour Deconvolution via FIJI ImageJ, and reported in the bar graphs. Data are presented as mean ± SEM (n=3-4/group).*

ETS EXPOSURE AUGMENTED CELLULAR SENESCENCE INDUCED BY BLEOMYCIN TREATMENT

During this study, we also considered whether these two agents could induce an early onset of senescence. To assess the dysregulated transcript levels a customized NanoString panel focused on senescence genes was used.

The gene levels of cyclin-dependent kinase inhibitors (*CDKN1A, CDKN2B, CDKN2C, CDKN2D, CDKN1B*, and *CDKN1C*) were tested. Among these inhibitors, *CDKN1A* and *CDKN2B* gene expression levels were higher in Air+BLM and ETS+BLM groups than in Air+PBS group. Of note, only ETS+BLM mice showed a significant increment of these genes as opposed to control mice (Figure 16A). ETS+PBS group did not exhibit variations in the gene expression of CDKN1A and CDKN2B when compared to Air+PBS group (Figure 16A).

Moreover, other senescence-associated factors were tested. *SERPINE1* gene presented significantly higher levels of expression in ETS+BLM mice compared to either Air+PBS or ETS+PBS group. No differences among these two groups (Air+PBS and ETS+PBS) were observed for *SERPINE1* gene. The only treatment with bleomycin (Air+BLM) did not induce a significant increment with respect to control animals (Air+PBS) (Figure 15A).

Members of the Sirtuins family were also analysed in the customized panel. The gene expression of both *SIRT1* and *SIRT3* were lower in mice treated with bleomycin (Air+BLM) than control group (Air+PBS). A strong downregulation of these genes was likewise observed with the combined exposure to ETS and BLM. *SIRT1* and *SIRT3* gene expressions did not show variations when treated with ETS (ETS+PBS group) (Figure 16A).

Among the genes evaluated, it was interested to notice that the gene expression levels of Complement genes (*C1QA*, *C1QB*, *C1QC*, and *C3AR1*) were upregulated after BLM

administration either with air (Air+BLM) or ETS exposure (ETS+BLM). In addition, *C1QA*, *C1QB* and *C3AR1* showed a significant further increase in ETS+BLM group with respect to the Air+BLM group. Complement components genes were not changed in ETS+PBS mice as opposed to Air+PBS group (Figure 16A).

Eventually, to confirm the activation of the Complement system, we quantified the protein expression levels of C3 (Figure 16B). ETS and BLM exposure induce a significant increase of C3 alpha chain (C3A) compared to the other groups (Air+PBS and Air+BLM) (Figure 16B). Likewise, C3 alpha chain fragment (C3B) protein was significantly higher than Air+PBS group only in ETS+BLM group. On the other hand, C3 alpha chain fragment 2 (C3C) protein level was significantly upregulated both in Air+BLM and ETS+BLM group with respect to the control mice (Figure 16B). Withal, BLM alone did not induce the same upregulation observed in animals exposed to both agents (Figure 16B). Blot images are reported in Figure 16C.

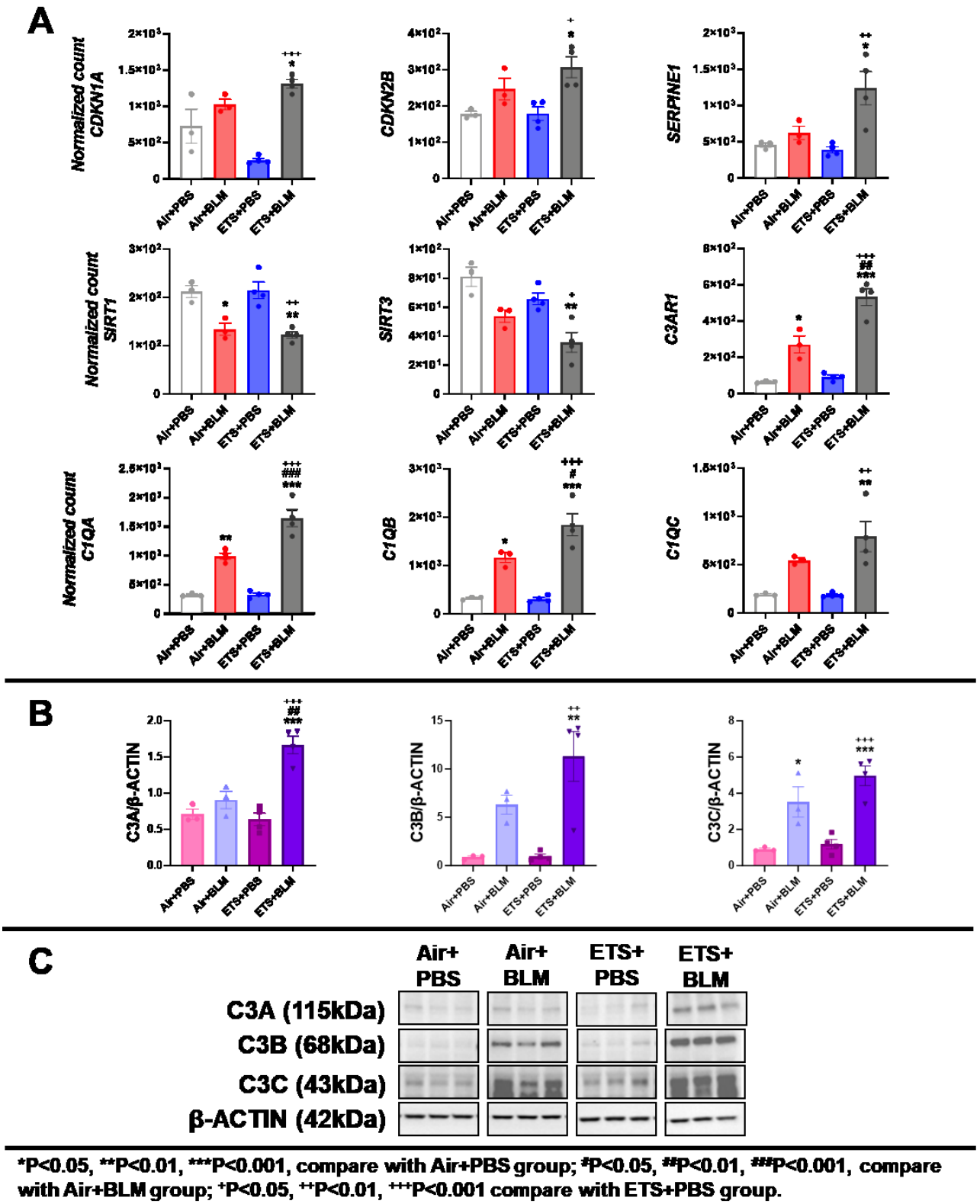

Figure 16: *(A) Total RNA isolated from the lungs was used to screen targets of interest. The expression of selected genes is reported with bar graphs. (B) Proteins were isolated from lung homogenates and C3 protein expression levels (C3A, C3B, and C3C) were analysed by Western blotting. (C) Blot images of each experimental group. Densitometry analyses are done individually, and β-ACTIN was used as endogenous control. Data are shown as mean ± SEM (n=3-4/group).*

COMPLEMENT SYSTEM ACTIVATION IN FIBROBLASTS CELLS LEADS TO A FIBROTIC PHENOTYPE

As previously reported in this thesis, the activation of the Complement system might have a relevant role in the early induction of senescence and therefore a potential role in pulmonary fibrosis progression.

In a pilot study, we investigated the role of C3 Complement component and receptor signalling in the activation of fibroblasts, and we demonstrated that the Complement system might have a key role in the activation of fibroblasts and their differentiation into myofibroblasts.

After 48 hours of treatment, NHLF exposed to C3 Complement component (Figure 17A) or C3aR antagonist (SB 290157) (Figure 17B) did not present a rise in the LDH release.

Of interest, 200nM C3 Complement component induced a noteworthy upregulation of *ACTA2* and *FN1* in these cells (Figure 17C).

We further confirmed that the activation of C3 pathway in fibroblasts is crucial to fibrosis progression by inhibiting his receptor (C3aR). A specific antagonist of C3aR (SB 290157) prompted a downregulation of the same genes previously evaluated (*COL1A1*, *ACAT2*, and *FN1*) in a dose-dependent manner (Figure 17D).

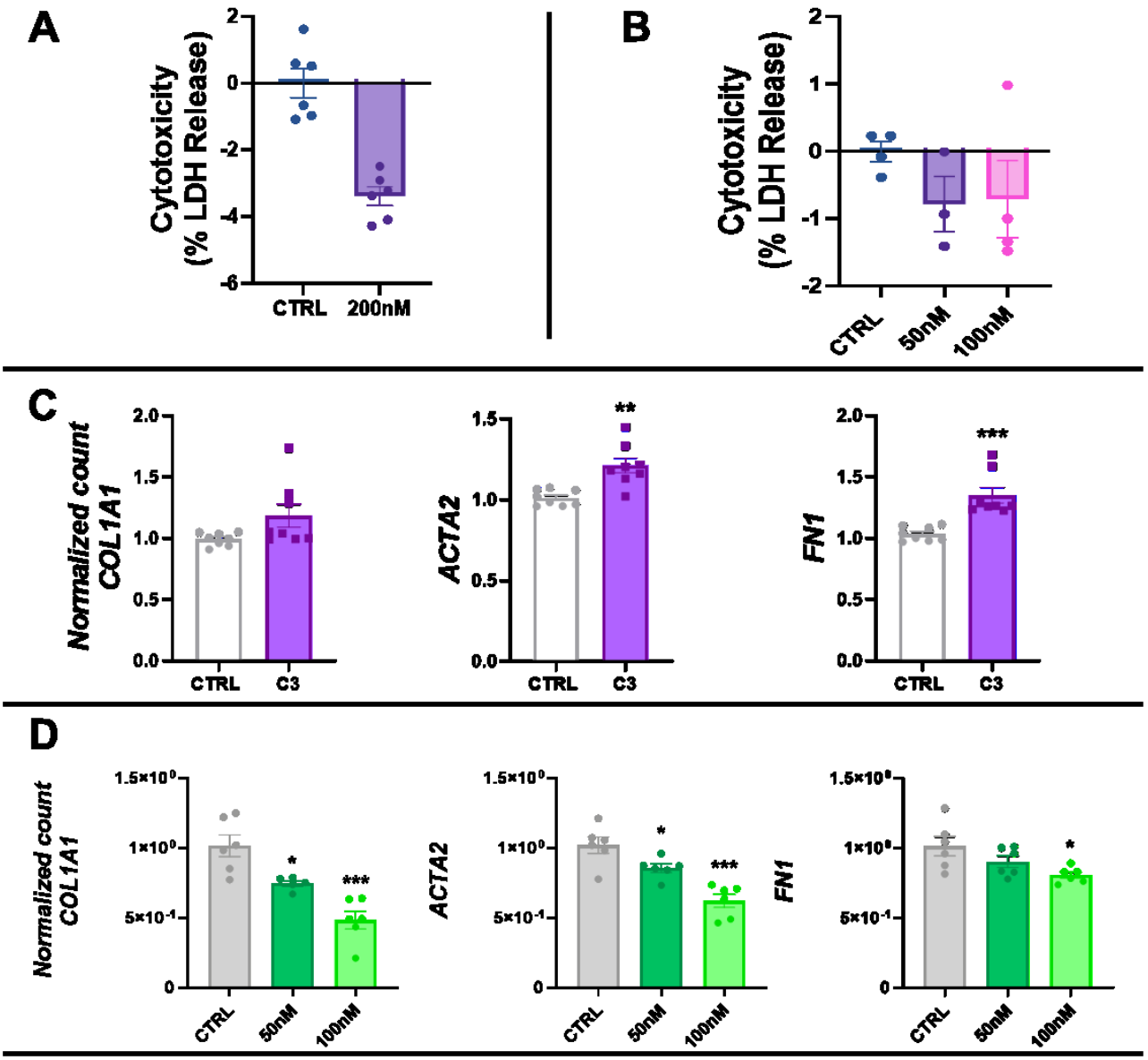

Figure 17: *The LDH release was measured in conditioned media from NHLF exposed to C3 Complement component (A) and SB290157 (C3a receptor antagonist) (B). RNA isolated from cells treated with C3 Complement component (C) or C3a receptor antagonist (D) was used to screen targets of interest (COL1A1, ACTA2 and FN1) via RT-PCR. GAPDH was used as the endogenous control. Data are presented as mean ± SEM (n=6-8/group).*

In addition, we investigated the capacity of this treatment to prompt fibroblasts transition to myofibroblasts with a double immunofluorescence (Figure 18). This analysis confirmed an increased expression of FIBRONECTIN after C3 treatment. We also observed some cells expressing alpha-smooth muscle actin (α-SMA), one of the principal markers used to identify myofibroblasts. A quantification of the intensity of the immunofluorescence is also reported in Figure 18. This result represents just a preliminary analysis; therefore, more investigations are required to complete this study. It is clear although a predominant role of innate immunity in the activation of fibroblast cells.

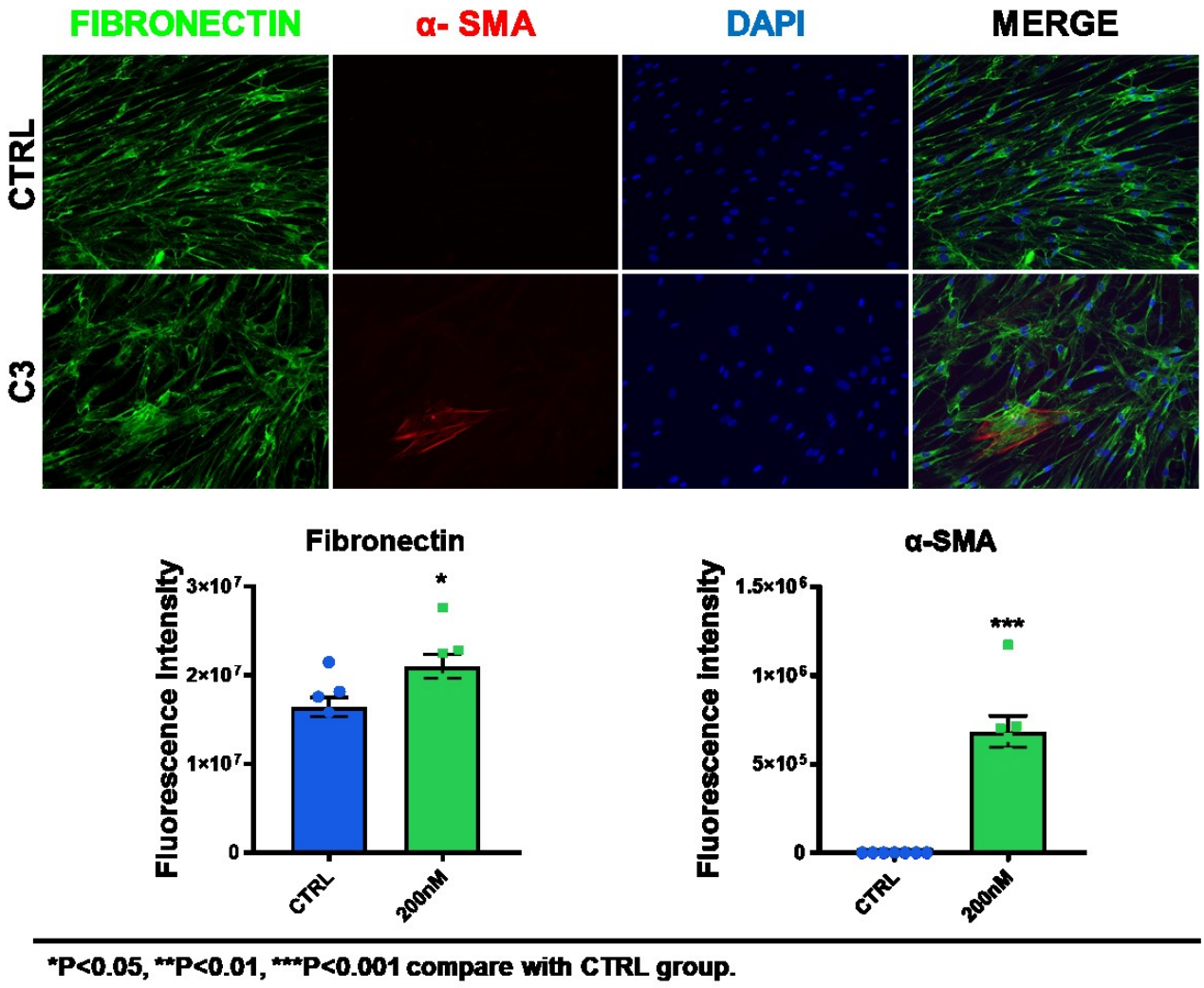

Figure 18: *NHLF cells were fixed, and stained with FIBRONECTIN (green) and α-SMA (red). Following the administration of C3 Complement component, few fibroblasts began expressing α-SMA and at the same time, the expression of fibronectin increased. The fluorescence intensity, quantified using FIJI ImageJ, is reported as bar graph. Data are shown as mean ± SEM (n=7/group).*

DISCUSSION

Environmental tobacco smoke (ETS) consists in a mixture of tobacco smoke from the side-stream of cigarettes and the exhaled smoke from active smokers. ETS has shown correlations with asthma and COPD development; so far, no clinical evidence showed how ETS exposure may favour fibrogenesis development [94, 95]. Notwithstanding, environmental tobacco smoke exposure is considered a risk factor for several respiratory conditions; moreover, evidences indicated that pre- and post-natal exposure to ETS may lead to poorer respiratory health [96].

Recent studies reported that cigarette smoke (CS) worsens the fibrotic progression induced by different agents such as bleomycin, lipopolysaccharides (LPS), and polyhexamethylene guanidine [97 - 100]. The exposure to CS further increased hydroxyproline and collagen deposition induced by bleomycin administration in different animal models [97, 98].

In our study, the pulmonary fibrosis observed after the administration of bleomycin was mildly intensifies by a short exposure to ETS. Of interest, the ETS exposure favoured the fibrogenesis induced by bleomycin, through collagen biosynthesis and modifications mediate by MMPs and LOX, and further activates the C3 Complement signalling [101].

Following BLM administration, increased collagen deposition was observed in lung lesion areas, withal, no additional collagen deposition was induced by ETS exposure (Figure 12). However, ETS is considered a low dose of tobacco smoke; thus, a longer exposure duration might be needed to develop more evident alterations, as observed in animals treated with cigarette smoke and bleomycin [98].

Several collagen types were taken into consideration, especially the ones known as pro-fibrotic. Subtypes of collagen IV were included in this analysis even though they are not

fibrillar collagens but components of basement membranes including the alveolar basement membrane (Figure 13).

COL4A1 and *COL5A3* genes recorded significantly increased RNA expression levels in ETS+BLM animals with respect to the Air+BLM group. Other collagen genes (*COL1A1*, *COL1A2*, *COL3A1*, and *COL4A2*) were found upregulated in the ETS+BLM group, although non-significantly when compared to Air+BLM (Figure 13). In addition, a significant increment of COL1A1 protein was found in animals exposed to ETS+BLM with respect to the Air+BLM group (Figure 14A).

In their work, Zhou and colleagues reported that the activation of the TGF-β/SMAD2 signalling pathway may be at the origin of the fibrotic process exacerbation mediated by cigarette smoke exposure [98]. We also evaluated the expression of TGF-β and its receptors in our study; even so, no significant modifications were acknowledged between Air+BLM and ETS+BLM groups. Additional study, with longer exposure to ETS, could shed more light on how ETS contributes to the fibrogenesis development. Other pathways might be already activated at the time point here analysed.

Our gene expression results showed further activation of ECM degradation, and collagen modifications. Therefore, our next goal was to assess the expression and activation of MMPs and lysyl oxidases, enzymes responsible for ECM remodelling (Figure 13). Among the MMPs, the protein expression levels of MMP2 was found increased either in animal models of lung fibrosis or fibrotic clinical samples [102]. In agreement with the previous work, bleomycin administration increased the expression of several MMPs genes in our study. We also demonstrate that ETS exposure further upregulated the active form of MMP2 protein; although, no significant differences were noticed in ETS+BLM compared to the Air+BLM group (Figure 14).

Another enzyme tested in this study is lysyl oxidase. This is a copper-dependent amine oxidase that helps to stabilize the ECM structure creating crosslink between collagen and elastin fibres [103]. In a previous work, an upregulation of lysyl oxidase was identified in bleomycin-induced lung fibrotic injury in mice and in the fibrotic areas of lung patients [104]. During fibrogenesis, an over activation of lysyl oxidases enzymes leads to severe crosslinking of collagen and elastin fibres, that contributes to irreversible scarring by avoiding degradation of fibrous matrix [105]. In this study, we first acknowledged that ETS exposure could alter the lysyl oxidase-mediated collagen dynamics, therefore causing an exacerbation of the fibrotic process. More specifically, the expression of *LOX*, *LOXL1*, and *LOXL2* genes were altered after the administration of bleomycin, although no significant differences were appreciated between the ETS+BLM and Air+BLM groups (Figure 13). However, a significant increase of active LOX protein was found especially in the fibrotic lesion areas in the ETS+BLM group with respect to the Air+BLM group, suggesting that ETS exposure influences bleomycin-induced upregulation of LOX (Figure 14).

As already mentioned, lung disorders like COPD and IPF are senescence/aging-related [106, 107]. The accumulation of senescent cells in the lungs promotes the spread of early senescence between neighbouring cells, but also allows the propagation of pulmonary fibrosis and airways remodelling. Thus, we customized a senescence-focused NanoString transcriptomic panel to assess whether the pathways associated with cellular senescence were altered by ETS exposure and bleomycin administration. The cellular senescence is established when molecular checkpoint systems responsible for DNA damage, cell cycle, apoptosis, and other routine cellular functions are disrupted and become irreversible [107, 108]. After bleomycin administration, we observed increased gene expressions of different cyclin-dependent kinase inhibitors (*CDKN1A*, and *CDKN2B*). Then, mice, previously exposed to ETS, showed a further non-significant increase of *CDKN1A* and *CDKN2B*

compared to Air+BLM animals (Figure 16A). CDKN1A encodes the protein p21, which can provoke cell cycle arrest by inhibiting CDK2 and CDK4 [109]. It is reported that both smoke exposure and bleomycin can increase *CDKN1A* in the alveolar epithelium [110]. In line with the previous study, our results further showed that ETS exposure could magnify bleomycin-induced *CDKN1A* upregulation. After bleomycin administration, *SERPINE1* gene showed a slight upregulation, but a noteworthy upward trend was found in the ETS+BLM group (Figure 16A). *SERPINE1* is known as a cellular senescence marker; however emerging data showed that this factor could be a mediator of cellular senescence [111]. In this regard, Jiang et al. demonstrated that *SERPINE1* increased p53 and p21 protein levels, and activated the p53-p21-Rb pathway, thus inducing alveolar epithelial cells type II senescence [111]. Therefore, the upregulation of *SERPINE1* observed in ETS+BLM group might have a key role in the onset of cellular senescence.

Of interest, a dysregulation of some members of Sirtuins family was also observed. The specific role of Sirtuins in cellular senescence is still debated; nonetheless, recent evidences suggested an essential role in delaying cellular senescence. Indeed, expression levels of SIRT1 and SIRT6 are decreased in cells exposed to oxidants, while an overexpression of these Sirtuins is correlated to a suppression of cellular senescence [112].

Among the family of NAD-dependent deacetylases, SIRT3 is the primary mitochondrial deacetylase that takes part in the regulation of numerous process by acetylating proteins involved in oxidative stress response, mitochondrial anti-oxidant response and respiratory chain [105, 106]. Curiously, evidences reported that mice knock-out for SIRT3 gene develop spontaneous fibrosis in lung associated with an increased synthesis of TGF-β [113, 114].

In our study, mice exposed to Air+BLM showed a downregulation of *SIRT1* and *SIRT3*; whereas, a further decrease was appreciated in mice treated with both agents (ETS+BLM) (Figure 16A).

Both these enzymes are physiologically involved in the process of ageing; thus, a reduction in the expression of *SIRT1* might be associated with a premature induction of senescence [85]. The combined exposure of mice to two agents able to induced oxidative stress and DNA damage further augments the downregulation of this enzyme, thus accelerating the onset of cellular senescence.

In a different study, a downregulation of SIRT3 in aging murine model of pulmonary fibrosis suggests that this NAD-dependent deacetylase plays a role in lung fibrogenesis during aging [114]. Moreover, Sundaresan and co-workers reported that hearts of 8-month-old SIRT3-KO mice showed higher levels of immature and mature forms of TGF-β1 and demonstrated a role of SIRT3 in regulating TGF-β1 synthesis [115]. Both these works support our results, since we only observed a major reduction of *SIRT3* expression in mice exposed to cigarette smoke and bleomycin. Moreover, the significant increment in the expression of TGF-β1 observed in mice exposed to ETS+BLM validated the role of SIRT3 on TGF-β1 regulation. Therefore, the combined stimulation performed in this work might be associated with an abnormal matrix remodelling but also an early induction of senescence.

Furthermore, the transcriptomic panel showed a peculiar and irregular activation of the Complement system, which lately has been suggested to play an important role during cellular senescence and aging [116]. Recently it has been demonstrated that Complement C3 expression levels are positively correlated with age, and an inhibition of C3 could prevent senescence progression in the renal system [117]. Several researchers studied the role of Complement system in emphysema and IPF development [118, 119]. For

instance, the removal of C3 or C3A receptor (C3AR) prevented inflammation and airspace enlargement caused by chronic smoke exposure [118]. In the same work, chronic CS exposure augmented the protein levels of C3 and C3AR [118]. Nonetheless, in our model the exposure to ETS did not alter the gene and protein expressions of C3A and C3AR. Probably, a longer duration of ETS exposure should be considered to activate C3 and C3AR. Another study showed an increased C3A protein expression after bleomycin treatment [119]. In particular, Gu et al. demonstrated that an increase of C3A and C5A proteins prompts the expression of FIBRONECTIN and α-SMA in lung fibroblasts, suggesting a role of the Complement system in fibroblasts transition to myofibroblasts [119]. Our results agreed with the increased expression of C3 and C3AR observed following the administration of bleomycin (Figure 16A). Moreover, we identified that ETS exposure intensifies the bleomycin-induced activation of C3AR. Of interest in our study, C3A protein expression levels showed a significant increase in ETS+BLM compared to Air+BLM (Figure 16B).

However, a limited number of canonical factors associated to cellular senescence were significantly dysregulated in our model. Thus, increasing the duration of ETS exposure and evaluating the BLM-induced lung injury at longer time points could confirm and further extend the information that we already have about the role these cellular senescence mediators.

In conclusion, we showed that ETS exposure exacerbated bleomycin-induced overproduction of collagen subtypes and lysyl oxidase enzymes. Moreover, these results suggest that ETS exposure not only activated the TGF-β/SMAD2 pathway but also C3A-receptor signalling. Of note, the latter might be a crucial factor involved in the collagens dysregulation and in an earlier onset of cellular senescence.

As demonstrated in the previous animal model, the Complement system might have a relevant role in an early induction of senescence and in pulmonary fibrosis progression. For this purpose, a pilot study was conducted to evaluate the effects of C3 Complement component on primary human lung fibroblasts (NHLF).

The Complement system plays a crucial role in innate and adaptive immune responses. The activation of this system may occur through three different pathways: classical, lectin and alternative [116]. All three pathways converge to form effector molecules (i.e., C3 convertase) and generating a large numbers of activated Complement proteins with different biological functions (i.e., opsonisation, chemoattraction, and cell lysis through pore formation) [120].

The Complement system is associated with several inflammatory lung conditions including asthma and COPD [121]. The most potent chemotactic responses in acute inflammation are provided by Complement protein 3 (C3); but, more importantly, the active form, C3a, develops allergic lung inflammation and it is essential in acute pneumonia, by binding its receptor (C3aR) on dendritic cells [118]. In addition, Yuan and colleagues revealed a deep involvement of the Complement system in a cigarette smoke-induced model of emphysema. The release of the active cleaved products of C3 binds the C3aR on neutrophils and macrophages creating a positive feedback loop, with an upregulation of C3aR on neighbouring cells [118].

Previous studies have also reported a Complement activation in patients with IPF [121 - 123]. In line with this evidences, Gu H et al. demonstrate that both C3a and C5a components have a profibrotic role in IPF lung [119].

In our study, following 48-hours stimulation with C3 Complement component, normal human lung fibroblast (NHFL) responded with an upregulation of *COL1A1*, *FN1* and *ACTA2* genes, revealing an activation of these cells and possibly a transition to

myofibroblasts (Figure 17C). The double immunofluorescence against FIBRONECTIN and alpha-smooth muscle actin (α-SMA) antigens further attested an initial stage of fibroblasts differentiation (Figure 18). These results confirmed what Gu H and colleagues observed in a different model of 24-hours exposure to C3a or C5a fragment [119].

These evidences suggest that the activation of immune systems in lungs not only represent a first defence, but also may play a crucial role in maintaining a profibrotic environment. As a matter of fact, anaphylatoxins Complement components, commonly secreted and activated by immune cells in lungs, activate fibroblasts cells by binding to specific receptors. From this perspective, we evaluated if a blockage of C3a receptor (C3aR) might prevent the activation and differentiation of fibroblasts in our model [119].

In our preliminary study with NHLF, we observed a dose-dependent reduction in the expression of *COL1A1*, *FN1* and *ACTA2* genes after the administration of a potent C3aR antagonist (Figure 17D). The downregulation of these genes highlights how the continuous activation of the Complement system might promote fibroblasts activation and pulmonary fibrosis progression. Besides, inhibiting Complement protein receptors might be a useful tool to avoid a constant activation of a major source of inflammation [124].

In conclusion, we demonstrated that primary human lung fibroblasts (NHLF) are induced to differentiate into myofibroblasts just after 48 hours of treatment with C3 Complement component. Moreover, the blockade of C3aR induced a significant downregulation of genes associated to fibroblasts differentiation. These evidence confirm the essential role of the Complement system in fibroblasts activation and consequently pulmonary fibrosis progression.

Evidently, more analyses are required to better understand to what extent the Complement system activation is responsible for the instauration and perpetuation of lung fibrosis; however, its involvement is undoubted. Hence, future studies might show that the inhibition

of the Complement system is an excellent tool to slow or even arrest the progression of fibrosis.

SUMMARY

Tobacco smoke is known to be one of the major risks associated with chronic lung diseases. Recently, the environmental tobacco smoke (ETS) gain more attention, since its ability to induce inflammatory responses and lung injuries. However, how ETS exposure augments fibrogenesis is yet to be defined. In this chapter a new model of lung fibrosis was presented and it was reported that the sub-chronic exposure to ETS favours the fibrogenesis induced by bleomycin (BLM) administration.

The previous exposure to ETS already induced a dysregulation of collagen synthesis and degradation, which was then enhanced by BLM administration. The observed alterations in the extracellular matrix (ECM) dynamics were accompanied by the dysregulation of enzymes in charge of ECM organization (LOXs and MMPs).

Moreover, ETS exposure contributed to augment the premature senescence induced by BLM through the activation of the complement system and the dysregulation of other senescence markers (CDKN1A, SIRT1, SIRT3), suggesting that occupational ETS exposure could aggravate the severity of fibrotic lung disease.

In this regard, a pilot study was conducted to better evaluate the role of the complement system activation in normal human lung fibroblasts (NHLF). The results demonstrated that the activation of the complement system signalling leads to fibroblast differentiation into myofibroblasts and an upregulation of collagen and fibronectin. Overall, these data suggested a relevant role of the Complement in the early onset of cellular senescence and a potential role in pulmonary fibrosis progression.

CHAPTER 3

AIM OF THE STUDY

In this study, we evaluated the combined effects of two agents, namely cigarette smoke and TGF-β, in normal human lung fibroblasts (NHLF). Fibroblasts are one of the main cell populations involved in the fibrogenesis. Thus, the goal of this study was to reproduce a model characterized by the dysregulation of the same pathways already observed in the *in vivo* model, where mice were exposed to environmental tobacco smoke (ETS) and bleomycin (BLM).

MATERIALS AND METHODS

CELL CULTURE AND TREATMENTS

Primary human lung fibroblasts (NHLF) (Cat# CC-2512) were purchased from Lonza (Lonza, Morristown, NJ, USA). Lung fibroblasts were cultured in FGM-2 Fibroblast Growth Medium (Cat# CC-3132, Lonza, Morristown, NJ, USA) and maintained under 5% CO_2 and 95% humidity.

First, NHLF cells were seeded into 6 and 12 well plates ($5.0x10^5$ cells/well and $2.5x10^5$ cells/well respectively), after 24 hours, the cells were serum deprived for at least 6 hours before starting the treatments which were conducted in a serum-free media. Fibroblast cells were treated either with 0.5% of cigarette smoke extract (CSE) or 2.5 ng/ml recombinant human TGF-β protein (Abcam, Cambridge, UK) or both for a total of 72 hours. A detailed scheme of treatments is reported in Figure 19. At the end of the experiment, the cells were either lysed for RNA and protein quantification or fixed with 4% paraformaldehyde for immunofluorescence staining.

Figure 19: Schematic representation of cell treatments.

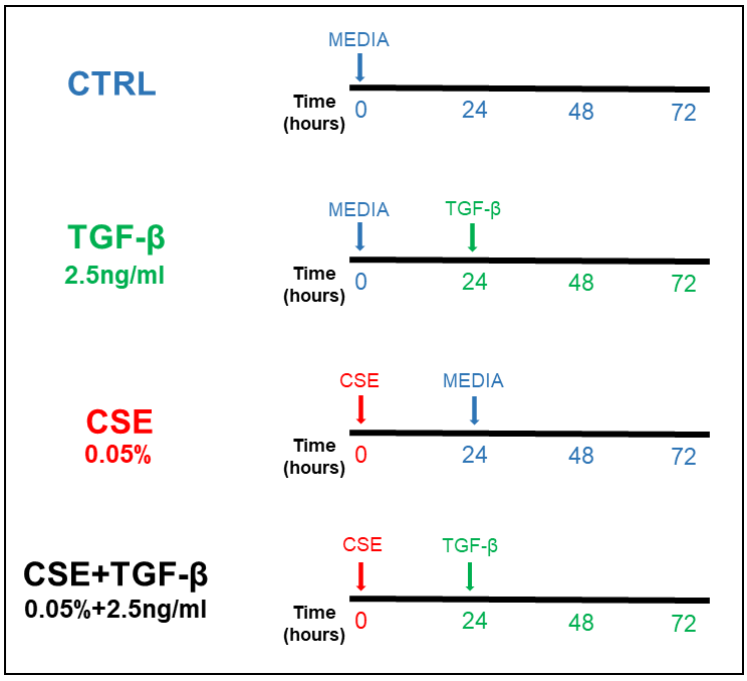

CIGARETTE SMOKE EXTRACT

Cigarette smoke extract (CSE) was prepared as previously described [125]. In brief, one cigarette (3R4F, University of Kentucky, KY, USA) was bubbled into 10 ml of culture media without fetal bovine serum (FBS). This represented the 10% CSE stock solution, that was standardized by measuring absorbance at 320 nm (OD= 1.00 ± 0.05) after being sterile-filtered with a 0.45 μm filter (Avantor, Radnor, PA, USA). Different concentrations of CSE were evaluated; finally, fibroblast cells were treated with 0,05% CSE for 24 hours. At the end of the treatment, media was removed and each well was washed with phosphate buffer saline (PBS). New serum-free media was added and then cells were collected at the end of the experiment (Figure 19).

LACTATE DEHYDROGENASE CYTOTOXICITY ASSAY

Lactate dehydrogenase (LDH) was quantified to assess the cytotoxicity of single and combine treatment (i.e. TGF-β, CSE and CSE+TGF-β). At the end of 72 hours' treatment, the conditioned media was collected and immediately place on ice. The release of LDH from damaged cells was determined by using the Cytotoxicity Detection Kit ^{PLUS} (LDH) (Roche Diagnostic Corporation, Indianapolis, IN, USA). In brief, a 96-well plate was loaded with 50 μL of each sample in duplicate, then 100 μL of reaction mixture was added and incubated at room temperature for 15 minutes. The incubation time was stopped by adding in each well 50 μL of stop solution. Absorbance was recorded at 490 nm using a microplate spectrophotometer system.

CYTOKINES RELEASE BY LUMINEX ASSAY

Release of cytokines and mediators in culture media were assessed with Bio-Plex Pro Human 27-Plex assay (Cat# M500KCAF0Y, BioRad, Hercules, CA, USA). Each sample

was diluted 1:4 with sample diluent, and the assay was performed accordingly to manufacturer's instructions. First, 50 µL of capture antibody-coupled beads were added in each well, then 50 µL of samples and standards were loaded and the plate was incubated for 30 minutes. After the recommended washing step with wash buffer, detection antibody was added and incubated for 30 minutes at room temperature. The same steps were followed before the incubation with streptavidin-PE. Lastly, the beads were resuspended in 125 µL of assay buffer. The plate was read on a FLEXMAP 3D System (Luminex, Austin, TX, USA). Results were obtained comparing treated groups with control. Data that showed a significant difference were plotted in a bar graph.

RNA ISOLATION AND qPCR

After 72 hours, cells were washed with PBS and incubated for 15 minutes at room temperature with QIAzol lysis reagent (Cat# 79306, Qiagen, Germantown, MD, USA). The RNA isolation was performed using the miRNeasy Mini Kit following the manufacturer's instructions (Cat# 217004, Qiagen, Germantown, MD, USA). In detail, the content of each well was collected and mixed with chloroform for 10 seconds. Then, the mixtures were centrifuged at 20,000 × *g* for 30 min, at 4 °C. Eventually, the aqueous phase was recovered and transferred to a new tube, to which was added with 1.5 of its volume of 100% ethanol. The samples were transferred to RNeasy Mini spin columns placed in a 2ml collection tube and centrifuge at 8,000 × *g* for 15 seconds at room temperature. After discarding the flow-through, 700 µL of Buffer RWT was added to each tube and centrifuge at 8,000 × *g* for 15 seconds to remove impurities. After discarding the flow-through, the same process was repeated two times for Buffer RPE. 500 µL of Buffer RPE were added each time and centrifuge at 8,000 × *g* for 15 seconds and 2 minutes respectively. Lastly, the mini columns were transferred to new 1.5mL tubes and in each column was added 50 µL of RNase free

water. Samples were centrifuge at 8,000 × *g* for 1 minute and then the concentrations and qualities of RNA were measured with Nano-drop spectrophotometer ND-1000 (NanoDrop Technologies, Wilmington, DE, USA).

cDNA synthesis was performed with RT^2 First Strand Kit (Qiagen, Germantown, MD, USA). For each sample 200ng of cDNA were used for real-time PCR quantification using RT^2 SYBR Green Fluor qPCR Mastermix, accordingly to instructions (Cat# 330513, Qiagen, Germantown, MD, USA). The pre-designed primers used in this study were: COL1A1 (Human, qHsaCED0043248), COL1A2 (Human, qHsaCED0003988), COL3A1 (Human, qHsaCED00046560), COL4A1 (Human, qHsaCID0010223), ACTA2 (Human, qHsaCID0013300), FN1 (Human, qHsaCID0012349), ELN (Human, qHsaCED0056732), LOX (Human, qHsaCID0007213), LOXL1 (Human, qHsaCID0006309), LOXL2 (Human, qHsaCED0044522), and GAPDH (Human, qHsaCED0038674). All primers were purchased from BioRad. mRNA expression of each gene was assessed with the following qPCR thermal cycle: 10 minutes at 95 °C, 40 cycles of 95 °C (15 seconds) and 60 °C (1 minute).

At the end, a melting curve was performed to check cDNA amplification quality. The BioRad CFX96 qPCR detection system was used, and data were presented as fold change, calculated based on $2^{-\Delta\Delta Ct}$ methods with GAPDH as housekeeping control.

NANOSTRING MEASURMENT

20ng of each RNA samples were used for NanoString analysis. In this study, we used the personalized nCounter Senescence Panel (NanoString Technologies, Inc., Seattle, WA, USA). More in detail, the hybridization reaction solution was prepared by mixing reporter codeset, and hybridization buffer. 8 µL of the reaction mixture was transferred in each tube where 5 µL of each samples were added. Next, 2 µL of capture codeset was added to

each sample. The mixtures were incubated at 65°C for 16 hours and stored at 4°C until further profiling. All the sample mixtures were loaded onto the NanoString running cartridge and then the gene expression profiling was performed via nCounter SPRINT Profiler (NanoString Technologies, Inc., Seattle, WA, USA). Gene expression results were analysed by nSolver 4.0 software, and reported as normalized count.

IMMUNOBLOTTING

Protein concentration from cell lysates was quantified by Pierce BCA Protein Assay (Cat# 23225 Thermo Fisher Scientific, Waltham, MA, USA). For each sample 20 µg of protein were separated on 4%-15% precast gels (Cat# 5671084, BioRad, Hercules, CA, USA). Following the electrophoresis, the separated proteins were transferred onto a nitrocellulose membrane (Cat# 1704159, BioRad, Hercules, CA, USA). After a wash with tris buffer saline containing 0.1% Tween 20 (TBS-T), the membranes were blocked for 1 hour at room temperature with 5% BSA, and then incubated overnight at 4°C with primary antibodies. The membranes were probed with: rabbit anti-Collagen 1α1 (1:1000, Novus Biologicals, Centennial, CO, USA); rabbit anti-LOX (1:1000, Abcam, Cambridge, UK); rabbit anti-fibronectin (1:1000, Abcam, Cambridge, UK); rabbit anti-αSMA (1:1000, Cell Signaling Technologies, Danvers, MA, USA); rabbit anti-SMAD2 (1:1000, Abcam, Cambridge, UK); rabbit anti-pan AKT (1:1000, Abcam, Cambridge, UK); rabbit anti-phospho-AKT1 (1:1000, Abcam, Cambridge, UK); rabbit anti phosphor-p44/42 MAPK (ERK 1/2) (1:1000, Cell Signaling Technologies, Danvers, MA, USA).

Following the overnight incubation, every membrane was washed three times with TBS-T and then probed with secondary antibody goat anti-rabbit IgG (H+L) HRP-conjugated (1:5000, BioRad, Hercules, CA, USA). At the end, a chemiluminescence substrate was used to detect bound complexes. Band density was calculated with Image Lab software

(v4.1, BioRad, Hercules, CA, USA), and expressed as fold change compared to control group. GAPDH was used as endogenous control (1:1000, Abcam, Cambridge, UK).

DOT BLOT

The amount of collagen released from NHLF cells was estimated with Bio-Dot Microfiltration Apparatus (BioRad, Hercules, CA, USA). Before assembling the apparatus, nitrocellulose membranes were soaked in tris buffer saline (TBS) for 10 minutes. Next, the membranes were laid on the gasket, and all the elements were assembled. Every well was filled with 30 µL of sample in duplicate and the volume was allowed to flow through the membrane by gravity. After 45 minutes, the membrane was removed from the gasket and blocked with 5% bovine albumin serum (BSA) for 1 hour at room temperature. Then, primary antibody rabbit anti-Collagen 1α1 (1:1000, Novus Biologicals, Centennial, CO, USA) was incubated overnight at 4°C. The following day, the membrane was probed with an appropriate secondary antibody goat anti-rabbit (H+L) HRP-conjugated (1:5000, BioRad, Hercules, CA, USA). Dots were detected with a chemiluminescence substrate. Image Lab software (v4.1, BioRad, Hercules, CA, USA) was used to perform the analysis, and data were reported as fold change compared to control group.

IMMUNOFLUORESCENCE

NHLF cells were seeded in chamber slides, and treated as reported in Figure 19. At the end of the treatment, fibroblasts were fixed with 4% paraformaldehyde for 15 minutes at room temperature. The wells were washed two times with tris buffer saline (TBS), and then blocked with 10% normal goat serum. Cells were incubated with the following antibodies: rabbit anti-fibronectin (1:50, Abcam, Cambridge, UK) and mouse anti-αSMA Alexa Fluor 594 conjugated (5 µL/10^6 cells, R&D System, Minneapolis, MN, USA) at 4 °C, overnight.

After at least 16 hours, the coverslips were washed with TBS three times and incubated with donkey anti-rabbit IgG (H+L) secondary antibody Alexa Fluor 488 (1:1000, Thermo Fisher Scientific, Waltham, MA, USA) for 1 hour at room temperature on a rocker. Following three washes, the slides were mounted with Prolong Diamond Antifade Mountant with DAPI (Life Technologies, Carlsbad, CA, USA). Images were acquired via a fluorescence microscopy.

ImageJ was used to quantify the fluorescence intensity with the following equation: integrated Density (IntDen) − (Area of cells * Mean fluorescence of background).

STATISTICAL ANALYSIS

All data were analysed through one-way ANOVA using GraphPad Prism software version 9.0 (GraphPad, San Diego, CA, USA). Results were presented as mean ± SEM and $P<0.05$ was considered significant.

RESULTS

AUGMENTED RELEASE OF CYTOKINES AND CHEMOKINES AFTER CSE AND TGF-β TREATMENTS

To determine the effects of TGF-β and CSE treatments, NHLF cells were seeded into 6 or 12-well plates and allowed to reach confluence.

2.5 ng/mL of TGF-β and 0.05% of CSE did not increase LDH release at 72 hours' post-treatment, whereas the combined exposure to these agents led to just a small increment of LDH release (1.95%) (Figure 20A).

NHLF cells released a different amount of cytokines and chemokines in response to specific treatments. After TGF-β administration, a statistically significant upregulation of interleukins like 6 (IL-6) and 8 (IL-8), monocyte chemoattractant protein 1 (MCP-1), and the macrophage inflammatory protein 1β (MIP-1β) was evident with respect to the control group (CTRL) (Figure 20B).

CSE exposure did not affect the expression levels of IL-6, IL-8 and MIP-1β when compared to CTRL group; the only exception was represented by MCP-1, which resulted more expressed in CSE exposed cells (Figure 20B).

The combined treatment (CSE+TGF-β) displayed a significant increment of the cytokine and chemokines evaluated, with respect to the CTRL group. The only exception was represented by the MIP-1β, where the upregulation was not significant when compare to CTRL group (Figure 20B).

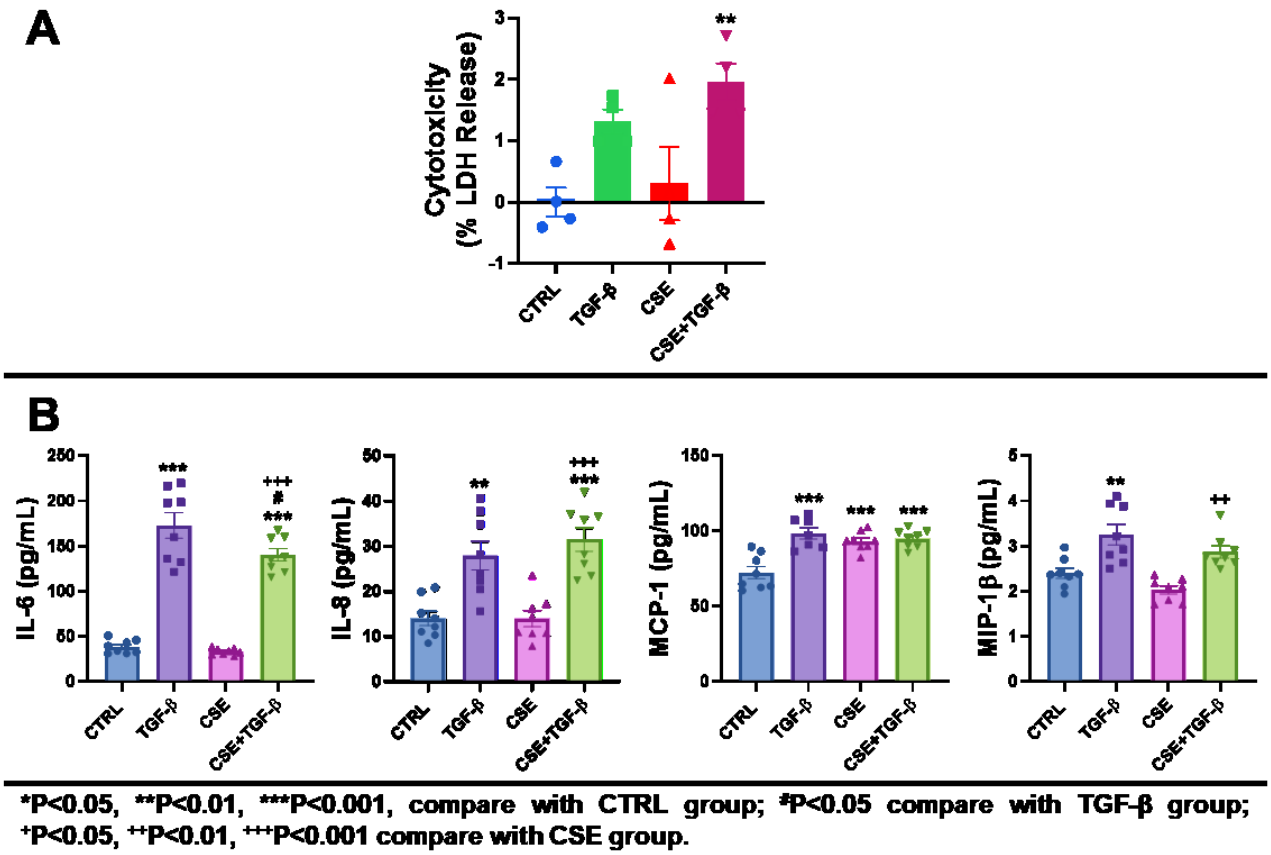

Figure 20: *(A) The LDH release was measured in conditioned media from each group and reported in the bar graph (n=4/group). (B) Likewise, the release of IL-6, IL-8, MCP-1 and MIP-1β was quantified with a Bio-Plex Pro Human 27-Plex assay. Data are presented as mean ± SEM (n=8/group).*

EXPOSURE TO CSE REDUCES THE EXPRESSION OF GENES AND PROTEINS ASSOCIATED TO FIBROBLASTS ACTIVATION WHEN COMBINED WITH TGF-β

To determine the role of smoke exposure associated to TGF-β-induced effects, RNA was isolated from treated cells, and fibrotic genes were measured via RT-PCR. As shown in Figure 21A, TGF-β increased mRNA expression of several collagens *COL1A1* (2.33-fold change), *COL1A2* (1.74-fold change), *COL3A1* (1.43-fold change), *COL4A1* (2.10-fold change) with respect to the control group. Likewise, other genes involved in ECM remodelling resulted upregulated following the exposure to TGF-β; *LOX* (1.75-fold change), *FN1* (2.21-fold change), and *ELN* (3.11-fold change) genes presented a significant increased expression in comparison to control group (Figure 21A). Fibroblast cells treated with TGF-β also exhibited a statistically significant increase in *ACTA2* expression levels with respect to the CTRL group (2.31-fold change) (Figure 21A). CSE exposure alone did not influence the mRNA levels of the upper mentioned genes; the only exception was represented by *COL3A1* which resulted downregulated as opposed to the control group (Figure 21A). When CSE was combined with TGF-β, collagens gene levels (*COL1A1*, *COL1A2*, *COL3A1*, *COL4A1*), as well as *LOX*, *FN1*, *ELN*, and *ACTA2* were significantly upregulated with respect to the control group (Figure 21A). Notwithstanding, *COL1A1*, *COL1A2*, *COL3A1*, and *LOX* genes resulted significantly downregulated in comparison to TGF-β group (Figure 21A). *ACTA2* and *COL4A1* expression levels seemed to be slightly lower than the ones observed for TGF-β treated-cells (Figure 21A). On the other hand, the combined treatment with CSE and TGF-β did not influence the expression of *FN1* and *ELN* genes whit respect to the TGF-β group (Figure 21A).

To further investigate the effects of the combined exposure of fibroblasts to CSE and TGF-β we evaluated the expression of proteins chiefly involved in ECM remodelling and fibroblasts activation via immunoblot.

Firstly, collagen biosynthesis and release were evaluated. Surprisingly, endogenous levels of COL1A1 protein were not affected by either TGF-β or CSE treatments. As a matter of fact, no differences were appreciated between each group and the control one (Figure 21B).

At the same time, a more in-depth analysis on collagen release from fibroblasts was performed via dot blot. Here, we noted a major release of COL1A1 induced by TGF-β, when compared to control group. Although no significant changes between TGF-β and CSE+TGF-β groups were depicted. CSE exposure did not influence the collagen release whit respect to the CTRL group (Figure 21D). Although these data are not in line with the COL1A1 protein expression, they might be justified since the immunoblot evaluated the expression of the endogenous protein, while the dot blot assessed the amount of collagen released in the media.

In Figure 21B LOX expression is also reported. The expression levels of this protein were similar in every group, without any variations. Of note, the active form of this enzyme resulted particularly expressed in NHLF cells treated with TGF-β, when compared to CTRL group. The only exposure to CSE did not influence the expression of the active-LOX. Unexpectedly, the exposure to both CSE and TGF-β resulted in a lower expression of the active-LOX when compared to TGF-β group. Although, fibroblasts treated with CSE+TGF-β presented higher expression levels of active-LOX whit respect to the CTRL group (Figure 21B).

The expression of alpha smooth muscle actin (α-SMA) protein was also tested. As reported in Figure 21B, cells exposed to CSE did not show a significant variation of α-SMA when compared to CTRL group. A statistically significant increment of α-SMA expression was only evident in cells exposed to TGF-β (Figure 21B). Surprisingly, the additional

exposure to CSE significantly downregulated the expression of α-SMA with respect to the TGF-β group. (Figure 21B).

Of interest, FIBRONECTIN expression levels of every treated groups were higher than control group. However, the combined administration of CSE and TGF-β was the only treatment able to induce a significant rise in the expression of this protein (Figure 21B). Blot images are reported in Figure 21C.

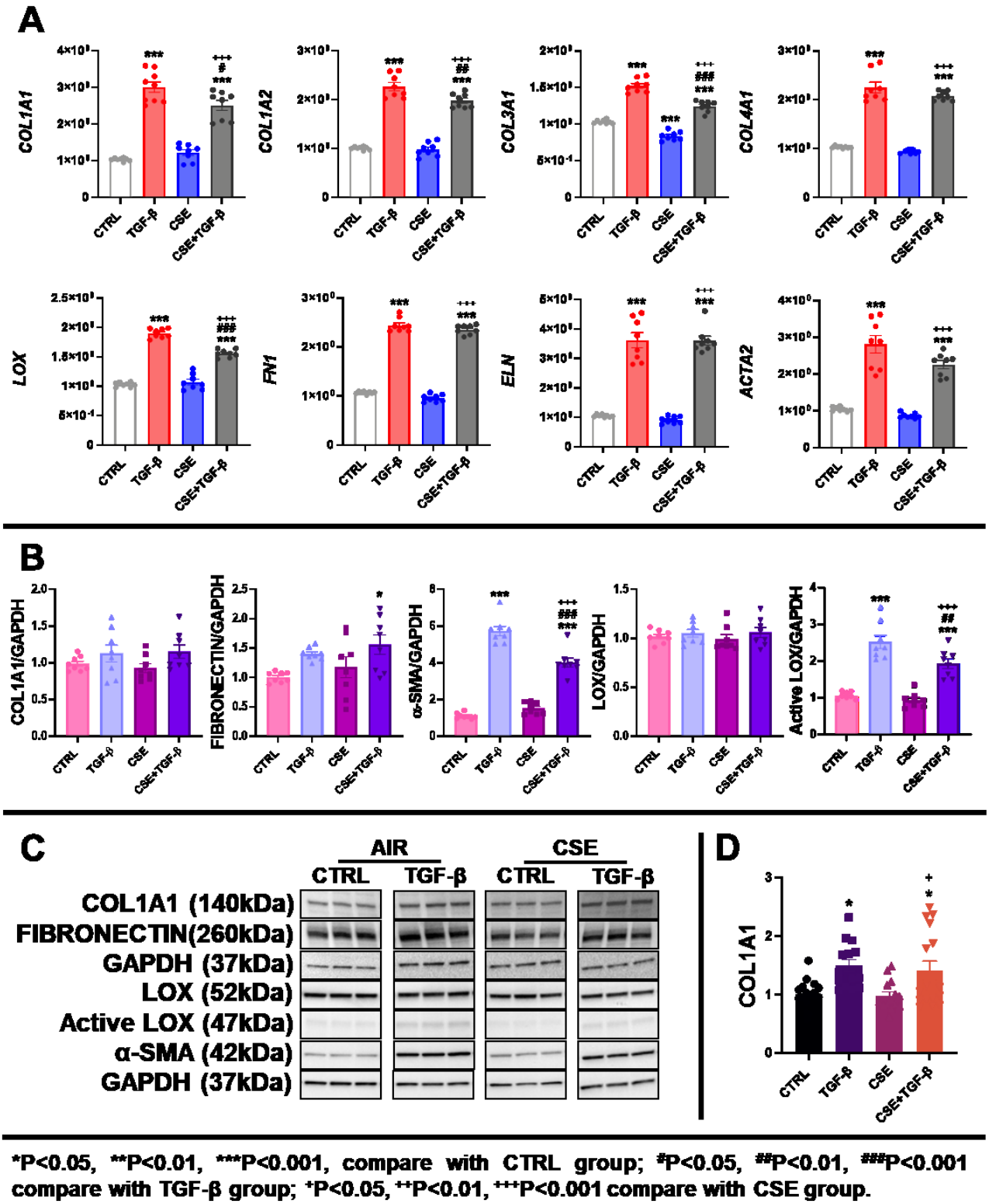

Figure 21: *(A) RNA isolated from cells was used to screen targets of interest* via RT-PCR. *GAPDH was used as the endogenous control. (B) Protein expressions were analysed by Western blotting from cell lysate. (C) Blot images of each experimental group. Densitometry analyses are done individually, and GAPDH was used as the endogenous control (n=8/group). (D) COL1A1 release from NHLF cells was quantified via dot blot analysis (n=15/group). Data are presented as mean ± SEM.*

A double immunofluorescence was performed to investigate the different distribution of α-SMA and FIBRONECTIN proteins. The results are reported in Figure 22 together with a quantification of the fluorescence intensity. Fibroblasts cells in CTRL and CSE groups did not express α-SMA. Instead, TGF-β induced a great expression of α-SMA already after 48 hours of treatment. Withal, this analysis depicted a marked decrease of α-SMA positivity in CSE+TGF-β cells (Figure 22). FIBRONECTIN expression increased after every treatment with a significant upregulation with TGF-β administration either with or without CSE (Figure 22). The immunofluorescence analysis corroborated the previous results.

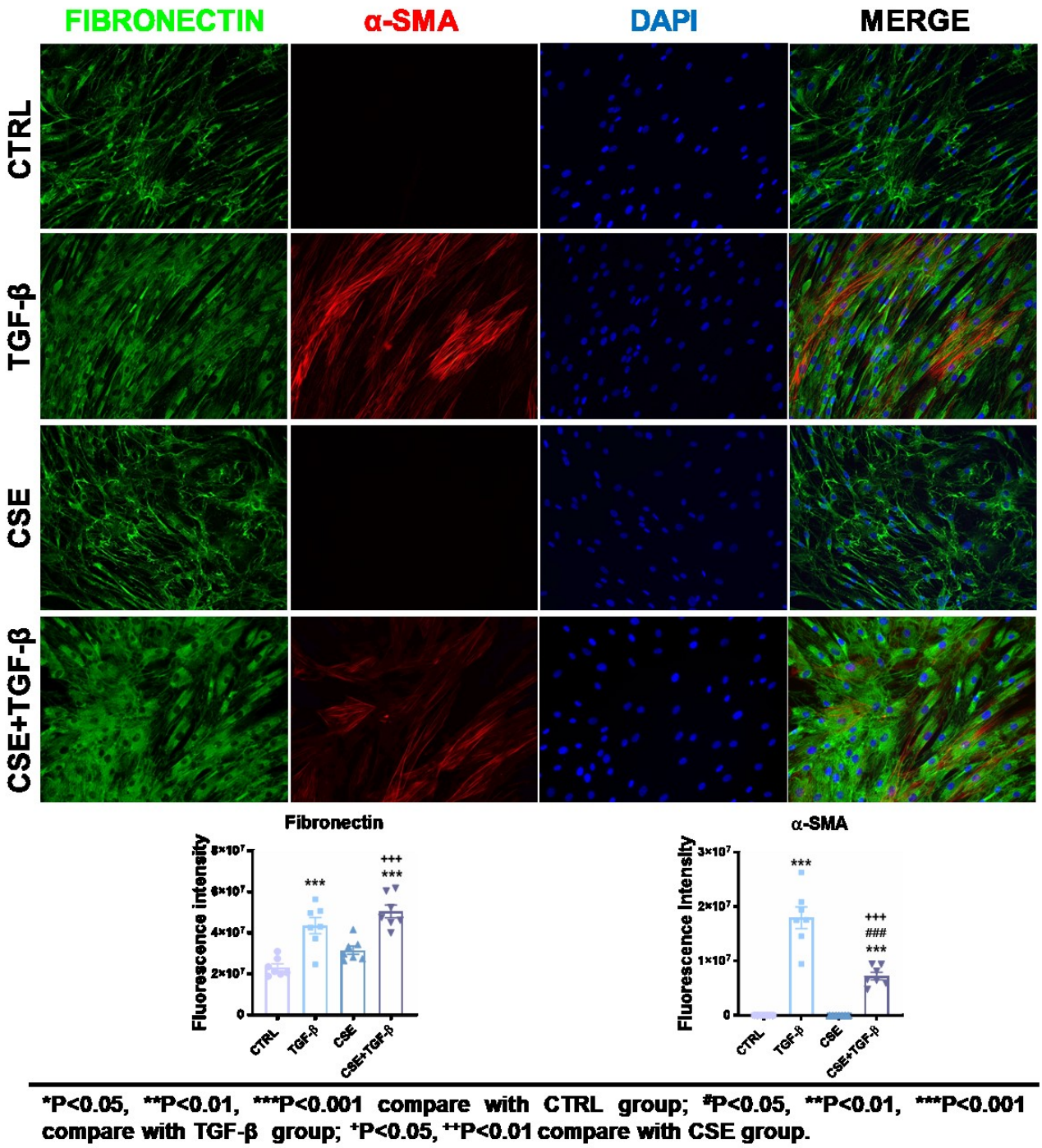

Figure 22: *NHLF cells were fixed, and stained with FIBRONECTIN (green) and α-SMA (red). The immunofluorescence revealed a great number of fibroblast expressing α-SMA and a significant increase in the expression of fibronectin following TGF-β treatment. The fluorescence intensity, quantified using FIJI ImageJ, is reported as bar graph. Data are shown as mean ± SEM (n=7/group).*

TGF-β DOWNSTREAM EFFECTORS WERE NOT ACTIVATED WITH COMBINED EXPOSURE TO CSE AND TGF-β

In this study, the initial hypothesis was that CSE exposure would enhance the fibrotic response of fibroblasts exposed to TGF-β. Notwithstanding, results obtained in our experimental conditions highlighted a possible interference between smoke exposure and TGF-β administration. Thus, further analyses were conducted in order to identify whether pathways, usually involve in fibroblasts activation, were negatively affected by the combination of these agents.

RNA was isolated from treated cells, and genes associated to TGF-β pathways were measured via NanoString profiling. As reported in Figure 23A, smoke exposure did not induce significant alterations of *AKT1*, *mTOR*, *PIK3CA* and *SMAD2* genes compared to control group. Of note, after TGF-β stimulation, the expression of these genes was lower than CTRL group. Likewise, CSE+TGF-β treatment induces a downregulation of *AKT1*, *mTOR*, *PIK3CA* and *SMAD2* genes, when compared to control group (Figure 23A).

Next, we evaluated the protein expression of downstream effectors of TGF-β like SMAD2, p-AKT1, pan-AKT1 and ERK1/2. Of interest, p-AKT1, pan-AKT1 and ERK1/2 presented a different trend from what was observed with the gene expression in the different experimental groups (Figure 23B). More in detail, TGF-β significantly upregulated the expression of p-AKT1, pan-AKT1, and ERK1/2 proteins with respect to the control group (Figure 23B). Smoke exposure induced an upregulation of ERK1/2 proteins, while the combined administration of these agents (CSE+TGF-β) did not prompt any rise with respect to the control group (Figure 23B).

We did not observe significant variation of SMAD2 protein expression at the different experimental conditions (Figure 23B). Even though, we cannot exclude a prime role of this

pathway, especially because we did not evaluate the expression of the phosphorylated form of SMAD2.

Unfortunately, so far, these data do not allow us to identify a specific pathway affected, especially if we think about the huge plethora of receptors, co-receptor and signalling activated by TGF-β. Blot images are reported in Figure 23C.

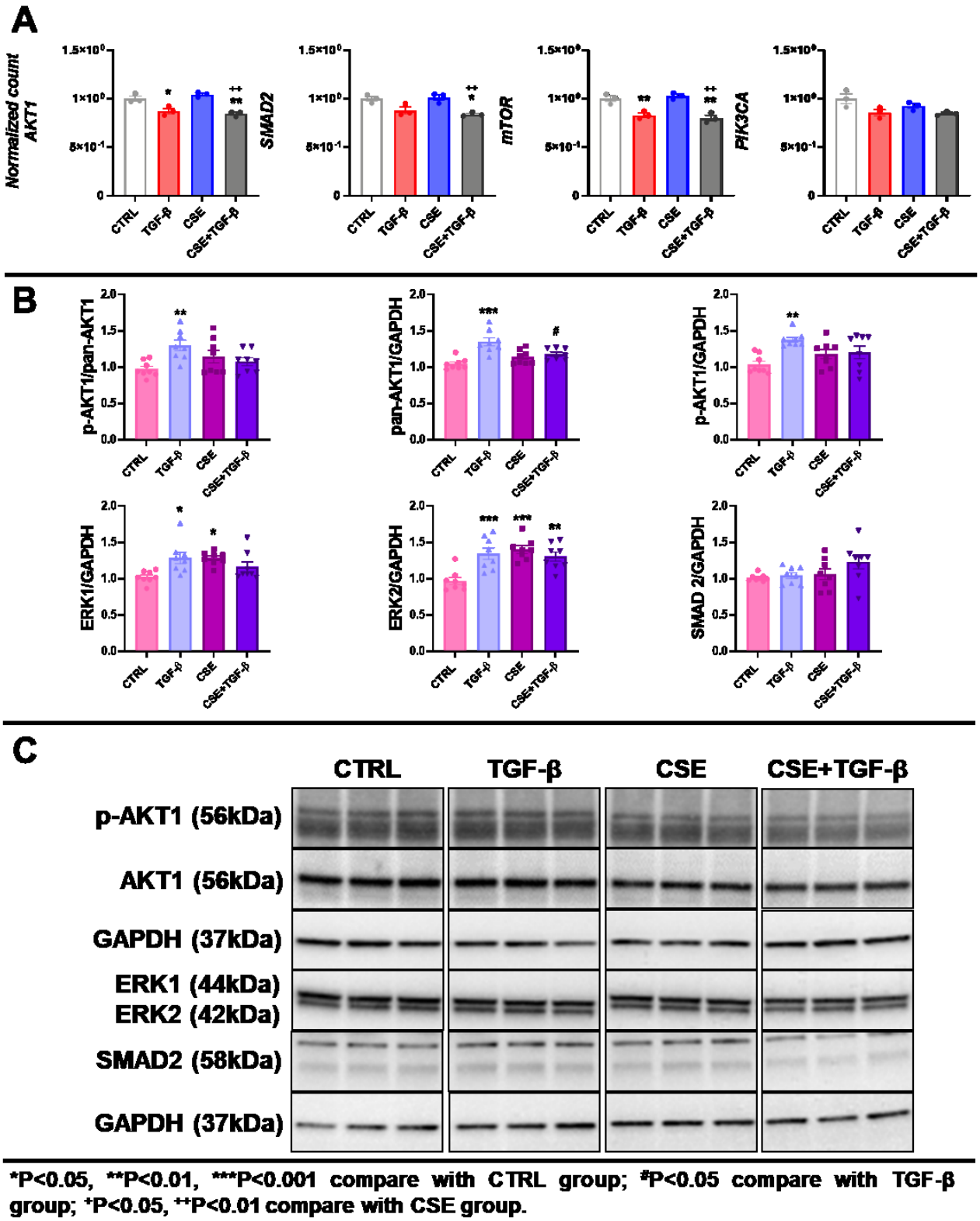

Figure 23: *(A) RNA isolated from cells was used to screen targets of interest via RT-PCR. GAPDH was used as the endogenous control (n=3/group). (B) Protein expressions were analysed by Western blotting from cell lysate. (C) Blot images of each experimental group. Densitometry analyses are done individually, and GAPDH was used as the endogenous control. Data are presented as mean ± SEM (n=8/group).*

DISCUSSION

Fibroblast cells are considered among the main players of fibrotic diseases. In pulmonary fibrosis, these cells are responsible for the release of massive amount of ECM proteins, cytokines, chemokines and growth factors that allow the propagation of fibrogenesis [126, 127]. Even if the role of these cells is well known, many aspects still need to be elucidated. Currently, there are several risk factors that might be involved in the initiation and exacerbation of fibrosis, and smoking is one of those. However, it is more likely that multiple micro-insults are necessary to the development of pulmonary fibrosis.

As already mentioned, bleomycin-induced pulmonary fibrosis is the most well studied model of lung fibrosis, yet it lacks some crucial characteristics such as the non-reversibility of this condition in human. Recently, several *in vivo* studies reported that the combined exposure to cigarette smoke and fibrotic agents (i.e., bleomycin, silica dust, fluorescent isothiocynate, paraquat) [100, 128] can reproduce some common features of pulmonary fibrosis, that seldom are observed in animal model induced by a single agent [97, 98].

Multiple intracellular signalling pathways have been implicated in the development of pulmonary fibrosis; yet, the specific molecular mechanisms are not clear. For instance, it is reported that an imbalance of ECM synthesis and degradation, and a dysregulation of ECM proteins crosslinking is crucial. Despite the complexity of this condition, the transforming growth factor β (TGF-β) is known to have a central role as regulator of tissue fibrosis. Indeed, the pro-fibrotic effects of TGF-β1 are well established in several *in vivo* studies [129].

In addition, *in vitro* studies were useful to elucidate some of the pathogenetic mechanisms of pulmonary fibrosis.

A dose-response study showed that TGF-β isoforms stimulate fibroblasts procollagen synthesis, and TGF-β1 resulted to be the predominant isoform implicated in pulmonary

fibrosis *in vivo* studies [130]. In a different study, human lung fibroblasts exposed to 10 ng/mL of TGF-β presented an increased expression of α-SMA and collagen production after 24 hours. These events were observed through the phosphorylation of ERK1/ERK2 within 30 minutes from the treatment with TGF-β [131].

In our study, we exposed, for a short time, normal human lung fibroblasts (NHLFs) to a very low dose of cigarette smoke extract (0.05%) followed by a treatment with TGF-β (2.5 ng/mL). The combination of these elements, able to induce a fibrogenic response in *in vivo* models, could amplify fibroblast cells activation, and their differentiation into myofibroblasts. The aim of this study was to evaluate whether some pathways involved in fibroblasts differentiation and activation were dysregulated, when multiple insults were combined.

After 24 hours of CSE exposure, we observed a slight increment in the gene expression of ECM elements and markers of fibroblasts differentiation. Thus, we thought that the combination with TGF-β would bring to a significant upregulation of these genes, in a short time. On the contrary, fibroblasts exposed to CSE+TGF-β presented a significant downregulation of collagens (*COL1A1*, *COL1A2*, *COL3A1*), and lysyl oxidase enzyme (*LOX*) genes when compared to TGF-β group. This trend was also confirmed with an evaluation of the protein expression via immunoblotting analysis. Indeed, cells exposed only to TGF-β presented higher levels of α-SMA, and LOX active form, than CSE+TGF-β treated fibroblasts. Instead, the expression of FIBRONECTIN was significantly increased following the exposure to TGF-β and cigarette smoke.

A possible explanation for the results obtained in this study could be attributable to the cell seeding density, as highlighted by different research groups. For instance, Wang and co-workers reported that high-density fibroblasts following the exposure to CSE were

stimulated to produce fibronectin, while at a lower cell density, CSE induced the opposite effects, in their experimental conditions [132].

In our model, high-density fibroblasts were able to produce a great amount of fibronectin even with a low dose of CSE. In addition, it was interesting to notice that NHLFs first exposed to CSE and then to TGF-β presented a further upregulation of fibronectin protein compared to CSE and TGF-β groups.

In a different study, Doolin and co-workers demonstrated that high-density culture of fibroblasts best mimic the microenvironment observed in fibrotic lung. In fact, in this condition (12.000 cells/cm^2), fibroblasts, exposed to TGF-β for 24, 48 or 72 hours, presented a higher incidence of transition to myofibroblasts, highlighted by a greater expression of α-SMA [133]. Even in our study, a pronounced expression of α-SMA protein was observed after 48 hours of exposure to TGF-β.

Therefore, we confirmed that high-density culture of normal human lung fibroblast cells presented a noteworthy degree of differentiation into myofibroblasts even when exposed to a relative low dose of TGF-β for just 48 hours.

However, this does not justify why we observed a downregulation of collagens and α-SMA when cigarette smoke and TGF-β were combined.

CSE is known to induce DNA damage and apoptosis in human fetal lung fibroblasts (HFL-1) in a dose and time-dependent manner through oxidative-mediated damage [134]. In this study, a high concentration of CSE (5%) induced a significant increase of DNA strand breaks from 3 hours onwards; nonetheless, the lower evaluated concentration of CSE (1.25%) was able to increase the percentage of DNA strand breaks compare to control cells, after 24 hours [134]. These results justify our decision to use a low dose of CSE, to avoid a significant mortality of cells that could introduce more bias to the study.

In addition, these authors evaluate the relationship between cell density and CSE-induced DNA strand breaks. In their model, 24-hours exposure to 5% CSE prompted around 95% of DNA strand breaks in fibroblasts seeded at low densities (1-2x10^5 cells/mL), while at higher cell densities (3-5x10^5 cells/mL) fibroblasts displayed less TUNEL-positive cells [134]. In our work, the applied cell density (2.5x10^5 cells/mL) might be considered among the higher cell densities used by Kim and colleagues that probably favours cellular survival. Based on this consideration, the extremely low percentage of cell deaths in fibroblasts exposed to CSE observed in our experimental condition might also be related to the higher cell density.

Notwithstanding, our model indicates that CSE does not amplify TGF-β-induced fibroblasts transition in cell culture. Confirming the above results, the quantification of the immunofluorescence depicted a reduction in the α-SMA expression in CSE+TGF-β treated NHLFs, whit respect to TGF-β treated cells. This suggests a lower activation of fibroblasts, hence a lower capacity of remodelling the extracellular matrix.

These data are inconsistent with the synergistic effects of these two agents reported in some *in vivo* studies [97, 98]. This could be due to the fact that within the lungs there are several cell populations that respond differently to the same noxious agent by activating distinctive molecular pathways.

Based on our data, we thought of evaluating whether the expression of some TGF-β downstream effectors were modified when CSE and TGF-β are combined. After 72 hours from the beginning of the experiment, a Nanostring panel was used to assess the gene expression. This analysis revealed that cells treated with TGF-β did not display an upregulation of *SMAD2*, *AKT1*, *PI3K*, *mTOR* genes, regardless the exposure to air or CSE. Still, the proteins expression of p-AKT1 (phospho-AKT1), pan-AKT1 and ERK1/2 in the TGF-β group appeared upregulated with respect to the control group.

PI3K/AKT signalling pathway is demonstrated to play a central role in human lung fibroblasts proliferation and differentiation, and TGF-β is reported to increase p-AKT levels [135]. Conte et al. affirmed that, through the inhibition of PI3K/AKT pathway, they were able to revert the proliferation rate, the α-SMA expression and the collagen production induced by TGF-β treatment, in *ex-vivo* human lung fibroblasts [135]. In line with these results, we observed a significant increase of p-AKT1 and pan-AKT1 in human lung fibroblasts treated with a lower concentration of TGF-β (2.5 ng/ml). As already mentioned, associated with the increment of p-AKT1 protein expression, we observed the upregulation of collagens and α-SMA gene and protein expression levels. Thus, these results confirmed what reported in the previous work [135].

It is well known that TGF-β exposure activates the extracellular signal-regulated kinase-1 and -2 (ERK1/2) pathway in several cell systems [136]. More importantly, it has been demonstrated that this specific pathway is crucial for fibroblasts differentiation into myofibroblasts, and an inhibition of ERK1/2 attenuates the expression of α-SMA induced by TGF-β exposure [131]. In our study, we did not assess the expression of phospho-ERK1/2; nonetheless, we observed a significant increment of ERK1/2 protein levels even after 48 hours of exposure to TGF-β. As reported by D'Anna et al., CSE stimulates the expression of pro-inflammatory transcription factors ERK1/2. In this regard, in our work, we noticed a significant increase of ERK1/2 in the CSE group, even after the removal of the media with the CSE [137]. Of interest, the combination of CSE and TGF-β did not further upregulate the expression of p-AKT1, pan-AKT1, and ERK1/2 whit respect to the TGF-β group. Moreover, no significant changes of SMAD2 expression levels were observed between the different experimental groups.

Usuki and co-workers in their paper stated that, after 1-hour exposure to TGF-β, a great percentage of murine lung fibroblasts assumed an elongated spindle-shape, and, after 24

hours of treatment, the majority of fibroblasts were expressing α-SMA [138]. Usuki and colleagues also assessed the co-expression of α-SMA and phosphorylate-SMAD2/3 (p-SMAD2/3), and they observed that, after 1-hour exposure to TGF-β, a large number of cells were positive for p-SMAD2/3, but less than 10% of those were also positive for α-SMA. Rather, after 24 hours, the positive staining for p-SMAD2/3 was significantly decrease, whereas more than 50% of the lung fibroblasts were positive for α-SMA [138]. Even if in our work, the phosphorylated form was not evaluated, we analysed SMAD2 gene and protein expressions, and no changes were depicted after 48 hours' exposure to TGF-β. This might be due to the time point chosen for this treatment; therefore, based on what Usuki et al. reported, the expression levels of p-SMAD2 would have been reduced, in our experimental conditions. Moreover, we can speculate that the absence of SMAD2 protein variations associated with an increment of α-SMA expression may be indicative of an already fibroblasts differentiation.

Corroborating our hypothesis, another work reported that SMAD2 phosphorylation should be maintained for at least 6 hours through TGF-β stimulation in order to induce fibroblasts differentiation [139]. Indeed, Ard et al. demonstrated that the deletion of p-SMAD2 results in a decrease α-SMA, COL1A1 and FN1 expression [139].

From this perspective, NHLF cells first exposed to cigarette smoke for 24 hours may already have activated TGF-β downstream effectors; thus at the end of the experiment (72 hours, with 48 hours of TGF-β treatment) there might be a switching off of SMADs pathway. This would also justify a lower expression of collagens, active LOX, and α-SMA, confirming an essential role of SMAD2 phosphorylation in myofibroblasts differentiation.

Of course, further analyses are required to better understand the activation of SMAD2 pathway in our *in vitro* model.

On the other side, researches conducted on human lung and gingival fibroblasts reported that TGF-β ability of inducing α-SMA expression was compromised by the previous or concomitant administration of nicotine [140, 141]. For this reason, the previous exposure to CSE might be detrimental for the expression of α-SMA and collagen synthesis as demonstrated by the decrement of those in our experimental conditions.

This might also explain the results obtained from the cytokines analysis performed on the conditioned media collected from each group. The release of cytokines revealed an upregulation of interleukins like 6 and 8 (IL-6 and IL-8), monocyte chemoattractant protein 1 (MCP-1), and the macrophage inflammatory protein 1β (MIP-1β). TGF-β induced a significant increment in the expression of MIP-1β and IL-6; however, when combined with the CSE the quantity of these cytokines was lower than TGF-β group. Interestingly, a major amount of IL-8 was detected in culture media from NHLF cells exposed to CSE+TGF-β; while no differences were appreciated between TGF-β, CSE and CSE+TGF-β groups for MCP-1. Our data partially corresponded with what Sato et al. reported in their work, where they demonstrated that human fetal lung fibroblasts release IL-8 and MCP-1 following the exposure to cigarette smoke [142].

In conclusion, this study confirms the ability of TGF-β to induce fibroblasts differentiation, and the upregulation of ECM components within human primary lung fibroblasts. Besides, this work highlights a possible interference between CSE and TGF-β.

In this chapter, I reported data obtained during my last months of the exchange period.

The experimental project reported here do not produce the expected results may be due to some limitations; one of these is represented by the concentration of the extract and the time point chosen for evaluating the effects only produced by the CSE exposure. Moreover, as reported by other authors, there might be an interference produced by some elements present in the CSE, as nicotine.

Thus, future analysis should be made to identify doses and time points of CSE exposure able to prompt more evident responses, and to assess the presence of cigarette smoke components that might interfere with TGF-β signalling pathways. Furthermore, earlier time points than those evaluated in this study should be included both to identify the different signalling activated by the treatments tested, and to avoid switching off of those pathways. Lastly, as already reported in this discussion, due to distinct feedbacks elicited with diverse cell densities, more in-depth evaluations with primary cell cultures are required to gain more knowledge about this topic.

SUMMARY

Fibroblasts are one of the main cell populations that contribute to the progression of pulmonary fibrosis through the excessive production of collagens. It has also observed that these cells can differentiate into a different type of fibroblast, known as myofibroblasts, which can secrete even higher amounts of collagens. In this chapter the differentiation of fibroblasts was induced with the administration of TGF-β, but it was also tested the effect of cigarette smoke extract (CSE) in combination with TGF-β. Surprisingly, the combination of these agents did not result in the amplification of fibroblast differentiation, but instead showed an interference of their effects. This was demonstrated by a reduction in the expression of collagens (COL1A1, COL1A2, COL3A1, COL4A1), lysyl oxidase enzyme (LOX) and more importantly by a lower expression of α-SMA, the canonical marker of myofibroblasts.

This study presented some limitations that should be overcome with future experiments; nevertheless, the observed interference with the combined exposure to CSE and TGF-β could be an interesting starting point for new investigations to understand the effects of these two agents.

NOTE

The analyses reported in the first chapter were conducted during my first and last year of the PhD program at the University of Siena, and were supervised by Professor Monica Lucattelli. These experiments were conducted to accomplish previous works.

The experiments reported in the other chapters were performed during my 1-year exchange program at the University of Rochester (NY, USA), and were supervising by Dr. Irfan Rahman and Dr. Qixin Wang. At the same time, Professor Monica Lucattelli was updated about the ongoing experiments with monthly meetings.

Hence, I would like to thank Dr. Irfan Rahman for granting me the possibility to work in his laboratory for 1 year and for his support during this time. I would also like to express all my gratitude to Dr. Qixin Wang, Dr. Gagandeep Kaur, Dr. Joseph Lucas, and Cortney Pang, for their assistance and encouragement during this year at the University of Rochester.

Last but not least, I would like to thank Professor Monica Lucattelli for giving me the opportunity to spend 1 year abroad and for her constant support during the last 3 years.

REFERENCES

1. Kisseleva T, Brenner DA. “Mechanisms of Fibrogenesis”. *Exp Biol Med*. **2008**; 233: 109-122.
2. Wynn TA. “Common and unique mechanisms regulate fibrosis in various fibroproliferative diseases”. *J Clin Invest*. **2007**; 117: 524-529.
3. Karakioulaki M, Papakonstantinou E, Stolz D. “Extracellular matrix remodelling in COPD”. *Eur Respir Rev*. **2020**; 29: 190124.
4. Burgstaller G, Oehrle B, Gerckens M, White ES, Schiller HB, Eickelberg O. “The instructive extracellular matrix of the lung: basic composition and alterations in chronic lung disease”. *Eur Respir J*. **2017**; 50: 1601805.
5. Dunsmore SE. “Treatment of COPD: a matrix perspective”. *Int J Chron Obstruct Pulmon Dis*. **2008**; 3: 113-122.
6. Liu G, Philp AM, Corte T, Travis MA, Schilter H, Hansbro NG, Burns CJ, Eapen MS, Sohal SS, Burgess JK, Hansbro PM. “Therapeutic targets in lung tissue remodelling and fibrosis”. *Pharmacol Ther*. **2021**; 225: 107839.
7. White ES. “Lung extracellular matrix and fibroblast function”. *Ann Am Thorac Soc*. **2015**; 12: S30-S33.
8. Burgess JK, Harmsen MC. “Chronic lung diseases: entangled in extracellular matrix”. *Eur Respir Rev*. **2022**; 31: 210202.
9. Hynes RO, Naba A. “Overview of the matrisome--an inventory of extracellular matrix constituents and functions”. *Cold Spring Harb Perspect Biol*. **2012**; 4: a004903.
10. Walker C, Mojares E, Del Río Hernández A. “Role of Extracellular Matrix in Development and Cancer Progression”. *Int J Mol Sci*. **2018**; 19: 3028.

11. Hackett TL, Osei ET. “Modeling Extracellular Matrix-Cell Interactions in Lung Repair and Chronic Disease”. *Cells*. **2021**; 10: 2145.
12. Burgess JK, Mauad T, Tjin G, Karlsson JC, Westergren-Thorsson G. “The extracellular matrix - the under-recognized element in lung disease?” *J Pathol*. **2016**; 240: 397-409.
13. Cui N, Hu M, Khalil RA. “Biochemical and Biological Attributes of Matrix Metalloproteinases”. *Prog Mol Biol Transl Sci*. **2017**; 147: 1-73.
14. Elkington PT, Friedland JS. “Matrix metalloproteinases in destructive pulmonary pathology”. *Thorax*. **2006**; 61: 259-266.
15. Bonnans C, Chou J, Werb Z. “Remodelling the extracellular matrix in development and disease”. *Nat Rev Mol Cell Biol*. **2014**; 15: 786-801.
16. Aumiller V, Strobel B, Romeike M, Schuler M, Stierstorfer BE, Kreuz S. “Comparative analysis of lysyl oxidase (like) family members in pulmonary fibrosis”. *Sci Rep*. **2017**; 7: 149.
17. Laczko R, Csiszar K. “Lysyl Oxidase (LOX): Functional Contributions to Signaling Pathways”. *Biomolecules*. **2020**; 10: 1093.
18. Migulina N, Tjin G, Faiz A, Borghuis T, Zhao F, Kaper HJ, Matzlar M, van DiJk E, Sharma PK, Timens W, Gosens R, Brandsma C, Burgess JK. “Differential roles for lysyl oxidase (like), family members in chronic obstructive pulmonary disease; from gene and protein expression to function”. *FASEB J*. **2022**; 36: e22374.
19. Erasmus M, Samodien E, Lecour S, Cour M, Lorenzo O, Dludla P, Pheiffer C, Johnson R. “Linking LOXL2 to Cardiac Interstitial Fibrosis”. *Int J Mol Sci*. **2020**; 21: 5913.
20. Guo T, He C, Venado A, Zhou Y. “Extracellular Matrix Stiffness in Lung Health and Disease”. *Compr Physiol*. **2022**; 12: 3523-3558.

21. Amendola PG, Reuten R, Erler JT. “Interplay Between LOX Enzymes and Integrins in the Tumor Microenvironment”. *Cancers (Basel)*. **2019**; 11: 729.
22. Ito JT, Lourenço JD, Righetti RF, Tibério IFLC, Prado CM, Lopes FDTQS. “Extracellular Matrix Component Remodeling in Respiratory Diseases: What Has Been Found in Clinical and Experimental Studies?” *Cells*. **2019**; 8: 342.
23. Glasser SW, Hagood JS, Wong S, Taype CA, Madala SK, Hardie WD. “Mechanisms of Lung Fibrosis Resolution”. Am J Pathol. **2016**; 186: 1066-1077.
24. Chilosi M, Poletti V, Rossi A. “The pathogenesis of COPD and IPF: distinct horns of the same devil?” *Respir Res*. **2012**; 13: 3.
25. Pauwels RA, Buist AS, Calverley PM, Jenkins CR, Hurd SS, GOLD Scientific Committee. “Global strategy for the diagnosis, management, and prevention of chronic obstructive pulmonary disease. NHLBI/WHO Global Initiative for Chronic Obstructive Lung Disease (GOLD) Workshop summary”. *Am J Respir Crit Care Med*. **2001**; 163: 1256-1276.
26. Lettieri S, Bertuccio FR, Del Frate L, Perrotta F, Corsico AG, Stella GM. “The Plastic Interplay between Lung Regeneration Phenomena and Fibrotic Evolution: Current Challenges and Novel Therapeutic Perspectives”. *Int J Mol Sci*. **2023**; 25: 547.
27. Marshall RP, McAnulty RJ, Laurent GJ. “The pathogenesis of pulmonary fibrosis: is there a fibrosis gene?”. *Int J Biochem Cell Biol*. **1997**; 29: 107-120.
28. Aghali A, Koloko Ngassie ML, Pabelick CM, Prakash YS. “Cellular Senescence in Aging Lungs and Diseases”. *Cells*. **2022**; 11: 1781.
29. Barnes PJ, Baker J, Donnelly LE. “Cellular Senescence as a Mechanism and Target in Chronic Lung Diseases”. *Am J Respir Crit Care Med*. **2019**; 200: 556-564.

30. Chung KF, Adcock IM. “Multifaceted mechanisms in COPD: inflammation, immunity, and tissue repair and destruction”. *Eur Respir J*. **2008**; 31: 1334-1356.
31. Lee SH, Hwang ED, Lim JE, Moon S, Kang YA, Jung JY, Park MS, Kim SK, Chang J, Kim YS, Kim SY. “The Risk Factors and Characteristics of COPD Among Nonsmokers in Korea: An Analysis of KNHANES IV and V”. *Lung*. **2016**; 194: 353-361.
32. Brandsma CA, Van den Berge M, Hackett TL, Brusselle G, Timens W. “Recent advances in chronic obstructive pulmonary disease pathogenesis: from disease mechanisms to precision medicine”. *J Pathol*. **2020**; 250: 624-635.
33. MacNee W. “Pathology, pathogenesis, and pathophysiology”. *BMJ*. **2006**; 332: 1202–1204.
34. Hogg JC. “Pathophysiology of airflow limitation in chronic obstructive pulmonary disease”. *Lancet*. **2004**; 364: 709-721.
35. Mecham RP. “Elastin in lung development and disease pathogenesis”. *Matrix Biol*. **2018**; 73: 6-20.
36. Kim V, Rogers TJ, Criner GJ. “New concepts in the pathobiology of chronic obstructive pulmonary disease”. *Proc Am Thorac Soc*. **2008**; 5: 478-485.
37. Churg A, Tai H, Coulthard T, Wang R, Wright JL. “Cigarette smoke drives small airway remodeling by induction of growth factors in the airway wall”. *Am J Respir Crit Care Med*. **2006**; 174: 1327-1334.
38. Jones RL, Noble PB, Elliot JG, James AL. “Airway remodelling in COPD: It's not asthma!” *Respirology*. **2016**; 21: 1347-1356.
39. Wrobel JP, McLean CA, Thompson BR, Stuart-Andrews CR, Paul E, Snell GI, Williams TJ. “Pulmonary arterial remodeling in chronic obstructive pulmonary disease is lobe dependent”. *Pulm Circ*. **2013**; 3: 665-674.

40. Siafakas NM, Antoniou KM, Tzortzaki EG. “Role of angiogenesis and vascular remodeling in chronic obstructive pulmonary disease”. *Int J Chron Obstruct Pulmon Dis*. **2007**; 2: 453-462.
41. Pardo A, Selman M. “Molecular mechanisms of pulmonary fibrosis”. *Front Biosci*. **2002**; 7: d1743-d1761.
42. Kato S, Inui N, Hakamata A, Suzuki Y, Enomoto N, Fujisawa T, Nakamura Y, Watanabe H, Suda T. “Changes in pulmonary endothelial cell properties during bleomycin-induced pulmonary fibrosis”. *Respir Res*. **2018**; 19: 127.
43. Wolters PJ, Collard HR, Jones KD. “Pathogenesis of idiopathic pulmonary fibrosis”. *Annu Rev Pathol*. **2014**; 9: 157-179.
44. Selman M, Pardo A. “Idiopathic pulmonary fibrosis: an epithelial/fibroblastic cross-talk disorder”. *Respir Res*. **2002**; 3: 3.
45. Raghu G, Chen SY, Hou Q, Yeh WS, Collard HR. “Incidence and prevalence of idiopathic pulmonary fibrosis in US adults 18-64 years old”. *Eur Respir J*. **2016**; 48: 179-186.
46. Noble PW, Barkauskas CE, Jiang D. “Pulmonary fibrosis: patterns and perpetrators”. *J Clin Invest*. **2012**; 122: 2756-2762.
47. American Thoracic Society, European Respiratory Society. American Thoracic Society/European Respiratory Society International Multidisciplinary Consensus Classification of the Idiopathic Interstitial Pneumonias. This joint statement of the American Thoracic Society (ATS), and the European Respiratory Society (ERS) was adopted by the ATS board of directors, June 2001 and by the ERS Executive Committee, June 2001 [published correction appears in *Am J Respir Crit Care Med.* 2002; 166: 426]. *Am J Respir Crit Care Med*. **2002**; 165: 277-304.

48. Travis WD, Costabel U, Hansell DM, King TE Jr, Lynch DA, Nicholson AG, Ryerson CJ, Ryu JH, Selman M, Wells AU, Behr J, Bouros D, Brown KK, Colby TV, Collard HR, Cordeiro CR, Cottin V, Crestani B, Drent M, Dudden RF, Egan J, Flaherty K, Hogaboam C, Inoue Y, Johkoh T, Kim DS, Kitaichi M, Loyd J, Martinez FJ, Myers J, Protzko S, Raghu G, Richeldi L, Sverzellati N, Swigris J, Valeyre D, ATS/ERS Committee on Idiopathic Interstitial Pneumonias. "An official American Thoracic Society/European Respiratory Society statement: Update of the international multidisciplinary classification of the idiopathic interstitial pneumonias". *Am J Respir Crit Care Med*. **2013**; 188: 733-748.
49. Selman M, Buendía-Roldán I, Pardo A. "Aging and Pulmonary Fibrosis". *Rev Invest Clin*. **2016**; 68: 75-83.
50. Steele MP, Speer MC, Loyd JE, Brown KK, Herron A, Slifer SH, Burch LH, Wahidi MM, Philips JA 3rd, Sporn TA, McAdams HG, Schwarz MI, Schwartz DA. "Clinical and pathologic features of familial interstitial pneumonia". *Am J Respir Crit Care Med*. **2005**; 172: 1146-1152.
51. Rafii R, Juarez MM, Albertson TE, Chan AL. "A review of current and novel therapies for idiopathic pulmonary fibrosis". *J Thorac Dis*. **2013**; 5: 48-73.
52. Kropski JA, Blackwell TS, Loyd JE. "The genetic basis of idiopathic pulmonary fibrosis". *Eur Respir J*. **2015**; 45: 1717-1727.
53. Pardo A, Selman M. "The Interplay of the Genetic Architecture, Aging, and Environmental Factors in the Pathogenesis of Idiopathic Pulmonary Fibrosis". *Am J Respir Cell Mol Biol*. **2021**; 64: 163-172.
54. Sgalla G, Iovene B, Calvello M, Ori M, Varone F, Richeldi L. "Idiopathic pulmonary fibrosis: pathogenesis and management". *Respir Res*. **2018**; 19: 32.

55. Sack C, Raghu G. “Idiopathic pulmonary fibrosis: unmasking cryptogenic environmental factors”. *Eur Respir J*. **2019**; 53: 1801699.
56. Moss BJ, Ryter SW, Rosas IO. “Pathogenic Mechanisms Underlying Idiopathic Pulmonary Fibrosis”. *Annu Rev Pathol*. **2022**; 17: 515-546.
57. Hadjicharalambous MR, Lindsay MA. “Idiopathic Pulmonary Fibrosis: Pathogenesis and the Emerging Role of Long Non-Coding RNAs”. *Int J Mol Sci*. **2020**; 21: 524.
58. Willis BC, Liebler JM, Luby-Phelps K, Nicholson AG, Crandall ED, du Bois RM, Borok Z. “Induction of epithelial-mesenchymal transition in alveolar epithelial cells by transforming growth factor-beta1: potential role in idiopathic pulmonary fibrosis”. *Am J Pathol*. **2005**; 166: 1321-1332.
59. Wynn TA. “Cellular and molecular mechanisms of fibrosis”. *J Pathol*. **2008**; 214: 199-210.
60. Frangogiannis N. “Transforming growth factor-β in tissue fibrosis”. *J Exp Med*. **2020**; 217: e20190103.
61. Fernandez IE, Eickelberg O. “The impact of TGF-β on lung fibrosis: from targeting to biomarkers”. *Proc Am Thorac Soc*. **2012**; 9: 111-116.
62. Ramos C, Montaño M, García-Alvarez J, Ruiz V, Uhal BD, Selman M, Pardo A. “Fibroblasts from idiopathic pulmonary fibrosis and normal lungs differ in growth rate, apoptosis, and tissue inhibitor of metalloproteinases expression”. *Am J Respir Cell Mol Biol*. **2001**; 24: 591-598.
63. Andersson-Sjöland A, de Alba CG, Nihlberg K, Becerril C, RamÍrez R, Pardo A, Westergren-Thorsson G, Selman M. “Fibrocytes are a potential source of lung fibroblasts in idiopathic pulmonary fibrosis”. *Int J Biochem Cell Biol*. **2008**; 40: 2129-2140.

64. Willis BC, Borok Z. “TGF-beta-induced EMT: mechanisms and implications for fibrotic lung disease”. *Am J Physiol Lung Cell Mol Physiol*. **2007**; 293: L525-L534.
65. Rock JR, Barkauskas CE, Cronce MJ, Xue Y, Harris JR, Liang J, Noble PW, Hogan BL. “Multiple stromal populations contribute to pulmonary fibrosis without evidence for epithelial to mesenchymal transition”. *Proc Natl Acad Sci*. **2011**; 108: E1475-E1483.
66. Hashimoto N, Phan SH, Imaizumi K, Matsuo M, Nakashima H, Kawabe T, Shimokata K, Hasegawa Y. “Endothelial-mesenchymal transition in bleomycin-induced pulmonary fibrosis”. *Am J Respir Cell Mol Biol*. **2010**; 43: 161-172.
67. Hung C, Linn G, Chow YH, Kobayashi A, Mittelsteadt K, Altemeier WA, Gharib SA, Schnapp LM, Duffield JS. “Role of lung pericytes and resident fibroblasts in the pathogenesis of pulmonary fibrosis”. *Am J Respir Crit Care Med*. **2013**; 188: 820-830.
68. World Medical Association; American Physiological Society. “Guiding principles for research involving animals and human beings”. *Am J Physiol Regul Integr Comp Physiol*. **2002**; 283: R281-R283.
69. Cavarra E, Bartalesi B, Lucattelli M, Fineschi S, Lunghi B, Gambelli F, Ortiz LA, Martorana PA, Lungarella G. “Effects of cigarette smoke in mice with different levels of alpha (1)-proteinase inhibitor and sensitivity to oxidants”. *Am J Respir Crit Care Med*. **2001**; 164: 886-890.
70. De Cunto G, Bartalesi B, Cavarra E, Balzano E, Lungarella G, Lucattelli M. “Ongoing Lung Inflammation and Disease Progression in Mice after Smoking Cessation: Beneficial Effects of Formyl-Peptide Receptor Blockade”. *Am J Pathol*. **2018**; 188: 2195-2206.

71. De Cunto G, Brancaleone V, Riemma MA, Cerqua I, Vellecco V, Spaziano G, Cavarra E, Bartalesi B, D'Agostino B, Lungarella G, Cirino G, Lucattelli M, Roviezzo F. "Functional contribution of sphingosine-1-phosphate to airway pathology in cigarette smoke exposed mice". *Br J Pharmacol*. **2020**; 177: 267–281.
72. De Cunto G, De Meo S, Bartalesi B, Cavarra E, Lungarella G, Lucattelli M. "Smoking cessation in mice does not switch off persistent lung inflammation and does not restore the expression of HDAC-2 and SIRT-1". *Int J Mol Sci*. **2022**; 23: 9104.
73. Balzano E, De Cunto G, Goracci C, Bartalesi B, Cavarra E, Lungarella G, Lucattelli M. "Immunohistochemical Study of Airways Fibrous Remodeling in Smoking Mice". *J Histochem Cytochem*. **2023**; 71: 577-599.
74. Winer J, Jung CK, Shackel I, Williams PS. "Development and validation of real-time quantitative reverse transcriptase-polymerase chain reaction for monitoring gene expression in cardiac myocytes in vitro". *Anal Biochem*. **1999**; 270: 41–49.
75. Bateman G, Guo-Parke H, Rodgers AM, Linden D, Bailey M, Weldon S, Kidney JC, Taggart CC. "Airway Epithelium Senescence as a Driving Mechanism in COPD Pathogenesis". *Biomedicines*. **2023**; 11:2072.
76. Salminen A, Kauppinen A, Kaarniranta K. "Emerging role of NF-κB signaling in the induction of senescence-associated secretory phenotype (SASP)". *Cell Signal*. **2012**; 24: 835-845.
77. Hogg JC, Chu F, Utokaparch S, Woods R, Elliott WM, Buzatu L, Cherniack RM, Rogers RM, Sciurba FC, Coxson HO, Paré PD. "The nature of small-airway obstruction in chronic obstructive pulmonary disease". *N Engl J Med*. **2004**; 350: 2645-2653.

78. Bartalesi B, Cavarra E, Fineschi S, Lucattelli M, Lunghi B, Martorana PA, Lungarella G. “Different lung responses to cigarette smoke in two strains of mice sensitive to oxidants”. *Eur Respir J*. **2005**; 25: 15-22.
79. Wang RD, Wright JL, Churg A. “Transforming growth factor-beta1 drives airway remodeling in cigarette smoke-exposed tracheal explants”. *Am J Respir Cell Mol Biol*. **2005**; 33: 387-393.
80. Cantin AM. “Cellular response to cigarette smoke and oxidants: adapting to survive”. *Proc Am Thorac Soc*. **2010**; 7: 368-375.
81. Birch J, Barnes PJ, Passos JF. “Mitochondria, telomeres and cell senescence: Implications for lung ageing and disease”. *Pharmacol Ther*. **2018**; 183: 34-49.
82. Childs BG, Durik M, Baker DJ, van Deursen JM. “Cellular senescence in aging and age-related disease: from mechanisms to therapy”. *Nat Med*. **2015**; 21: 1424-1435.
83. Thannickal VJ, Murthy M, Balch WE, Chandel NS, Meiners S, Eickelberg O, Selman M, Pardo A, White ES, Levy BD, Busse PJ, Tuder RM, Antony VB, Sznajder JI, Budinger Budinger GR. “Blue journal conference. Aging and susceptibility to lung disease”. *Am J Respir Crit Care Med*. **2015**; 191: 261-269.
84. Conti V, Corbi G, Manzo V, Pelaia G, Filippelli A, Vatrella A. “Sirtuin 1 and aging theory for chronic obstructive pulmonary disease”. *Anal Cell Pathol (Amsterdam)*. **2015**; 2015: 897327.
85. Rahman I, Kinnula VL, Gorbunova V, Yao H. “SIRT1 as a therapeutic target in inflammaging of the pulmonary disease”. *Prev Med*. **2012**; 54: S20-S28.
86. Yeung F, Hoberg JE, Ramsey CS, Keller MD, Jones DR, Frye RA, Mayo MW. “Modulation of NF-kappaB-dependent transcription and cell survival by the SIRT1 deacetylase”. *EMBO J*. **2004**; 23: 2369-2380.

87. Alharbi KS, Fuloria NK, Fuloria S, Rahman SB, Al-Malki WH, Javed Shaikh MA, Thangavelu L, Singh SK, Rama Raju Allam VS, Jha NK, Chellappan DK, Dua K, Gupta G. “Nuclear factor-kappa B and its role in inflammatory lung disease”. *Chem Biol Interact*. **2021**; 345: 109568.
88. Gaffey K, Reynolds S, Plumb J, Kaur M, Singh D. “Increased phosphorylated p38 mitogen-activated protein kinase in COPD lungs”. *Eur Respir J*. **2013**; 42: 28-41.
89. Roux PP, Blenis J. “ERK and p38 MAPK-activated protein kinases: a family of protein kinases with diverse biological functions”. *Microbiol Mol Biol Rev*. **2004**; 68: 320-344.
90. Lagoumtzi SM, Chondrogianni N. “Senolytics and senomorphics: Natural and synthetic therapeutics in the treatment of aging and chronic diseases”. *Free Radic Biol Med*. **2021**; 171: 169-190.
91. Zhang L, Pitcher LE, Prahalad V, Niedernhofer LJ, Robbins PD. “Targeting cellular senescence with senotherapeutics: senolytics and senomorphics”. *FEBS J*. **2023**; 290: 1362-1383.
92. Wang Q, Sundar IK, Blum JL, Ratner JR, Lucas JH, Chuang T, Wang Y, Liu J, Rehan VK, Zelikoff JT, Rahman I. “Prenatal Exposure to Electronic-Cigarette Aerosols Leads to Sex-Dependent Pulmonary Extracellular-Matrix Remodeling and Myogenesis in Offspring Mice”. *Am J Respir Cell Mol Biol*. **2020**; 63: 794-805.
93. Wang Q, Sundar IK, Lucas JH, Muthumalage T, Rahman I. “Molecular clock REV-ERBα regulates cigarette smoke-induced pulmonary inflammation and epithelial-mesenchymal transition”. *JCI Insight*. **2021**; 6: e145200.
94. Eisner MD, Balmes J, Katz PP, Trupin L, Yelin EH, Blanc PD. “Lifetime environmental tobacco smoke exposure and the risk of chronic obstructive pulmonary disease”. *Environ Health*. **2005**; 4: 7.

95. Bellou V, Belbasis L, Evangelou E. “Tobacco Smoking and Risk for Pulmonary Fibrosis: A Prospective Cohort Study From the UK Biobank”. *Chest*. **2021**; 160: 983-993.
96. Vanker A, Gie RP, Zar HJ. “The association between environmental tobacco smoke exposure and childhood respiratory disease: a review”. *Expert Rev Respir Med*. **2017**; 11: 661-673.
97. Cisneros-Lira J, Gaxiola M, Ramos C, Selman M, Pardo A. “Cigarette smoke exposure potentiates bleomycin-induced lung fibrosis in guinea pigs”. *Am J Physiol Lung Cell Mol Physiol*. **2003**; 285: L949-L956.
98. Zhou LL, Wang M, Liu F, Lu YZ, Song LJ, Xiong L, Xiang F, He XL, Shuai SY, Xin JB, Ye H, Yu F, Ma WL. “Cigarette smoking aggravates bleomycin-induced experimental pulmonary fibrosis”. *Toxicol Lett*. **2019**; 303: 1-8.
99. Shin YJ, Kim SH, Park CM, Kim HY, Kim IH, Yang MJ, Lee K, Kim MS. “Exposure to cigarette smoke exacerbates polyhexamethylene guanidine-induced lung fibrosis in mice”. *J Toxicol Sci*. **2021**; 46:487-497.
100. Fang L, Cheng Q, Zhao F, Cheng H, Luo Y, Bao X, Li Y, Liang X, Huang Y, Xu J, Han J, Tang Y, Tang S, Liu W, Luo Z, Feng D. “Cigarette smoke exposure combined with lipopolysaccharides induced pulmonary fibrosis in mice”. *Respir Physiol Neurobiol*. **2019**; 266: 9-17.
101. Wang Q, Goracci C, Sundar IK, Rahman I. “Environmental tobacco smoke exposure exaggerates bleomycin-induced collagen overexpression during pulmonary fibrogenesis”. *J Inflamm (London)*. **2024**; 21:9.
102. Bormann T, Maus R, Stolper J, Tarrés MT, Brandenberger C, Wedekind D, Jonigk D, Welte T, Gualdie J, Kolb M, Maus UA. “Role of matrix metalloprotease-2 and MMP-9 in experimental lung fibrosis in mice”. *Respir Res*. **2022**; 23: 180.

103. Smith-Mungo LI, Kagan HM. “Lysyl oxidase: properties, regulation and multiple functions in biology”. *Matrix Biol*. **1998**; 16: 387-398.

104. Wang Q, Sundar IK, Lucas JH, Park JG, Nogales A, Martinez-Sobrido L, Rahman I. “Circadian clock molecule REV-ERBα regulates lung fibrotic progression through collagen stabilization”. *Nat Commun*. **2023**; 14: 1295.

105. Tjin G, White ES, Faiz A, Sicard D, Tschumperlin DJ, Mahar A, Kable EPW Burgess JK. “Lysyl oxidases regulate fibrillar collagen remodelling in idiopathic pulmonary fibrosis”. *Dis Model Mech*. **2017**; 10: 1301-1312.

106. MacNee W. “Is Chronic Obstructive Pulmonary Disease an Accelerated Aging Disease?” *Ann Am Thorac Soc*. **2016**; 13 Suppl 5: S429-S437.

107. Venosa A. “Senescence in Pulmonary Fibrosis: Between Aging and Exposure”. *Front Med (Lausanne)*. **2020**; 7: 606462.

108. Fulda S, Gorman AM, Hori O, Samali A. “Cellular stress responses: cell survival and cell death”. *Int J Cell Biol*. **2010**; 2010: 214074.

109. Campisi J, d'Adda di Fagagna F. “Cellular senescence: when bad things happen to good cells”. *Nat Rev Mol Cell Biol*. **2007**; 8: 729-740.

110. Tsuji T, Aoshiba K, Nagai A. “Cigarette smoke induces senescence in alveolar epithelial cells”. *Am J Respir Cell Mol Biol*. **2004**; 31: 643-649.

111. Jiang C, Liu G, Luckhardt T, Antony V, Zhou Y, Carter AB, Thannickal VJ, Liu RM. “Serpine 1 induces alveolar type II cell senescence through activating p53-p21-Rb pathway in fibrotic lung disease”. *Aging Cell*. **2017**; 16: 1114-1124.

112. Lee SH, Lee JH, Lee HY, Min KJ. “Sirtuin signaling in cellular senescence and aging”. *BMB Rep*. **2019**; 52: 24-34.

113. Jablonski RP, Kim SJ, Cheresh P, Williams DB, Morales-Nebreda L, Cheng Y, Yeldandi A, Bhorade S, Pardo A, Selman M, Ridge K, Gius D, Budinger GR, Kamp

DW. “SIRT3 deficiency promotes lung fibrosis by augmenting alveolar epithelial cell mitochondrial DNA damage and apoptosis”. *FASEB J*. **2017**; 31: 2520-2532.

114. Sosulski ML, Gongora R, Feghali-Bostwick C, Lasky JA, Sanchez CG. “Sirtuin 3 Deregulation Promotes Pulmonary Fibrosis”. *J Gerontol A Biol Sci Med Sci*. **2017**; 72: 595-602.
115. Sundaresan NR, Bindu S, Pillai VB, Samant S, Pan Y, Huang JY, Gupta M, Nagalingam RS, Wolfgeher D, Verdin E, Gupta MP. “SIRT3 Blocks Aging-Associated Tissue Fibrosis in Mice by Deacetylating and Activating Glycogen Synthase Kinase 3β”. *Mol Cell Biol*. **2015**; 36: 678-692.
116. Zheng R, Zhang Y, Zhang K, Yuan Y, Jia S, Liu J. “The Complement System, Aging, and Aging-Related Diseases”. *Int J Mol Sci*. **2022**; 23: 8689.
117. Wu X, Lin L, Cui J, Chen Y, Yang L, Wan J. “Complement C3 deficiency ameliorates aging related changes in the kidney”. *Life Sci*. **2020**; 260: 118370.
118. Yuan X, Shan M, You R, Frazier MV, Hong MJ, Wetsel RA, Drouin S, Seryshev A, Song LZ, Cornwell L, Rossen RD, Corry DB, Kheradmand F. “Activation of C3a receptor is required in cigarette smoke-mediated emphysema”. *Mucosal Immunol*. **2015**; 8: 874-885.
119. Gu H, Fisher AJ, Mickler EA, Duerson F 3rd, Cummings OW, Peters-Golden M, Twigg HL 3rd, Woodruff TM, Wilkes DS, Vittal R. “Contribution of the anaphylatoxin receptors, C3aR and C5aR, to the pathogenesis of pulmonary fibrosis”. *FASEB J*. **2016**; 30: 2336-2350.
120. Pandya PH, Wilkes DS. “Complement system in lung disease”. *Am J Respir Cell Mol Biol*. **2014**; 51: 467-473.
121. Okamoto T, Mathai SK, Hennessy CE, Hancock LA, Walts AD, Stefanski AL, Brown KK, Lynch DA, Cosgrove GP, Groshong SD, Cool CD, Schwarz MI, Banda NK,

Thurman JM, Yang IV, Holers VM, Schwartz DA. “The relationship between complement C3 expression and the MUC5B genotype in pulmonary fibrosis”. *Am J Physiol Lung Cell Mol Physiol*. **2018**; 315: L1-L10.

122. Meliconi R, Senaldi G, Sturani C, Galavotti V, Facchini A, Gasbarrini G, Vergani D. “Complement activation products in idiopathic pulmonary fibrosis: relevance of fragment Ba to disease severity”. *Clin Immunol Immunopathol*. **1990**; 57: 64-73.
123. Sikkeland LIB, Ueland T, Lund MB, Durheim MT, Mollnes TE. “A role for the terminal C5-C9 complement pathway in idiopathic pulmonary fibrosis”. *Front Med (Lausanne)*. **2023**; 10: 1236495.
124. Cipolla E, Fisher AJ, Gu H, Mickler EA, Agarwal M, Wilke CA, Kim KK, Moore BB, Vittal R. “IL-17A deficiency mitigates bleomycin-induced complement activation during lung fibrosis”. *FASEB J*. **2017**; 31: 5543-5556.
125. Sundar IK, Nevid MZ, Friedman AE, Rahman I. “Cigarette smoke induces distinct histone modifications in lung cells: implications for the pathogenesis of COPD and lung cancer”. *J Proteome Res*. **2014**; 13: 982-996.
126. Kendall RT, Feghali-Bostwick CA. “Fibroblasts in fibrosis: novel roles and mediators”. *Front Pharmacol*. **2014**; 5: 123.
127. Plikus MV, Wang X, Sinha S, Forte E, Thompson SM, Herzog EL, Driskell RR, Rosenthal N, Biernaskie J, Horsley V. “Fibroblasts: Origins, definitions, and functions in health and disease”. *Cell*. **2021**; 184: 3852-3872.
128. Tashiro J, Rubio GA, Limper AH, Williams K, Elliot SJ, Ninou I, Aidinis V, Tzouvelekis A, Glassberg MK. “Exploring Animal Models That Resemble Idiopathic Pulmonary Fibrosis”. *Front Med (Lausanne)*. **2017**; 4:118.

129. Xu Q, Norman JT, Shrivastav S, Lucio-Cazana J, Kopp JB. “In vitro models of TGF-beta-induced fibrosis suitable for high-throughput screening of antifibrotic agents”. *Am J Physiol Renal Physiol*. **2007**; 293: F631-F640.

130. Coker RK, Laurent GJ, Shahzeidi S, Lympany PA, du Bois RM, Jeffery PK, McAnulty RJ. “Transforming growth factors-beta 1, -beta 2, and -beta 3 stimulate fibroblast procollagen production in vitro but are differentially expressed during bleomycin-induced lung fibrosis”. *Am J Pathol*. **1997**; 150: 981-991.

131. Caraci F, Gili E, Calafiore M, Failla M, La Rosa C, Crimi N, Sortino MA, Nicoletti F, Copani A, Vancheri C. “TGF-beta1 targets the GSK-3beta/beta-catenin pathway via ERK activation in the transition of human lung fibroblasts into myofibroblasts”. *Pharmacol Res*. **2008**; 57: 274-282.

132. Wang H, Liu X, Umino T, Kohyama T, Zhu YK, Wen FQ, Spurzem JR, Romberger DJ, Kim HJ, Rennard SI. “Effect of cigarette smoke on fibroblast-mediated gel contraction is dependent on cell density”. *Am J Physiol Lung Cell Mol Physiol*. **2003**; 284: L205-L213.

133. Doolin MT, Smith IM, Stroka KM. “Fibroblast to myofibroblast transition is enhanced by increased cell density”. *Mol Biol Cell*. **2021**; 32: ar41.

134. Kim H, Liu X, Kobayashi T, Conner H, Kohyama T, Wen FQ, Fang Q, Abe S, Bitterman P, Rennard SI. “Reversible cigarette smoke extract-induced DNA damage in human lung fibroblasts”. *Am J Respir Cell Mol Biol*. **2004**; 31: 483-490.

135. Conte E, Fruciano M, Fagone E, Gili E, Caraci F, Iemmolo M, Crimi N, Vancheri C. “Inhibition of PI3K prevents the proliferation and differentiation of human lung fibroblasts into myofibroblasts: the role of class I P110 isoforms”. *PLoS One*. **2011**; 6: e24663.

136. Finlay GA, Thannickal VJ, Fanburg BL, Paulson KE. “Transforming growth factor-beta 1-induced activation of the ERK pathway/activator protein-1 in human lung fibroblasts requires the autocrine induction of basic fibroblast growth factor”. *J Biol Chem*. **2000**; 275: 27650-27656.

137. D'Anna C, Cigna D, Costanzo G, Ferraro M, Siena L, Vitulo P, Gjomarkaj G, Pace E. “Cigarette smoke alters cell cycle and induces inflammation in lung fibroblasts”. *Life Sci*. **2015**; 126: 10-18.

138. Usuki J, Matsuda K, Azuma A, Kudoh S, Gemma A. “Sequential analysis of myofibroblast differentiation and transforming growth factor-β1/Smad pathway activation in murine pulmonary fibrosis”. *J Nippon Med Sch*. **2012**; 79: 46-59.

139. Ard S, Reed EB, Smolyaninova LV, Orlov SN, Mutlu GM, Guzy RD, Dulin NO. “Sustained Smad2 Phosphorylation Is Required for Myofibroblast Transformation in Response to TGF-β”. *Am J Respir Cell Mol Biol*. **2019**; 60: 367-369.

140. Lei W, Lerner C, Sundar IK, Rahman I. “Myofibroblast differentiation and its functional properties are inhibited by nicotine and e-cigarette via mitochondrial OXPHOS complex III”. *Sci Rep*. **2017**; 7: 43213.

141. Fang Y, Svoboda KK. “Nicotine inhibits myofibroblast differentiation in human gingival fibroblasts”. *J Cell Biochem*. **2005**; 95: 1108-1119.

142. Sato E, Koyama S, Takamizawa A, Masubuchi T, Kubo K, Robbins RA, Nagai S, Izumi T. “Smoke extract stimulates lung fibroblasts to release neutrophil and monocyte chemotactic activities”. *Am J Physiol*. **1999**; 277: L1149-L1157.